THE UNIVERSITY OF CHICAGO

MECHANISMS OF REMODELING TRANSLATION DURING STRESS

A DISSERTATION SUBMITTED TO
THE FACULTY OF THE DIVISION OF THE BIOLOGICAL SCIENCES
AND THE PRITZKER SCHOOL OF MEDICINE
IN CANDIDACY FOR THE DEGREE OF
DOCTOR OF PHILOSOPHY

GRADUATE PROGRAM IN BIOCHEMISTRY AND MOLECULAR BIOPHYSICS

BY
CHRISTOPHER DANIEL KATANSKI

CHICAGO, ILLINOIS
MARCH 2019

"The recent concepts about the function of the system are fascinating, yet the system looks so complex that it might still hold some other surprises in store for us."

-Ferruccio Ritossa, discoverer of the heat shock response [1]

Table of Contents

List of Figures

ACKNOWLEDGMENTS

This work was only possible with the guidance and support of my advisor, Allan Drummond, and the entire Drummond lab. I was able to take advantage of the patience, and eventually expertise, of everyone in the lab to grow both scientifically and personally. I am especially thankful to Allan for his support as a mentor. He filled this role in the traditional sense, advising where and how to direct the science, but also offered support personally which made my continued growth possible.

I am grateful to everyone in the Drummond lab for making it a great place to work. Edward was a mentor to me and showed me genuine excitement for science. Jamie kept the wheels on the bus for many years. Evgeny showed me what true expertise looks like. Josh was a wonderful collaborator and friend. Cat showed me many new things and modeled a disciplined approach to science. Haneul has been a great collaborator and kind ear to listen. Sammy, Hendrik, and Jared have been fun and inspire faith that the lab will continue to thrive.

I would like to thank my sources of financial support. I have been supported by the Molecular and Cellular Biology training grant T32 GM007183 and also the Protein Translation Research Network.

I would like to thank my family for their support during my thesis work. I always had a bed to come back to. I always had a holiday to unwind. I was never asked to choose between work or family. Their support helped make this possible. I would also like to thank my mother for assistance in editing grammar.

I am grateful to my many friends who have supported me emotionally and with the occasional free drink. Old friendships were neglected for years, but were preserved through great patience and grace, for which I am truly grateful. I am also grateful to the many new friends I made during my time at the University of Chicago. Science loves company and my cohort in the molecular biosciences was great company. I am especially grateful to have

spent so much time with the real first years of BMB, Alyssa Harker, Katherine Leon, Kevin Hunt, and Phil McGilvray.

ABSTRACT

How do cells sense and respond to changes in the environment? Studying the cellular stress response has led to many insights regarding gene regulation – a central theme in post-genomic biology. Much of our knowledge about the stress response remains phenomenological without precise functions and mechanisms assigned. In particular, a wide variety of stressors trigger the formation of massive phase-separated assemblies containing many different protein and RNA species. These structures are believed to sequester their components and contribute to attenuation of translation and protect the contents. However, questions remain about these structures, including: what they made of, how they form, and their precise function. The aim of my thesis work has been to better understand the role of these structures in their native biological context. The work presented is highly collaborative, representing the effort of many researchers from the Drummond lab and others.

Chapter 1 is a review of the heat shock response, including changes in gene regulation, changes in translation, and the function of molecular chaperones. Additionally, the growing field of phase separation in biology is reviewed. Material is reviewed with a focus on historical observations, such as the first observations of phenomena.

Chapter 2 details work seeking to identify the protein components of heat induced assemblies. Formation of large structures during stress has historically been observed using fluorescence microscopy by following the subcellular localization of a small number of proteins during stress. We used a combination of sedimentation and mass spectrometry to identify the set of proteins that join large structures during stress. This technique allowed us to identify proteins that aggregate faster and at less severe stresses than traditional protein markers of these structures. Additionally, we identified that drugs which prevent formation of visible foci do not prevent the formation of sedimentable species - a result that requires reexamination of proposed mechanisms of focus formation.

Chapter 3 discusses autonomous temperature sensing of a particular protein component,

poly(A)-binding protein, and how phase separation is a plausible mechanism for native assembly formation. We were able to reconstitute the assembly behavior of one canonical component of heat-stress-induced assemblies in yeast: poly(A)-binding protein (Pab1). We have further shown assembly of Pab1 proceeds via a phase separation mechanism and this process is adaptive. Unlike other phase separating proteins, Pab1 phase separation is modulated, but not caused by a low-complexity domain. Also, the hydrophobic content of this low-complexity domain influences phase separation, in contrast with other proteins where ionic and hydrogen bond interactions are dominant. Point mutations that disrupt phase separation prevent cell growth at high temperature and under starvation conditions.

Chapter 4 explores the molecular details behind an adaptive function of poly(A)-binding protein assembly. We asked what are the molecular and cellular functions of stress-triggered phase separation of Pab1? Several observations about both heat shock protein (HSP) regulation and Pab1 lead to a possible model. (1) Pab1 can repress translation via binding A-rich regions in the 5' translated region (UTR) of an mRNA. (2) The mRNA encoding HSPs possess conserved A-rich 5' UTRs. (3) Phase-separated Pab1 does not bind RNA. We show that Pab1 binds to the 5' UTR of several heat induced mRNAs *in vivo*, and that Pab1 releases these regions of mRNA during during stress. We can reconstitute the release of RNA *in vitro*. We show that translation of mRNAs bearing A-rich 5' UTRs are specifically repressed by Pab1 *in vitro*. However, phase-separated Pab1 has little effect on translation. Together these results support a model where Pab1 phase separation facilitates highly efficient translation of HSPs during stress. Chaperones disperse Pab1 phase-separated assemblies, restoring Pab1 to its original monomeric RNA-binding-competent state. Pab1 binds the 5' UTRs of HSP mRNA and represses further translation.

Chapter 5 summarizes many conclusions from chapters 2, 3, and 4. From these conclusions, future directions are suggested to further understand regulation of stress-induced phase separation and chaperone production. Together, the published and unpublished data

presented in this thesis demonstrate that protein aggregation is not strictly proteotoxic, but instead represents adaptive regulated assembly processes.

CHAPTER 1

INTRODUCTION

The effects of environmental temperature on biology can be seen in every day life. Examples range from the dramatic, like coral bleaching, to the benign, like the process of lagering beer - storing it at cooler temperatures resulting in a different flavor profile [2, 3]. But why bother studying how organisms sense and respond to environmental temperature? The summer of 2018 saw exceptional heat waves in both Europe and California, resulting in crops failures projected to cost billions of dollars [4, 5]. The biology of heat stress is also important in human disease and immunity. Fever promotes survival in patients with bacterial infection [6]. In the model organism *C. elegans*, the genes involved in the cellular response to heat also affect longevity [7]. Humans can detect temperature with special temperature-sensitive channels in neurons; however, it remains unclear how single cells, which lack neurons and temperature-sensitive channels, are able to detect temperature [8]. Decades of research have focused on understanding how temperature affects not just whole organisms, but also individual cells and even the biomolecules, like proteins, inside of cells. Previous work has identified genes that respond to temperature and help cells and organisms adapt to heat and other stresses [9]. The regulation of these genes is a topic of ongoing research.

This thesis explores the connection between an old scientific field, the heat shock response, and a new field, phase separation of biological molecules. In this introduction, I review important observations and findings about the heat shock response. Then I review the growing field of phase separation in biology - which has roots in the biology of heat stress. Finally, I provide a primer about a particular gene that is the focus of chapters 3 and 4, poly(A)-binding protein (PABP, PAB1 in *S. cerevisiae*). This gene serves as an example for how biology of the heat shock response is related to modern research on phase separation.

1.1 The heat shock response

The heat shock response was discovered in *Drosophila melanogaster* when an incubator was accidentally shifted up in temperature. The shift resulted in observable differences in the puffing pattern of the chromosomes of salivary glands of the organism, which were subsequently discovered to represent new RNA synthesis [1, 10]. This observation led to identification of the genes up-regulated by heat and other stresses, in addition to observations of other cellular changes.

1.1.1 Chaperones are produced during stress

The puffs in larval *D. melanogaster* salivary glands were eventually assigned to transcription of a small number of genes [11, 12]. The transcribed mRNAs were further translated into a small number of proteins known as heat shock proteins (HSPs) [13, 14]. So what is the function of these proteins, and how is their induction regulated?

An early hint as to the function of HSPs is that they localize to the nucleolus upon stress [15]. The nucleolus is thought to undergo catastrophic aggregation of unassembled ribosome components during stress; HSP70 tightly associates with the stressed nucleolus, but not with the unstressed nucleolus, and is released by ATP [15]. This led to a model wherein HSP70 resolubilizes aggregated proteins by binding and releasing individual proteins in an ATP-dependent cycle. Factors that could alter polypeptide folding, using information beyond that endcoded in their primary amino acid sequence, were referred to as chaperones [16, 17]. The definition of chaperone is mostly limited to a family of unrelated genes, including homologs of HSP70, HSP60, HSP40, small HSPs, and others. As chaperones, HSPs can work together to disaggregate and refold proteins: a set of 3 yeast genes, HSP104, HSP70, and HSP40 can return misfolded luciferase back to a functional form [18]. Additionally, these chaperones help to disperse protein aggregates that can form as a result of misfolding [19, 20]. The HSP genes are broadly conserved in the tree of life, and even in different cellular compartments

[17, 21, 22]. Chaperones are known to help cells adapt to new environments. For example, HSP104 is necessary for induced thermotolerance in yeast [23, 24, 25].

Transcription of the HSP genes is mediated by transcription factors. In bacteria transcription of the heat stress response genes is regulated by σ^{32} [26, 17]. In eukaryotes, transcription is regulated by a transcription factor called HSF1. HSF1 binds to a DNA element known as the heat shock element (HSE) matching the pattern "AGAAN" [17]. Broadly, HSF1 is activated upon trimerization followed by DNA binding. However, in yeast the protein is a constitutive trimer bound to DNA in the inactive state [17, 27, 28]. An early proposal for regulation of the heat shock response suggested that HSP70 could associate directly with the transcription factor HSF1 or σ^{32} [29]. It has been shown that HSP70 does directly bind HSF1, and dissociates during stress, leading to transcriptional activation [27, 28]. A model following from these observations posits that during stress HSP70 releases HSF1 by mass action as it engages new substrates - perhaps unassembled ribosomal proteins in the nucleolus. Activated HSF1 leads to production of a variety of HSP transcripts, including more HSP70. Once stress-induced HSP70 substrates are either mitigated, or the concentration of HSP70 rises to engage both substrate and HSF1, then transcription is again repressed. The genes under control of HSF1 are also induced during environmental stresses other than heat [30]. Moreover, there are additional transcription factors involved in the environmental stress response: MSN2 and MSN4. These transcription factors regulate a partially overlapping set of genes compared to HSF1, have different DNA binding sites, and are regulated by HSP70-independent phosphorylation pathways [31, 27, 28, 30].

1.1.2 Translation is globally attenuated during stress

One of the most striking changes to cells exposed to stress is the change in translation. In addition to dramatic production of stress genes, the production of proteins related to growth is repressed just as dramatically [32, 11, 13]. Bulk translation is reduced in stressed

cells, characterized by a phenomena known as polysome-collapse that results from reduced numbers of mRNAs being translated by multiple ribosomes [19, 33, 20, 14]. One mechanism known to cause reduced global translation is the phosphorylation of the translation initiation factor eIF2α, which ultimately blocks translation initiation [34]. However, there are examples of phosphorylation-independent repression of translation [35]. While bulk translation is reduced, production of HSPs continues robustly [11, 32, 14, 13, 36]. What about the HSP genes facilitates their continued translation? One feature of the mRNA of HSPs, which is important for continued translation is known: the 5' untranslated region (UTR) of the mRNA. Though the precise mechanism is unknown, initiation is thought to proceed via a cap-independent pathway - thus evading regulation by eIF2α - and aided by low secondary structure [37, 38, 39, 40, 41, 42, 43]. This is supported by the observation of efficient HSP initiation in stressed cells [44]. Moreover, translation competent lysate prepared from stressed cells can distinguish between HSP mRNAs and total cellular mRNA [32].

1.1.3 Protein assemblies form during stress

In addition to changes in gene expression during stress, structural changes occur in the cytoplasm. Initially observed in tomato leaves, micron-sized aggregates, or granules, not bounded by a membrane, appear in the stressed cytoplasm and are known as stress granules [45]. These structures contain specific proteins and mRNAs [46]. Immunofluorescence confirmed the formation of similar stress-induced structures in mammalian cells and further identified specific protein components and mRNA [47]. These structures were linked to changes in translation via phosphorylation of initiation factor eIF2α [47, 34, 48]. A role was established for both RNA binding domains and prion-related domains (PrD) in recruitment of specific proteins to these structures [47, 49]. Further research found that the set of proteins that localize to stress-induced structures varies with different stresses and in different organisms [50, 51, 52]. Even the material state of these structures varies from dynamic to largely

static between species [53, 54]. The relation between these cytoplasmic granules and changes in global translation was strengthened by chemical manipulation of translation. The drugs emetine and cyclohexamide, that stall translating ribosomes during elongation and freeze them on mRNA, were found to prevent formation of visible foci [53, 47, 55]. Puromycin, an inhibitor of translation initiation, stimulates focus formation. Together, these findings supported a model for granule formation where reduced translation initiation, resulting from eIF2α phosphorylation, results in ribosomes running off mRNA and leaves them unbound by protein [48, 56]. The mRNA is then bound, nonspecifically, by RNA binding proteins such as TIA-1 and TIAR, which themselves undergo aggregation mediated by their PrD [34, 48, 49]. While the exact function and biological benefit for the structures is uncertain, sequestration of non-translating mRNAs during stress has been proposed as a way to both protect the mRNAs and the shift translation over to the stress-induced HSP genes. While this model has been immensly useful, mounting evidence suggests that this model is incomplete - an alternative model is discussed in chapter 4.

1.2 Phase separation in biology

The observation of protein and RNA-rich aggregates during stress prompted the question, how do these structures form? Mounting evidence suggests that a driving force for formation of stress granules and other large structures is phase separation. Most people are familiar with phase separation in everyday life. Separation of oil and water in Italian dressing is a classic example. Phase separation describes a process at thermodynamic equilibrium describing how a mixture of molecules can spontaneously organize into separate compartments enriched or depleted for particular components. The thermodynamic properties of this process have been the topic of decades of research [57, 58]. The language and ideas from polymer physics and phase separation have been useful in understanding a variety of biological phenomena recently [59, 60].

While phase separation refers to an equilibrium process, some biological processes appear to be non-equilibrium processes, while still achieving sequestration or localization similar to phase separation [61, 20, 19]. A useful general term for large cellular structures that makes no assumption of the underlying physics is quinary structure [62, 63, 64, 61]. Such structures lack fixed stoichiometry, compared to quaternary interactions between proteins in a complex, and thus includes massive structures like long fibers, gels, and liquid phases. While some quinary assemblies are true phase separation processes and are thus spontaneously reversible, other assemblies are irreversible on biologically relevant timescales and require the activity of molecular chaperones to be dispersed.

1.2.1 Phase separation in diverse cellular processes

Non-membrane bound cellular compartments have been observed in a wide variety of cell biological processes. From many of these processes individual protein components of the compartments have been purified and found to autonomously form similar compartments by phase separation *in vitro*. The ability to phase separate has been related back to the *in vivo* processes providing new mechanisms for formation, localization, and cohesion of these compartments. Examples are briefly discussed below. This is not an exhaustive list; new examples will likely be published by the time of reading.

TIA-1 and TIAR along with Pabp were among the first proteins identified as components of stress granules [47]. Formation of assemblies during stress will be covered in greater detail in the next section. However, discussion of stress granules sets a useful framework for comparing other assembly processes. Both TIA-1 and TIAR are mammalian proteins that localize to the nucleus, but upon stress join cytoplasmic foci. Both proteins contain a glutamine-rich prion-like domain that enhances focus formation *in vivo*. Indeed, this glutamine-rich region is sufficient to drive autonomous phase separation *in vitro*; however, because the conditions used to reconstitute this activity are well outside of physiologically

relevant ranges, it is unclear if this domain does drive TIA-1 focus formation *in vivo* [65, 66]. Similarly, intrinsically disordered regions (IDRs) of several proteins were found to be sufficient to drive phase separation. Examples of proteins with these IDRs include Lsm4, Pub1, eIF4G, hnRNPA1, FUS. These proteins do localize to cellular foci under different conditions, so it is tempting to connect the two observations and conclude that each protein is undergoing phase separation *in vivo*. While this interpretation is possible, additional evidence is needed to directly connect the two phenomena and determine that a single domain is responsible for the activity. As a counterexample, the IDR of Pub1 is dispensable for phase separation *in vivo* [20].

A feature of IDRs is their composed; they are composed of a limited number of amino acids. Such regions are also referred to as low-complexity regions (LCRs); these regions are often associated with phase separation [65, 67, 68, 66]. However, these LCRs are often also associated with amyloid-like aggregation and prions; the term prion-like domain (PrD) has been used to describe and identify similar domains [49, 69, 70, 66]. A translation release factor, Sup35, is a well studied yeast protein capable of causing the [PSI+] amyloid-like prion, mediated by its LCR [71]. Thus amyloid-like prions and phase separation can both be mediated by LCRs. The Sup35 prion has been shown to increase organismal fitness in some circumstances; however, amyloids are often associated with cellular toxcicity and disease [72, 68]. This raises the question, what selective pressure shaped LCRs into amyloid-prone potentially toxic species? One hypothesis suggests these domains are primarily selected for their activity in phase separation, and amyloid fiber formation is a rare, unintended consequence of this activity [68]. In further support of this idea, Sup35 has been shown to undergo phase separation during starvation in yeast [73]. Phase separation can be reconstituted *in vitro* and supports cell survival during starvation compared to more amyloid-prone protein variants [73].

The human neurodegenerative disease amyotrophic lateral sclerosis (ALS) is character-

ized by fibrillar structures in the cytoplasm and is associated with mutation in the protein hnRNPA1. hnRNPA1 also localizes to stress granules, which are thought to be liquid-like, unlike fibrillar, possibly amyloid, structures. hnRNPA1 is capable of autonomously phase separating *in vitro*, mediated by both a low-complexity domain and RNA-binding domains [67, 66]. hnRNPA1 phase separation is reversible in response to temperature - a feature of equilibrium phase separation; mutations associated with ALS also promote formation of fibrillar structures that emerge from phase separated droplets [67]. These data support a proposed mechanism for ALS pathology wherein mutations in hNRNPA1 promote fiber formation from endogenous phase separated structures; moreover, these data also make a clear distinction between the process of phase separation and secondary fiber formation [67].

Amyotrophic lateral sclerosis (ALS) is also associated with mutations in a protein called FUS, which is involved in RNA transcription [68]. The low-complexity domain of FUS has been reconstituted to form amyloid-like structures [66]. FUS can also phase separate into a liquid-like phase, and fibrous structures can emerge from the liquid droplet; formation of fibers is enhanced by disease related mutations [68, 74].

RNA is capable of autonomously phase separating. Both poly(CAG) RNA and poly(G) RNA have been shown to undergo spontaneous self-association and phase separtion. These patterns fit a basic requirement for phase separation: the ability to make weak multivalent interactions. Phase separation is possible both *in vitro* and *in vivo* [75]. Moreover, phase separation affects gene regulation and requires a critical number of repeats - and this number roughly corresponds to the minimum number of repeats seen in nucleotide repeat expansion disorders such as Huntington's and amyotrophic lateral sclerosis (ALS) [75].

When the single-cell of a fertilized *C. elegans* embryo begins to divide, diffuse structures rich in RNA and proteins become polarized and accumulate in one half of the cell. After division, one daughter cell contains the structures - known as a P-granule - and will develop into germline cells in the mature organism, while the other cell will develop into somatic

tissue. P-granules are round, not membrane-bound, can fuse, drip, wet, and behave as a liquid-like phase within the cell [76]. A P-granule protein, Laf-1, has been shown to phase separate *in vitro*, displaying similar liquid-like properties to P-granules. Laf-1 droplets interact with RNA; phase separation is mediated by a low-complexity domain of Arg-Gly repeats; and Laf-1 knock down results in dispersal of P-granules *in vivo* [77]. Similar results were found in mammalian nuage for protein Ddx4 [78]. Together these data suggest that P-granules form by a liquid-liquid phase separation *in vivo* driven by specific proteins and specific domain interactions.

Inside the nucleus, ribosome assembly occurs in a subcompartment, the nucleolus; this dense structure appears dense, round, and not bound by membranes. The nucleolus of *Xenopus laevis* oocytes, germinal vesicles (GV), were found to fuse and flow with liquid-like properties - and even to contain smaller droplet-shaped phases [79]. While the nucleolus *in vivo* is dynamic and contains many different proteins and RNAs, many of the liquid-like properties of the compartment, even existence of liquid-like immiscible subcompartments, can be reconstituted with phase separating nucleolar proteins Npm1 and Fib1 *in vitro* [80]. Interestingly, a protein related to Npm1 called nucleoplasmin or Npm2 was the first protein described as a molecular chaperone, for its ability to support *in vitro* assembly of nucleosomes on DNA [16, 81, 82]. Plausibly, the chaperone activity of Npm2 could be mediated phase separation, creating a compartment of different solvent quality around DNA, which reduces irreversible protein aggregation during nucleosome assembly.

During cell division, the sister chromatids must be divided. This is achieved by cytoskeletal structures called microtubules, which are organized at opposite ends of the dividing cells. The microtubules are organized by structures known as centrosomes [83]. A core component of centrosome assembly is SPD-5 in *C. elegans* [83]. It has been found that SPD-5 autonomously phase separates [84]. Droplets of SPD-5 can recruit other microtubule organizing machinery, ultimately allowing reconstitution of spherical assemblies that can catalyze

microtubule polymerization, which resemble cellular structures [83].

The fungus *Ashbya gossypii* is polynucleated - containing many asynchronously dividing nuclei in a single cytoplasm. Nuclear division is controlled by accumulation of proteins known as cyclins. However, if cyclins freely diffuse in the cytoplasm, how can nuclei independently divide? A solution to this question is the observation that CLN3, a cyclin mRNA, is not evenly dispersed in the cytoplasm, but localized around individual nuclei in association with Whi3, a protein capable of phase separating [85]. The poly(Q) low-complexity domain of Whi3 is necessary for localization around individual nuclei; deletion of Whi3 results in diffuse CLN3 mRNA and synchrony of nuclear division [85, 86]. Further work has shown that the mRNA of genes including CLN3 and BNI1 controls the specificity of contents of Whi3 phases; this control is related to mRNA self-association and secondary structure [87, 88].

An enzyme called RuBisCO (Ribulose-1,5-bisphosphate carboxylase/oxygenase) is involved in photosynthesis and fixing CO_2 into glucose. RuBisCO is concentrated in non-membrane-bound compartments known as pyrenoids, which have recently been hypothesized to be liquid-like phase compartments [89]. It has recently been reported that RuBisCO and a repeat protein, EPYC1, are sufficient to form a functional pyrenoid-like phase *in vitro* [90]. These data suggest that the physiological pyrenoid is indeed a phase separated compartment, and phase separation is one way biological systems achieve high concentration of enzymes.

1.2.2 Phase separation during stress

Poly(U)-binding protein (Pub1 in *S. cerevisiae*) colocalizes with stress-induced foci during both heat stress and starvation. Pub1 is capable of autonomously phase separating *in vitro* in response to both heat and increased pH [20]. Interestingly, heat induced assemblies appear to be spontaneously irreversible, are solid-like, and require the activity of chaperones to be cleared; however starvation induced assemblies are spontaneously reversible and are liquid-like *in vivo* [20]. Phase separation of Pub1 is driven by electrostatic interactions and does

not require its intrinsically disordered region (IDR) [20].

During starvation, translation initiation factor eIF2B has been found to form filamentous structures, stimulated by cytoplasmic acidification [91]. Preventing filament formation results in increased bulk translation, suggesting that filament formation reduces activity of eIF2B and represses bulk translation. Blocking filament formation also reduces survival of yeast during long term starvation, though the precise mechanism is unclear [91].

Many proteins involved in glucose and nitrogen sensing pathways have been observed to form filamentous structures in the cytoplasm during starvation [92]. Among them is PFK1, a glycolytic enzyme with historic and recent evidence suggesting that the protein is capable of autonomous filament assembly [93, 94]. Another example of a filament forming enzyme is Gln1, involved in glutamine synthesis. Gln1 was found to join filamentous structures during starvation in yeast. Formation is driven by cytoplasmic acidification [95]. Assembly of Gln1 inactivates its enzymatic properties, and the protein is capable of autonomously forming high-order assemblies [95].

TOR (target of rapamycin) is a kinase that is involved in regulating cell growth [96]. TOR is part of a signaling complex with other proteins including Kog1. During heat stress, Kog1 forms cytoplasmic foci and coimmunoprecipitates with Pab1; coimmunoprecipitation is dependent on stress, but not sensitive to cycloheximide - circumstantial evidence of Kog1 and Pab1 coexisting in large stress-induced assemblies that are invisible by microscopy [97]. It is not known if components of the TORC1 complex are capable of protein autonomous phase separation [60]. Sequestration is known to regulate TOR signaling [97].

1.2.3 Chaperones disperse stress-induced foci

In *S. cerevisiae* it has been shown that dispersal of stress-induced assemblies is supported by the activity of chaperones. Deleting HSP104, a AAA-ATPase, results in slower dispersal of foci marked by Pabp and of foci marked by a model misfolded protein; dispersal of

sedimentable species is also slowed [19, 98]. Similarly, inhibition of an HSP70, SSA1, disrupts the dispersal of Pabp marked foci. Inhibition of HSP104 using a small molecule slows foci dispersal in heat stressed cells, but not starved cells, indicating some difference in the nature of these structures [20]. It has been shown that HSP104, HSP70 and HSP40 can reactivate a model aggregated protein substrate, though the precise relation between the model substrate and stress-induced structures is unclear [18].

1.3 Poly(A)-binding protein

A defining feature of eukaryotes compared to prokaryotes is a structure added to the 3' end of their mRNA: a non-genetically encoded poly(A)-tail [99]. These structures are tightly bound by a particular protein factor, poly(A)-binding protein (Pabp) [100, 101, 102, 103]. This protein is an abundant highly conserved eukaryotic RNA binding protein that is involved with a wide variety of cellular processes, including mRNA processing and export, mRNA stability, and mRNA translation [104]. PABP is an essential gene in yeast. While it is involved in many biological processes, many of these activities are dispensable, and the essential function is not known. However, evidence suggests that the essential function is within the nucleus [105, 106].

1.3.1 Pabp is best known for binding poly(A)-tails

Poly(A)-binding protein was identified as a factor that tightly binds to poly(A)-tails. Shortening of the poly(A)-tail is a required step for 5' to 3' mRNA decay. Pabp inhibits the activity of the principle deadenylase in yeast [107]. In this way Pabp is thought to prolong the life of mRNAs by protecting the tail, until it is ultimately digested to some critical length. Poly(A)-binding protein also plays a role in the second step of 5' to 3' mRNA decay: decapping. Removal of the 5' cap is inhibited by Pabp both directly, and indirectly through Pabp binding of eIF4G [108, 109]. Pabp is also thought to regulate the addition of poly(A)-

tails in the nucleus. This contrasts with the cytoplasm, where decay occurs. However, the functions of nuclear and cytoplasmic Pabp appear to be distinct [104, 105, 103]. Pabp is also involved in export of mature mRNAs from the nucleus, including the HSP genes during stress [110].

When bound to poly(A)-tails, Pabp also acts as a translation factor, stimulating the production of protein from mRNA. Pabp interacts with eIF4G. This interaction is thought to bring the 3' poly(A)-tail in close proximity with the 5' cap and promotes efficient translation, possibly by promoting recycling of the 40S ribosome [111, 112, 113]. In this capacity Pabp is included as a component of the 43S pre-initiation complex, along with the 40S ribosome, and a variety of other translation initiation factors [56]. In a model of stress granule formation driven by stalled initiation complexes, Pabp is ultimately recruited to stress granules via its association with mRNA poly(A)-tails and eIF4G [56].

1.3.2 Structure of Pabp is conserved

The structure of cytoplasmic Pabp is highly conserved in eukaryotes. Pabp is composed of 4 tandem RNA recognition motif domains (RRMs), followed by a proline-rich linker domain (P domain), and finally a C-terminal peptide binding domain [100, 104]. Polypeptides with similar architecture can be found in fungus, animals, and plants [104, 114]. The protein binds with full affinity, 5 nM, to poly(A) tracts of length 12 or greater [105, 100]. Pabp protects an RNA footprint of 25 bases; this feature distinguishes cytoplasmic from nuclear Pabp, since nuclear Pabp does not appear to protect poly(A) RNA in the same repeated 25 nt pattern [115, 116, 103]. The binding specificity for poly(A) comes from the first 2 RRMs, but each individual RRM has different binding specificity [105, 117]. The C-terminal domain is known to bind short peptides, a 12 amino acid motif known as PAM2, and plays a role in recruiting polyadenylation factors [118]. Pabp is thought to self interact, resulting in a circular conformation in the absence of RNA [119]. This self-interaction is important for

mRNA deadenylation and mediated by an interaction between RRM1 and the P domain; deletion of RRM3 enhances circularization and reduces binding to poly(A) [119]. Finally, human Pabp (PabpC1), is known to be targeted by a number of viral proteases, particularly in the P domain, possibly modifying host translation during infection [120, 121].

1.3.3 Pabp is a repressor of translation

An interesting conserved feature of the PABP gene is an A-rich tract of DNA just upstream of the start codon in the 5' untranslated region (UTR) [103, 101, 122, 123, 124]. Soon after discovery, it was suggested and later confirmed that Pabp does indeed bind this region of its own mRNA [103, 125, 126]. When bound to this region, Pabp acts to repress translation of its own transcript, in contrast to Pabp bound to the 3' poly(A)-tail, where it enhances translation [126, 125, 127, 128, 129]. This repression is enhanced by proximity to the 5' end. However, proximity is not required, suggesting that Pabp can block a scanning initiation complex [129]. Blocking the ribosome is dependent on the P domain and C-terminal domain of Pabp; moreover synthetically localizing just the P domain and C-domain to the 5' end of a transcript can block translation *in vivo* [129]. Recently, CLIP-seq results have confirmed that Pabp can bind to mRNA for other genes in a similar way and repress translation *in vivo* [130]. There is at least one conflicting report of Pabp binding to the 5' UTR and recruiting eIF4G to stimulate translation in a cap-independent manner; how to reconcile these two activities is unclear [131].

1.3.4 Pabp joins stress-induced assemblies

Pabp was one of the first proteins identified as part of large stress-induced structures known as stress granules during arsenite stress in mammalian cells [47]. Pabp is often used as a defining marker for stress granules in other species, including *S. cerevisiae* [132, 133, 55, 19, 64, 61]. A variety of stresses result in Pabp marked focus formation, including starvation, heat, ethanol,

and vanillin [134, 133, 132]. Pabp was also shown to join biochemically sedimentable species during stress [50, 19, 64]. Pabp localization to these structures was presumed to be a result of association with stalled initiation complexes [19, 56, 51, 135]. However, recent evidence has challenged this assumption [61, 136].

CHAPTER 2

IDENTIFICATION OF STRESS ASSEMBLING PROTEINS (WALLACE ET AL. 2015)

The following chapter appears as published work from 2015 [64]. My specific contributions to this work were generating a number of yeast strains with fluorescent proteins tagged to their C-terminus. These strains were used to verify a number of results from proteomic analysis. In particular, these strains were used to confirm that "superaggregator" proteins indeed form massive structures during mild stresses, which don't stimulate stress granule formation. Additionally, these strains confirmed formation of stress-induced assemblies in the nucleus and nucleolus.

2.1 Summary

Reversible, Specific, Active Aggregates of Endogenous Proteins Assemble upon Heat Stress

Authors:

Edward W.J. Wallace, Jamie L. Kear-Scott, Evgeny V. Pilipenko, Michael H. Schwartz, Pawel R. Laskowski, Alexandra E. Rojek, Christopher D. Katanski, Joshua A. Riback, Michael F. Dion, Alexander Franks, Edo M. Airoldi, Tao Pan, Bogdan A. Budnik, D. Allan Drummond

Heat causes protein misfolding and aggregation and, in eukaryotic cells, triggers aggregation of proteins and RNA into stress granules. We have carried out extensive proteomic studies to quantify heat-triggered aggregation and subsequent disaggregation in budding yeast, identifying >170 endogenous proteins aggregating within minutes of heat shock in multiple subcellular compartments. We demonstrate that these aggregated proteins are not

misfolded and destined for degradation. Stable-isotope labeling reveals that even severely aggregated endogenous proteins are disaggregated without degradation during recovery from shock, contrasting with the rapid degradation observed for many exogenous thermolabile proteins. Although aggregation likely inactivates many cellular proteins, in the case of a heterotrimeric aminoacyl-tRNA synthetase complex, the aggregated proteins remain active with unaltered fidelity. We propose that most heat-induced aggregation of mature proteins reflects the operation of an adaptive, autoregulatory process of functionally significant aggregate assembly and disassembly that aids cellular adaptation to thermal stress.

2.2 Introduction

Following heat shock—a rapid increase in temperature to stressful but non-lethal levels—cells accumulate protein aggregates, decelerate protein synthesis, and mount a transcriptional program called the heat-shock response. Upregulated transcripts encode so-called heat-shock proteins, of which many are molecular chaperones. The standard interpretation of these events is that heat causes endogenous (species-native) proteins to misfold into aggregation-prone species whose toxicity is mitigated and reversed by chaperones [137, 138, 139, 140]. Misfolding here refers to the deleterious loss of—or failure to attain— natively folded protein structure, sometimes by adopting stable non-native conformations.

Newly synthesized proteins are particularly susceptible to heat-induced misfolding and aggregation and appear to be the major triggers of the heat-shock response, as well as the main beneficiaries of its induction [141, 139]. In agreement, heat triggers rapid degradation of newly synthesized proteins, but not of bulk cellular protein [142].

Mature, folded proteins also aggregate in response to heat shock, forming protein/poly(A)+-RNA structures called heat-shock granules (HSGs). Discovered in plants [45], HSGs form upon robust heat shock in a range of eukaryotes, including budding yeast, trypanosome, insect, and mammalian cells [50, 143, 19, 35]. HSGs are functionally defined by their compo-

nents, notably poly(A)-binding protein and eukaryotic initiation factor 4G; some components are common to RNA/protein granules formed during other stresses [52, 144, 34]. The mechanism(s) of HSG formation remain unclear.

Many studies demonstrate aggregation and degradation of exogenous (heterologous or other non-species-native) proteins [19, 145, 146]. Colocalization of exogenous aggregated proteins and HSGs has been interpreted as signaling the presence of endogenous misfolded proteins in HSGs [19]. However, the identities and folding states of HSG-associated proteins are largely unknown.

When cells return to lower temperatures, HSG dissolution is promoted by the disaggregase Hsp104 and the chaperone Hsp70 [19], which also disaggregate misfolded proteins *in vitro* [18]. It is unknown what fraction of disaggregated proteins are degraded *in vivo*, although evidence that stress granules are degraded by autophagy [147] suggests that degradation might be the dominant fate of stress-induced aggregates. Here, using the model eukaryote budding yeast (*Saccharomyces cerevisiae*), we report the results of experiments aimed at answering many of these fundamental questions. Which endogenous proteins aggregate during heat shock, and how do proteins differ in their propensity to aggregate? What is the relationship between protein aggregation and the formation of granules and other large subcellular foci? How does heat affect the function and fidelity of proteins determined to aggregate in response to heat shock *in vivo* ? And what are the fates of endogenous aggregated proteins after heat shock?

2.3 Results

2.3.1 Aggregation Profiling Identifies Many Thermally Sensitive Proteins

We quantified aggregation of proteins into high-molecular-weight particles by biochemical separation into supernatant and pellet fractions using ultracentrifugation, stable-isotope

labeling, and liquid chromatography coupled to tandem mass spectrometry (LC-MS/MS) (Figure 2.1A)

With these data, we estimated the proportion of each protein in the supernatant (pSup) using a statistical method that controls for differences in fraction mixing and inter-experiment variability (Experimental Procedures and Figure 2.1). Here and throughout, we refer to pelletable species of proteins that are soluble before heat shock as "aggregates," without prejudging whether the particles result from misfolding, formation of protein/RNA granules, or other homogeneous or heterogeneous oligomerization processes.

We quantified protein aggregation in cells transferred from 30°C to 46°C for 2, 4, and 8 min and to 37°C and 42°C for 8 min 2.1 (See online publication [64] table S1. During these treatments, which are shorter than those typically used to study HSG formation [50, 19](Supplemental Experimental Procedures), genes upregulated in the transcriptional heat-shock response show no significant change in protein levels (2.9A). By contrast, aggregation is rapid and widespread and increases with time and temperature (2.1B and C).

2.3.2 Heat Triggers Rapid and Specific Protein Aggregation

In the 46°C time course, 982 proteins are detected with at least two unique peptides at all time points ("well-detected," 73% of the proteome by mass, 17% of verified open reading frames [148], upon which we focus. Most cellular proteins remain in the supernatant throughout (2.1B), and cytosolic and ribosomal proteins are the most enriched gene ontology (GO) terms describing these proteins (2.10). Proteins found in the pellet in all conditions are primarily membrane associated (2.10). Heat triggers the aggregation of a large group of proteins (177 well-detected proteins), classified by consistent and substantial movement from the supernatant in unheated cells to the pellet after a shift to 46°C (see online publication [64] table S3 S3 and Experimental Procedures). Only four proteins moved from pellet to supernatant in the same interval (see online publication [64] table S4).

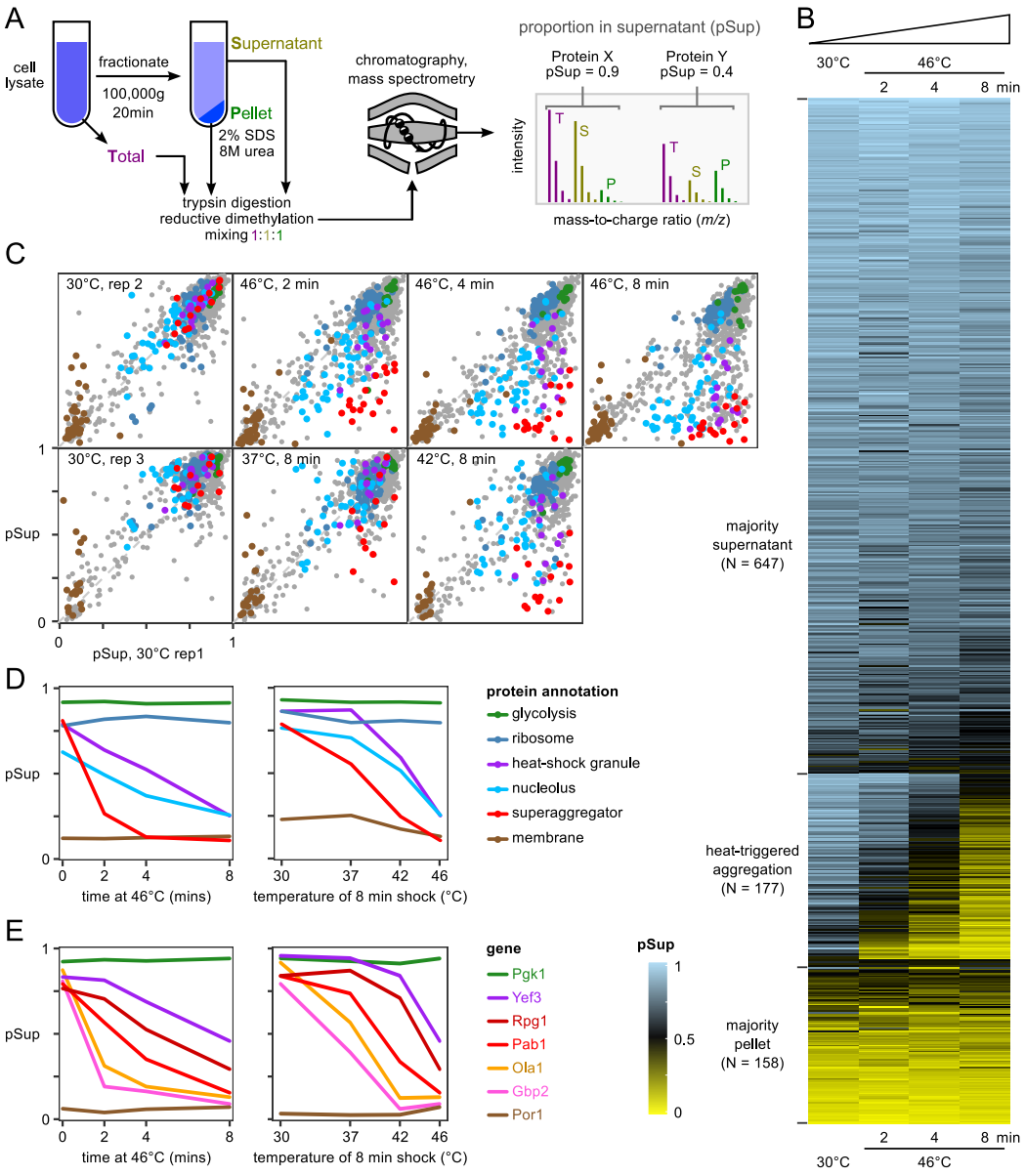

Figure 2.1: **Proteome-wide Aggregation Profiling**
Continued on the next page.

Figure 2.1: 2.1 continued. (A) Aggregation profiling by isotope labeling and mass spectrometry yields estimates of the proportion of each protein in the supernatant (pSup) before and after thermal stress. (B) pSup values in the 46°C time course for all well-detected proteins show proteins consistently found in the supernatant (top), consistently found in the pellet (bottom), and transitioning from supernatant to pellet during the 8 min heat shock (middle, see text). (C) Progressive protein aggregation quantified by proportion in the supernatant fraction (pSup) during a 46°C treatment compared to unshocked replicates (top) and with increasing 8 min shock temperature (bottom; see online publication [64] table S1 for design). Protein annotations in C and D are the same; superaggregators (see text) include five nucleolar proteins. (D) Behavior of proteins in various categories (cf. C) as a function of temperature, for 8 min, and time at 46°C. (E) Individual proteins aggregate at different rates in response to heat; more are shown in 2.11A. In D and E, 30°C rep 1 is shown in the time course plots, the same biological sample as the 46°C data; 30°C rep 3 is shown in the temperature course plots, the same biological sample as 37°C and 42°C, 8 min, data.

Of 18 HSG components identified in the literature (see online publication [64] table S2), we detected all but one (Ngr1). Twelve of these meet our criteria for heat-triggered aggregation, including poly(A)-binding protein (Pab1), eIF4G/Tif4631, and eIF3, where our data show aggregation of all five stably complexed eIF3 subunits (Nip1/Rpg1/Prt1, reported previously [50], and Tif34/Tif35 reported here) and eukaryotic release factors eRF1/Sup45 and eRF3/ Sup35 (2.11A). Of the remaining five, Whi3 is not well detected but aggregates, and three proteins (Dhh1, eIF4G2/ Tif4632, and small-subunit ribosomal protein Rps30A/B) do not clearly aggregate. The behavior of Rps30A/B is consistent with the lack of aggregation in 82 other well-detected ribosomal gene products from both subunits and with in situ hybridization against ribosomal RNA [19]. Our experimental conditions therefore allow us to quantify biochemically the aggregation of proteins reported to form HSGs by fluorescence microscopy.

In our data, 17 proteins aggregate more than any previously reported HSG component after 2 min heat shock at 46°C; we dub these "superaggregators" (see online publication [64] table S3 and Experimental Procedures). For example, the nuclear protein Ett1 plunges from a supernatant proportion of 0.93 to 0.15 after 2 min at 46C, while the mRNA-binding protein Gbp2 drops from 0.8 to 0.25. In the same interval, HSG-forming proteins such as

Pab1 and eIF3 remain mostly soluble (2.1C and 2.11). Notably, most super-aggregators also show clear aggregation after 8 min at 37°C and 42°C (2.1 C and D). At these temperatures and times, Pab1-marked HSGs do not form [19].

GO terms enriched in heat-aggregating proteins include the molecular functions RNA binding (exemplified by poly(A)-binding protein Pab1 along with Npl3, Pub1, and Gbp2) and RNA helicase activity (seven proteins, including Ded1 and Dbp2/3) (2.10). Enriched cellular components include cytosolic stress granules, polysomes, and notably the nucleolus (16 nucleolar proteins).

Six aminoacyl-tRNA-synthetases aggregate, including the yeast multisynthetase complex composed of methionyl- and glutamyl-tRNA synthetases Mes1 and Gus1 bound together by the aminoacylation cofactor Arc1. We return to this complex later.

Molecular chaperones, which colocalize with HSGs, largely remain soluble in our data, suggesting a biochemical distinction between aggregation and recruitment to aggregates. However, notable exceptions exist, including the ribosome-associated chaperone complex (RAC) discussed later. The small heat-shock proteins Hsp26 and Hsp42, despite poor detection in our dataset, partition into the pellet upon heat shock (2.11A).

2.3.3 Endogenous Proteins Aggregate in Distinct Compartments

To determine the subcellular location and morphology of aggregates for MS-identified aggregators, we imaged yeast strains engineered with fluorescent C-terminally tagged proteins at their native chromosomal loci. We tagged select proteins with mRuby2, a red fluorescent protein, and tagged the HSG marker Pab1 with Clover, a green fluorescent protein [149], mating these strains to form dual-tagged diploids (2.2). Fusions of the non-aggregating glycolytic enzyme Pgk1 stay cytosolic and diffuse when heat shocked, and diploids bearing Pab1 tagged with both fluorophores (no untagged Pab1 present) form cytosolic foci containing both colored tags (2.2B), indicating that these fluorophores neither cause nor prevent

aggregation.

Proteins detected to aggregate by mass spectrometry after an 8 min 46°C heat shock also form foci (2.2 B and C). Mes1 and Gus1, components of the multisynthetase complex, form cytosolic foci colocalized with Pab1. Arc1, the third multi-synthetase component, likewise forms fluorescent foci co-localized with Gus1 (2.2C). Ola1, a superaggregating cytosolic protein previously implicated in translation termination ([150], also forms foci colocalized with Pab1. These four proteins are all thus bona fide heat-shock granule components.

Some heat-aggregating proteins form nuclear foci. Gbp2, a nuclear poly(A)-RNA-binding protein involved in nuclear-cytosolic mRNA transport, forms sub-nuclear granules during heat shock (2.2B). Fpr3, a nucleolar component adopting the diagnostic nucleolar crescent shape under non-shock conditions, becomes increasingly granular within the nucleolus during heat shock (2.2B). Ett1, a nuclear protein and the most rapidly aggregating protein detected by mass spectrometry, forms nuclear foci during heat shock (2.2B) which colocalized with Gar1, a nucleolar protein that shows no heat-triggered aggregation by MS (2.12A). These results suggest that Ett1 aggregates in or near the nucleolus upon heat shock, possibly consistent with localization to the intranuclear quality-control compartment (INQ) [151]. We often observe multiple Ett1 foci per cell (2.12C).

2.3.4 Translation Inhibition Impedes Granule Formation but Does Not Prevent Stress-Triggered Protein Aggregation

Our data indicate clear distinctions between the heat-triggered *in vivo* formation of fluorescent foci and of submicroscopic, biochemically detectable aggregates. After milder shocks, several proteins producing pelletable aggregates did not form foci, such as Ett1 (at 37°C) and Pab1 (at 42°C) (2.12B and C). Also, Hsp104 forms foci colocalized with Pab1 upon heat shock ([19] while remaining highly soluble (2.11A), showing its recruitment to, but not stable association with, substrates within heat-shock granules.

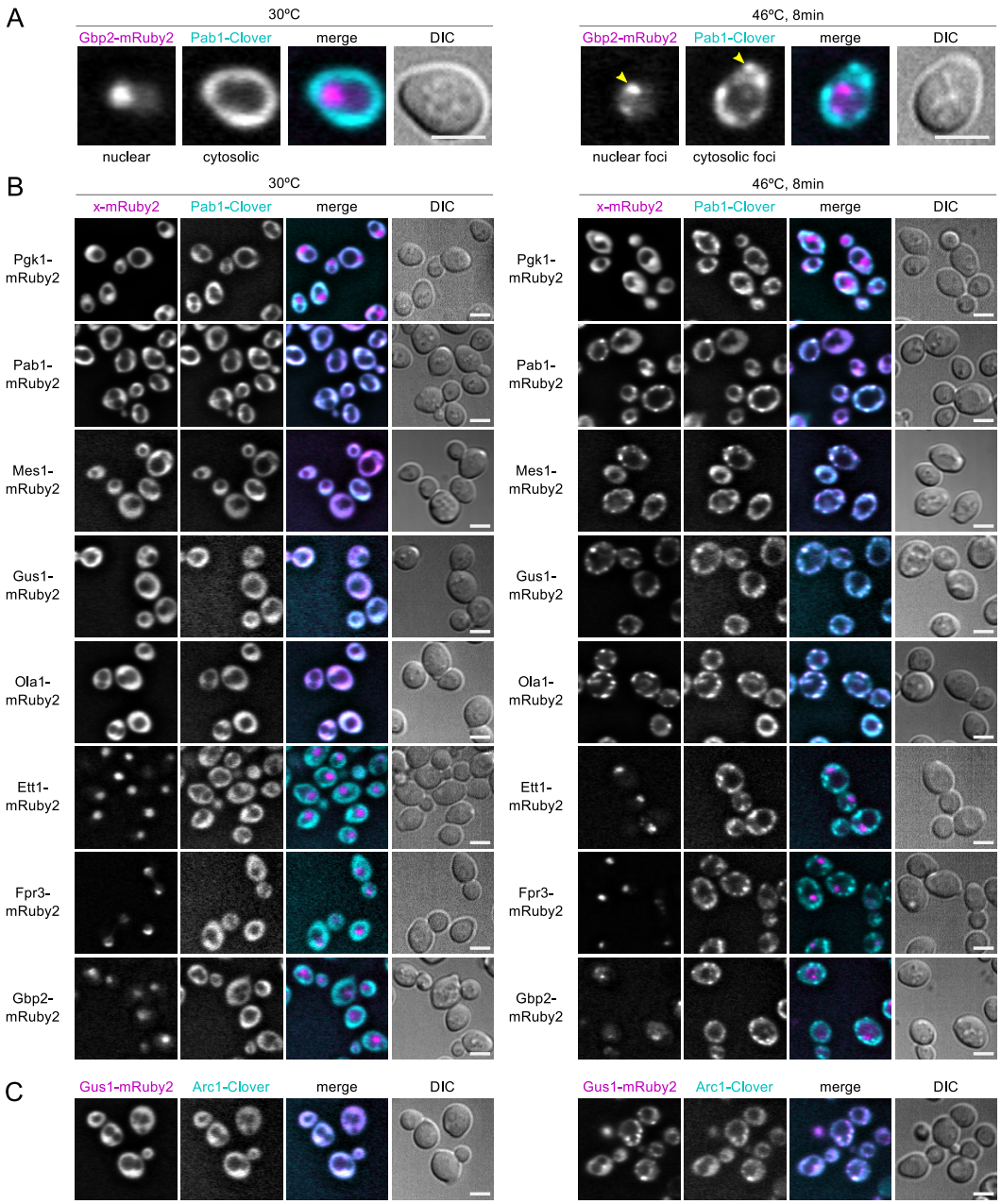

Figure 2.2: **Live-Cell Microscopy Identifies Heat-Aggregating Proteins Forming Cytosolic or Nuclear Granules**
Continued on the next page.

Figure 2.2: 2.2 continued. Diploid strains containing the HSG component Pab1 tagged with the green fluorescent protein (FP) Clover (cyan in merged images) and test proteins tagged with the red FP mRuby2 (magenta in merge) were imaged at 30°C and after 8 min heat shock at 46°C. Scale bar, 5μm. (A) Heat-induced nuclear and cytosolic aggregation of Gbp2-mRuby2 and Pab1-Clover, respectively. (B) Non-aggregating Pgk1-mRuby2 remains diffuse during heat shock, while Pab1-Clover forms HSGs. Pab1-Clover and Pab1-mRuby2 form colocalized foci during heat shock. Fusions of MS-identified heat-aggregating proteins form foci that colocalize with Pab1 during heat shock (Mes1, Gus1, Ola1) or form sub-nuclear foci (Ett1, Fpr3, Gbp2). (C) The aminoacylation cofactor in the multisynthetase complex, Arc1, forms heat-induced foci colocalized with Gus1.

A series of studies has demonstrated the preferential retention of cytosolic heat-induced protein aggregates by mother cells during budding [152, 153, 154]; these cytosolic Hsp104 foci are heat-shock granules [154] observe that Hsp104 focus formation during heat shock is blocked by the translation elongation inhibitor cycloheximide (CHX) and conclude that heat-induced aggregation requires active translation. By contrast, [155] observe that CHX blocks Hsp104 foci during arsenite stress, but not during heat shock. We wondered whether biochemical detection might shed useful light on the relationship between aggregation, heat-shock granules, and translation.

To study these phenomena, we treated cells with 100 mg/ml CHX for 5 min and then subjected them to either a 42°C heat shock for 30 min as in [154] or to a 46°C heat shock for 8 min. This dose of CHX attenuates formation of visible fluorescent foci by tagged Pab1 (2.3A and B). However, the cytosolic heat aggregators Yef3 and Ola1 still form some fluorescent foci in the presence of CHX (2.3A and B). Thus, translation inhibition attenuates the heat-triggered formation of foci for some, but not all, cytosolic proteins.

We also measured protein aggregation biochemically during identical heat shocks by analyzing 100,000 g pelleting particles. Pab1, Ssz1, and Yef3 all enter the 100,000 g pellet after a 46°C, 10 min heat shock, with reduced aggregation after a 42°C, 30 min shock. Surprisingly, biochemical aggregation was unaffected by CHX (2.3C).

The data are consistent with a model of multi-stage aggregation in which initial forma-

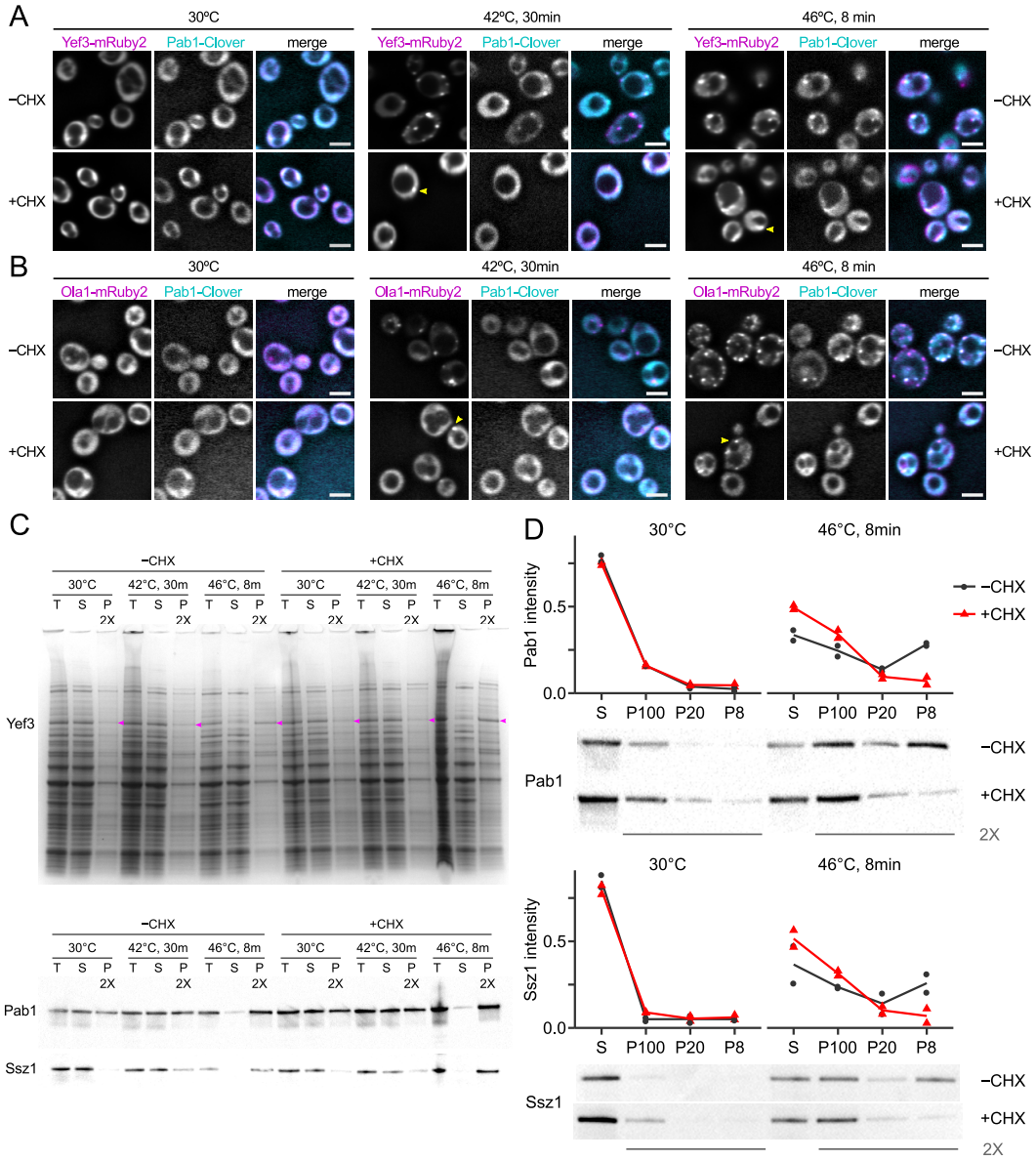

Figure 2.3: **Heat-Triggered Protein Aggregation Does Not Require Ongoing Translation** (A) Cycloheximide (CHX; 100 mg/ml) blocks formation of heat-triggered cytosolic foci by fluorescently tagged Pab1 and attenuates formation of foci by Yef3. Scale bars, 5μm; arrows indicate foci. (B) Ola1 forms fluorescent foci in response to heat shock in the presence of CHX. (C) Pab1, Ssz1, and Yef3 (arrows on gel) are found in the 100,000 g supernatant (S) in lysate from unshocked cells but enter the 100,000 g pellet (P) after heat shock independent of CHX treatment. Coomassie-stained protein gel and western blots against native proteins are shown. T, total protein. (D) CHX inhibits Pab1 and Ssz1 entry into large aggregates, but not into small aggregates. Cell lysate was progressively fractionated at 8,000 g (pellet, P8), 20,000 g (P20), then 100,000 g (P100), and pellets and residual supernatant (S) were western blotted against Pab1 and Ssz1; intensity as proportion of total was quantified in two biological replicates (2.13), and a representative blot is shown.

tion of biochemical aggregates is followed by CHX-sensitive collection of these aggregates into larger bodies visible as foci. To test this model, we progressively fractionated cell lysate first at 8,000 g X 3 min (pellet, P8, largest aggregates), then fractionated the supernatant at 20,000 g X 5 min (pellet, P20, smaller aggregates), and then fractionated the second supernatant at 100,000 g X 20 min (pellet, P100, smallest aggregates), collecting residual 100,000 g supernatant (S). Western blotting against native Pab1 showed that 75% of Pab1 remained in the supernatant from unshocked cells regardless of CHX treatment (2.3D and 2.13). In cells heat shocked for 8 min at 46°C, most Pab1 entered P8 and P100; treatment with CHX blocked formation of P8 particles and increased levels of P100 particles, as predicted (2.3D). Ssz1 shows the same pattern (2.3D), as does Yef3 (total protein gel, 2.13).

These results support a CHX-blockable secondary assembly of aggregates into cytosolic foci, which does not affect heat-induced formation of smaller aggregates.

2.3.5 Translation-Related Proteins Aggregate in Coherent Groups

The heat-triggered aggregation of eIF3 and the multisynthetase complex prompted us to examine aggregation of other protein complexes involved in translation. Translation factors partition into heat aggregators and non-aggregators (2.4A). Assuming that aggregated translation factors are inactive, the observed aggregation of eIF2B, eIF4B/G, eEF3, or eRF1 would be individually sufficient to substantially reduce net protein synthesis [156].

Each stable protein complex falls into a single category: of the components of eukaryotic elongation factor 1 (eEF1), all elements of the stable subcomplex eEF1B heat aggregate, but Tef1/eEF1a does not (2.4A). All components of eIF2 have similar high pSup across conditions, while all components of eIF3 heat aggregate with similar kinetics (2.4B). Aggregation of the multisynthetase complex is particularly synchronous (2.4B).

Complexes with shared interaction partners show distinct aggregation patterns: for example, the nascent-polypeptide-associated complex (NAC; Egd1/Egd2) and the ribosome-

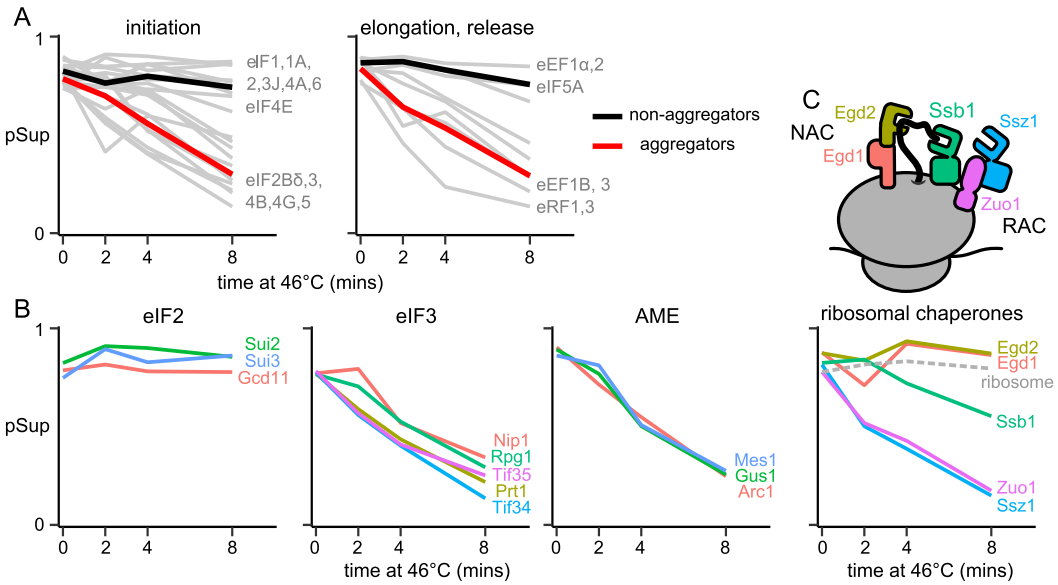

Figure 2.4: **Stable Translation-Related Complexes Aggregate Coherently** Proportion in supernatant (pSup) is plotted against time of heat shock at 46°C; each panel shows one or more complexes and each line a protein component. (A) pSup of all well-detected translation factors. Mean is shown for aggregators and non-aggregators in each plot. (B) Aggregation of translation initiation factors 2 and 3 and of the multi-tRNA-synthetase complex. (C) Aggregation of chaperone complexes involved in co-translational folding.

associated chaperone complex (RAC; Ssz1/Zuo1), along with Ssb1/2, bind the ribosome near the nascent peptide exit tunnel [157]. Both detected NAC components remain soluble across conditions, as do ribosomes; in contrast, RAC components aggregate swiftly and in lockstep (2.4C). More broadly, proteins associated in annotated complexes ([158] have more similar pSup trajectories than expected by chance (2.14).

2.3.6 The Yeast Multisynthetase Complex Forms Active Heat-Triggered Aggregates in vitro

The tight correlation of the three yeast multisynthetase components during heat-triggered aggregation (2.4) and their aggregation into the same subcellular location (2.2) prompted us to ask how heat affects this complex and its activity in isolation. The complex, dubbed AME, is a heterotrimer formed by the aminoacylation cofactor Arc1 (A), methionyl-tRNA synthetase Mes1 (M), and glutamyl-tRNA synthetase Gus1 (E), which interact through eukaryote-specific N-terminal domains in each protein [159].

Recombinant reconstituted AME remains in the supernatant of a 100,000 g, 20 min spin but after a severe 46°C 15 min treatment aggregates completely into pelletable material and cannot be resolubilized by dilution and 1 hr incubation at 30°C with or without substrates (2.5A).

Gentler centrifugation revealed that AME pellets as a stoichiometric complex (2.5A) despite wide variation in the aggregation propensity of its constituents (2.14C). Severely heat-shocked AME retains substantial activity, all of which resides in the aggregated fraction, as indicated by absence of activity in the supernatant after centrifugation (2.5B). Similarly, the activity of heat-treated Mes1 is reduced >7-fold after spinning out aggregates (2.5B). Gus1's non-catalytic N-terminal domain proved necessary and sufficient for heat-induced Gus1 aggregation (2.14D).

We next assessed the fidelity of tRNA-Met aminoacylation by AME before and after heat

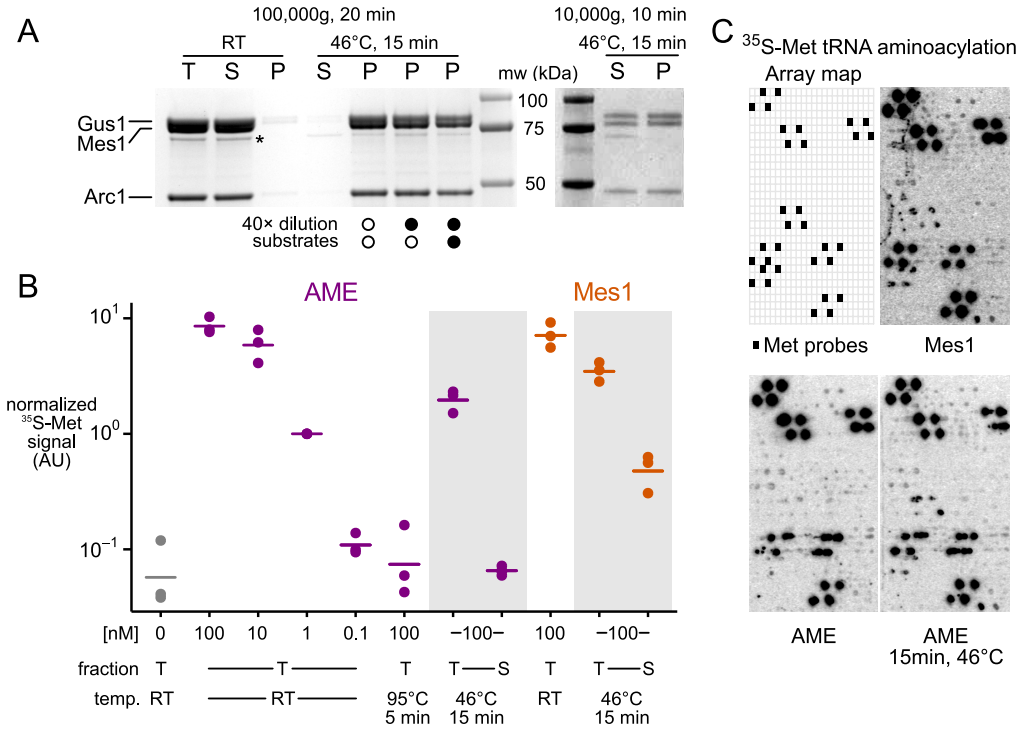

Figure 2.5: **The Yeast Multisynthetase Complex Forms Active Aggregates in Response to Heat Shock *in vitro*** (A) Recombinant purified AME complex is soluble before heat treatment and fully aggregated after (stained SDS PAGE; T, total; S, supernatant; P, pellet). A minor soluble degradation product is starred. Three heat-treated samples were incubated at room temperature (RT) for 1 hr (undiluted) or incubated for 1 hr at 30°C after 40 X dilution and after addition of substrates as indicated (see Experimental Procedures). (Right) Stoichiometry in aggregates revealed by lower-speed centrifugation. mw, molecular weight marker. (B) Activity measured by aminoacylation of total yeast tRNA with ^{35}S-labeled methionine in a filter-binding assay. Three replicates are shown, with signal normalized by 1 nM AME RT levels. Lines indicate means. (C) Fidelity measured by aminoacylation of tRNA- microarray-immobilized tRNAs with ^{35}S-labeled methionine. Each cell contains probes complementary to a single tRNA species, with tRNA-Met probes arrayed as indicated.

shock using tRNA microarrays. Under conditions in which AME is fully aggregated (2.5A), it retains fidelity indistinguishable from untreated AME or Mes1 (2.5C).

Bacterial inclusion bodies can contain active exogenous enzymes ([160]. Our results reveal heat-induced formation of endogenous, active, stoichiometric aggregates with normal fidelity. Here, reduced activity may indicate partial loss of function or reduced ability of large tRNA substrates to penetrate these *in vitro* aggregates.

2.3.7 Global Profiling of Disaggregation during Recovery Reveals Near-Complete Reversibility of Aggregation

Heat-shock granules slowly disappear after cells are returned to non-shock temperatures [19, 23], yet it has remained unclear whether endogenous aggregate dispersion is due to disaggregation followed by degradation and resynthesis or due to disaggregation back into a stable soluble pool.

To measure disaggregation and new synthesis at the proteome scale without blocking synthesis or degradation, we performed a media-shift experiment (2.6A and Experimental Procedures) in which cells are grown on a first set of stable-isotope-labeled amino acids, shifted to media containing a second set of labels, then heat shocked at 42°C and allowed to recover for a defined time at 30°C. Upon collection, these cells are mixed with cells from an unshocked (30°C) reference sample grown on a third label. Supernatant fractions of these mixtures measured after 0, 20, and 60 min of recovery allowed us to observe the depletion of aggregating proteins from the supernatant after shock followed by their recovery in both the pre- and post-shock labels, indicating new synthesis, or only in the pre- shock label, indicating disaggregation.

Heat-insensitive proteins, such as the glycolytic enzyme Pgk1, show minimal change in pre-shock ratio in the supernatant, indicating no aggregation, and a slight increase in post-shock ratio, indicating low levels of new synthesis during recovery (2.6B). Heat-aggregating

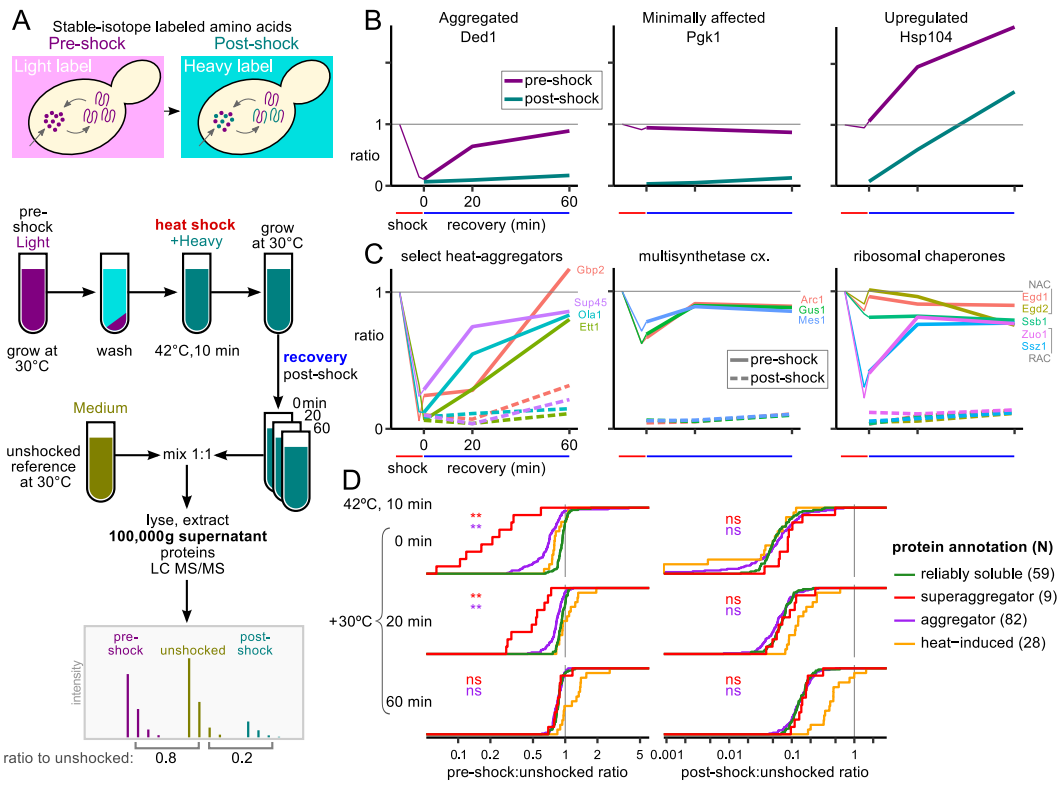

Figure 2.6: **Heat-Aggregated Proteins Disaggregate during Recovery** (A) Schematic experimental design for SILAC media-shift measurement of soluble protein dynamics during recovery from heat shock. (B) SILAC ratios measure aggregation or synthesis of example proteins Ded1, Pgk1, and Hsp104. Thin lines show pSup after 42°C, 8 min. heat shock from 2.1. (C) Select groups of heat-aggregating proteins during recovery after heat shock (others in 2.11B). (D) Heat-aggregated proteins disaggregate during recovery, while many proteins change minimally and known heat-induced proteins are synthesized. Cumulative distributions of the normalized ratio in the supernatant are plotted for reliably soluble proteins, superaggregators, other heat aggregators (annotated in the 46°C time course), and proteins whose ribosome occupancy increases at least 20-fold during 42°C, 20 min heat shock [161]. Wilcoxon rank sum test was used to compare the distributions of reliably soluble proteins to superaggregators and other aggregators, respectively, at each time point (**p $<$ 0.001; ns, not significant).

proteins have low pre-shock ratio immediately after shock, and their disaggregation is indicated by increase of the pre-shock ratio during recovery with only background-level changes in the post-shock ratio, as seen for the RNA helicase Ded1 (2.6B). Proteins synthesized in response to heat shock, such as the chaperone Hsp104, show an increase in both pre- and post-shock ratios, indicating new synthesis; increased signal in both channels reflects incorporation of imported post-shock amino acids and residual or recycled pre-shock amino acids (2.6B). Aggregated, degraded, and resynthesized proteins would show a low pre- shock ratio after shock and an increase in post-shock ratio; we do not observe this pattern.

A biological replicate with isotopic labels permuted shows the same behavior (2.9B). An additional time point 180 min post-shock, after a full cell doubling, shows that, as expected, the majority of the proteome incorporates the post-shock label (2.9C).

Proteins previously identified as superaggregators by MS aggregate aggressively at 42°C and disaggregate fully after 1 hr of recovery (2.6C and 2.11B). Complexes which aggregate coherently also disaggregate coherently, including the multisynthetase complex and the RAC (2.6C).

To examine proteome-scale trends, we compared groups of genes identified as reliably soluble, heat aggregators, or super-aggregators in the 46°C heat-shock data set. Immediately after heat shock, aggregators and superaggregators synthesized from pre-shock amino acids are depleted from the supernatant compared to reliable soluble proteins (2.6D). After 20 min recovery at 30°C, the differences between these populations are smaller though still significant, and after 60 min of recovery, the distributions are indistinguishable, indicating complete disaggregation (2.6D). The post-shock ratios of aggregators and superaggregators are indistinguishable from those of reliably soluble proteins, indicating approximately the same level of new synthesis. At the same time, proteins whose ribosome occupancy increases at least 20-fold during heat shock ([161] show a substantial increase in new protein synthesis (2.6D). New synthesis post shock correlates well with ribosome occupancy during shock

(2.9D).

In summary, the data show virtually complete disaggregation of endogenous aggregated proteins during recovery without elevated levels of degradative turnover.

2.4 Discussion

The standard model of heat stress holds that heat causes protein damage and misfolding, disrupting function and causing exposure of natively buried hydrophobic residues, which triggers protein aggregation [139]. This model was shaped by, and explains well, a wide array of observations, particularly the behavior of endogenous nascent polypeptides. A more recent regulatory interpretation holds that evolutionarily conserved heat-induced aggregation of some proteins into specific subcellular locations reflects a mechanism for attenuating translation [50, 35, 19] and protecting the cell during stress [162].

Our study provides multiple lines of evidence indicating that many phenomena that correlate tightly for nascent polypeptides and exogenous unstable reporter constructs—phenomena such as heat-induced aggregation, loss of function, formation of sub-cellular foci, and degradation—are in many cases completely separable and thus causally unrelated for endogenous mature eukaryotic proteins under acute stress. The standard misfolding model incompletely describes the behavior of most mature proteins during heat shock.

To illustrate, consider the aggressive yet fully reversible thermally induced aggregation of nuclear proteins, exemplified by Ett1 and Gbp2, in light of recent studies on nuclear quality control. The ubiquitin ligase San1 targets nuclear misfolded proteins for degradation [163, 146]. GFP constructs engineered with stretches of hydrophobic residues that promote formation of fluorescent nuclear foci and pelletable aggregates undergo San1-mediated degradation detectable within 1 hr [146]. Our expectation was that endogenous nuclear proteins that aggregate should be similarly degraded. However, despite aggressive aggregation of Ett1 and Gbp2 in the nucleus, they are restored to solubility without degradation.

The organized deposition of aggregated proteins into particular subcellular sites, such as stress granules, may provide fitness benefits to organisms during stress [162]. Stress granules may facilitate preferential translation of certain mRNAs during stress [48]. By providing a view into how proteins reversibly form large assemblies during stress, without necessary restriction to granular structures or particular sites, our study reveals a separate layer of phenomena that is rich with exciting functional possibilities. We hypothesize that the heat-induced aggregation of mature proteins reflects the action of a vast, fast-acting regulatory system based on massive molecular assembly and disassembly. This system couples rapid protein-autonomous stress-responsive assembling elements with slower-acting disassembly machines.

Such a system invokes transient interactions beyond quaternary structure, termed quinary organization [164]. Molecular mechanisms and components of quinary regulation may include multivalent interactions [165], low-complexity sequences [66], and phase-separation phenomena, including protein and protein/RNA liquids [166] and hydrogels [66]. Our studies do not offer a mechanistic picture of aggregation or new evidence for particular physical states of quinary assemblies but do identify targets for study.

Because heat stress necessarily involves an influx of thermal energy, it would be efficient for aggregation to result from evolved, thermally induced conformational changes that promote quinary interactions. Such processes could be all but indistinguishable from misfolding at the molecular level [167]. The fundamental distinction is in fitness: misfolding is deleterious, whereas evolved quinary regulation is beneficial, suggesting testable and opposing predictions about the fitness consequences of blocking aggregation. We also anticipate that, as in the case of the aminoacyl-tRNA synthetases, evolved quinary interactions will be domain specific, organized, and rapidly reversible without degradation, unlike the behavior of misfolded proteins.

Our data suggest several mechanisms for focusing translation on stress-induced tran-

scripts (2.7). Translation initiation on most yeast mRNAs depends upon initiation factors (eIFs) and auxiliary proteins (such as the RNA helicase Ded1). We find that these factors partition into two major classes, the heat-resistant factors (including eIF-1, 1A, 2) and heat-sensitive factors (including eIF-2B, 3, 4G, 5, Ded1). Shirokikh and Spirin ([168]) demonstrated assembly of a normal AUG-associated translation initiation complex on uncapped mRNA *in vitro* in the absence of eIF-2B/3/4A/4B/4G/4E if a poly(A) leader sequence is present. This poly(A)-mediated cap-independent initiation mechanism may explain the cap-independent translation of heat-shock mRNAs [41, 38, 37], which often possess unstructured, A-rich 5' UTRs [22] with reduced dependence on RNA unwinding [32]. We hypothesize that stress-sensitive aggregation of initiation and unwinding factors inhibits translation on most non-stress-relevant mRNAs.

The enzyme components of the AME complex, the aminoacyl-tRNA synthetases Mes1 and Gus1, have secondary transcriptional and translational activities in the nucleus and mitochondria, respectively, and are excluded from these compartments by complexing with Arc1 [159]. We hypothesize that autonomous heat-sensitive self-assembly of AME complexes discovered here confines active AME components to the cytosol, suppressing secondary activities in other compartments and focusing aminoacylation activity in the cytosol, where it is needed during stress (2.7).

Molecular chaperones may act as regulatory disassembly factors quite separate from their role in protein folding and misfolding. For example, chaperone-mediated dissolution of AME assemblies would permit return of Gus1 and Mes1 to duty in other cellular compartments. Chaperone-mediated restoration of helicases and cap-dependent initiation factors to solubility would derepress translation of most mRNAs, titrating translational activity away from stress-induced messages and thus closing a feedback loop (2.7). Consistent with this, deletion of the disaggregase Hsp104 delays both heat-shock granule dissolution and reassembly of polysomes after heat shock [19]. Which factors (chaperones or other proteins) disassemble

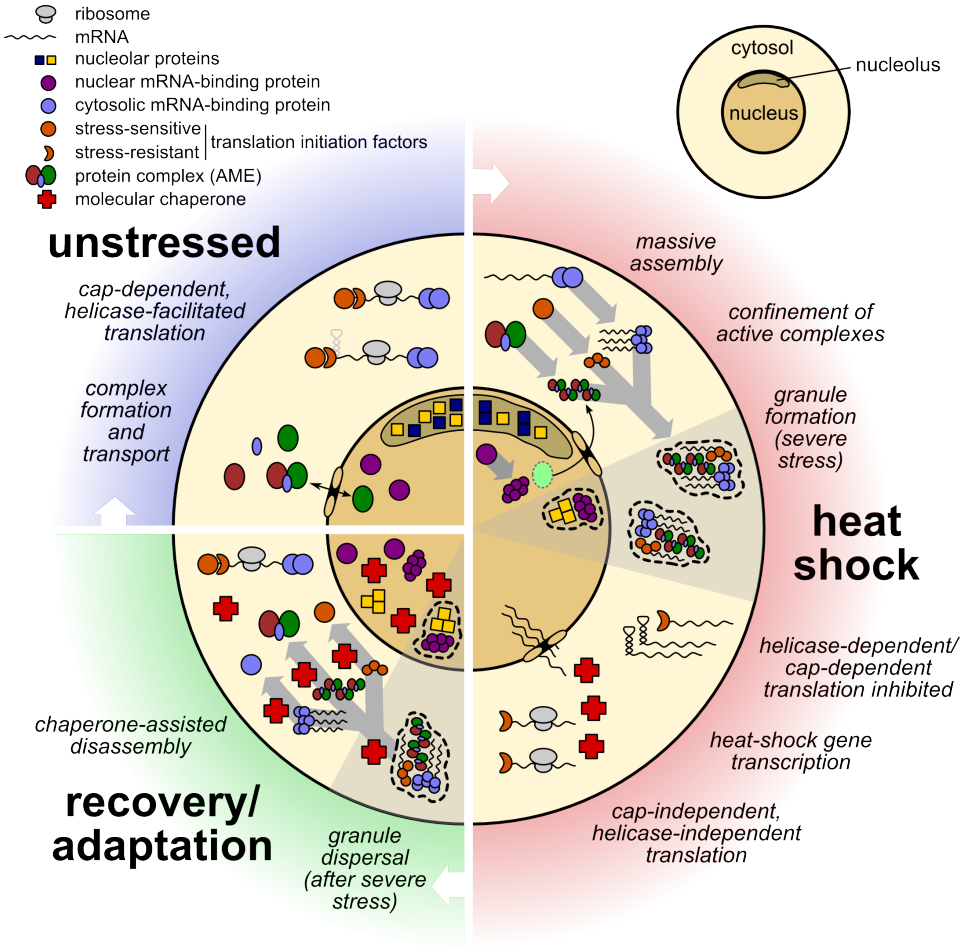

Figure 2.7: **Mechanisms for Enhancing Cellular Remodeling by Massive Assembly during Heat Stress**

which assemblies, and whether and how specificity is achieved, can be addressed in large part using the methods that we have introduced here.

A similar autoregulatory mechanism has been proposed as a way to link protein quality control and translation through assembly of stress granules [19]. Our study suggests that neither misfolding nor stress-granule formation need be involved; indeed, heat stress/ aggregation/ chaperones seem likely to be a special case of a broader class of signal/ assembly/ disassemblase regulatory systems, each involving stress-specific quinary interactions. It seems likely that certain proteins will form assemblies under a wide range of stress conditions (e.g., translation initiation factors) but by stress-specific mechanisms, such as binding sites revealed by phosphorylation, pH- driven self-association, and thermally induced local unfolding. Stress-triggered formation of massive but unanchored assemblies of undamaged proteins, when reversible by stress-induced disassembly activity, allows for a fast-acting autoregulatory response.

2.5 Supplemental figures

2.6 Methods

2.6.1 Comparison to previous proteome-scale measurements of heat-induced protein aggregation

Our rapid kinetic measurements capture aggregation behavior distinct from that observed after longer stresses. As reported in the main text, our conditions capture aggregation in the majority of known heat-shock granule components forming at the same timescale. A recent study reported 117 proteins forming aggregates after two hours at 42C ([171]; in these data, Pab1 is the only HSG component identified. We detect 90 of these 117 proteins, yet identify aggregation in only three (Pab1, Ura8, Tum1). These results indicate that aggrega-

tion measured at different times diers, or that the experimental protocols are incompatible. The two-hour measurements occur long after production of molecular chaperones, whose presence is expected to remodel, reverse, and prevent further aggregation of many proteins; by contrast, our measurements precede detectable induction of molecular chaperones.

2.6.2 Yeast growth, heat shock, and cell fractionation

Yeast strain BY4741 was grown, with shaking, at 30C in SC complete media in a baed Erlenmeyer flask, to mid-exponential phase (OD_{600} 0.5). 50 mL cell culture was transferred to a 50 mL conical tube and centrifuged for 1 min at 2, 500g at RT, and the media decanted. The tube containing cell pellet with residual medium was placed in a water bath at specified temperature (30°C, 37°C, 42°C, 46°C) for the specified amount of time (0, 2, 4, 8 minutes), after which the pellet was resuspended in 1 mL ice-cold Buffer S0 (120 mM KCl, 2 mM EDTA, 20 mM HEPES-KOH, pH 7.4), transferred to a chilled 1.5 mL microcentrifuge tube, and centrifuged again for 30 seconds at 5, 000 g, 4°C. The supernatant was discarded and pellet was resuspended in 100 L Buffer S [Buffer S0 + 0.5mM DTT, 1:100 protease inhibitor cocktail IV (Calbiochem 539136), 1mM PMSF], divided in half and flash-frozen into two half-aliquots. One aliquot here became the total protein sample (T), resuspended in 400 L Buffer T [20mM HEPES-NaOH, pH7.4, 150 mM NaCl, 3% SDS, 5 mM EDTA, 2 mM DTT, 1:100 PMSF, 1:1000 protease inhibitors IV), and lysed by boiling for 20 minutes at 95°C and vortexing. The other aliquot was placed in a 2 mL Eppendorf "Safe-Lok" tube containing a 7 mM stainless steel ball (Retsch) pre-chilled in liquid nitrogen (LN). Cells were lysed with 4 X 90s 30Hz pulses in a Retsch MM100 mixer mill, chilling in LN between pulses. 400 L ice-cold Buffer S was added, then the thawed lysate was clarified by centrifugation at 3,000g for 30 seconds at 4°C. The clarified supernatant was transferred to a 1.5mL ultracentrifuge tube, and centrifuged at 100,000 g for 20 minutes at 4°C; the aqueous portion of this is the supernatant (S) sample. The pellet was washed in 500 L Buffer S, and centrifuged

again at 100,000 g for 20min at 4°C. The remaining pellet was mixed with 500 L Buffer P [8 M urea, 20 mM HEPES-NaOH, pH7.4, 150 mM NaCl, 2% SDS, 2 mM EDTA, 2 mM DTT, 1:100 PMSF, 1:1000 protease inhibitors IV), by vortexing vigorously for 30 minutes. The resuspended pellet was centrifuged at 20,000g at RT for 5 minutes, and the aqueous phase was designated as the pellet (P) fraction. Protein from total, supernatant, and pellet fractions was precipitated by chloroform/methanol extraction ([172]).

SILAC recovery assay

Yeast auxotrophic for arginine and lysine (RK) were grown with light (rep. 2, heavy) isotope labeled RK (Cambridge Isotope Laboratories) at 30°C to mid-exponential phase, transferred to heavy (rep 2, light) isotope labeled RK, heat shocked for 10 minutes at 42°C, and allowed to recover at 30°C for 0, 20, 60 or 180 minutes. For the 180 minute timepoint in rep 2, cells were diluted in pre-warmed labeled media to ensure they stayed in exponential phase. Cells were harvested, mixed evenly with unheated cells grown in medium-isotope-labeled RK, and flash-frozen. Mixed samples were lysed and fractionated as above, and only the supernatant fraction was chloroform-methanol extracted, trypsin digested, and submitted for LC-MS/MS.

2.6.3 Sample preparation for mass spectrometric analysis

Samples were measured to 100 g of total protein each. Samples were digested with trypsin using a FASP protocol ([173]). For dimethyl labeling of T, S, P, samples, digested samples were labeled as described by [174]; total was labeled +28Da (light), supernatant was labeled +32Da (medium), and pellet was labeled +36Da (heavy). Subsequently, T, S, P, samples from the same experiment were mixed evenly. An aliquot of each sample was taken, and submitted directly for mass spectrometry analysis. The remaining sample was fractionated by high-performance liquid chromatography (HPLC). The HPLC 1200 Agilent system with fraction collector (Agilent Technologies, Santa Clara, CA) was used for ERLIC (electrostatic

repulsion-hydrophilic interaction chromatography, Alpert (2008)) separation on a PolyWAX LP column (200 x 2.1 mm, 5m, 300, PolyLC Inc, Columbia, MD). Sample was fractionated into 20 fractions on a 70 minute LC gradient. Individual or combined fractions were submitted for mass spectrometry analysis.

2.6.4 Mass spectrometry

Mass spectra were measured on an Orbitrap Velos Pro (Thermo Fisher, San Jose, CA). Samples injected from an autosampler (Waters, NanoAquity, Milford, MA) were loaded into the trapping column (75 m column ID, 5 cm packed with 5 m beads on 200 pores, from Michrom Bioresources, Inc.), washed for 15 minutes and then eluted to an analytical column with a gradient from 2 to 32% of buffer B [0.1% formic acid in acetonitrile] over a 90 minute gradient for each fraction. Instrument was set up to run TOP 20 method for MS/MS in the ion trap with an exclusion function turned on, followed by a MS1 scan in Orbitrap with 60K resolving power at mass of 400 m/z. Obtained runs were analyzed jointly by MaxQuant Software, version 1.5.0.30 ([175]), http://maxquant.org/). Searches were done against verified and uncharacterized ORFs from the R64-1-1 release of the S288C genome proteome database (yeastgenome.org), and common contaminants added to the database from the Global Proteome Machine (http://www.thegpm.org/crap/). Searches were done with trypsin enzyme specificity, allowing 2 missed cleavages. Possible modifications included in the search parameters were: protein N-terminus acetylation, methionine oxidation, deamidation of asparagine and glutamine amino acids, and phosphorylation of serine, threonine, and tyrosine. For triplex dimethyl labeling, labels on primary amines for light (+28 Da), medium (+32 Da) and heavy (+36 Da) were searched for as variable modifications. For SILAC, labels of medium lysine (+4 Da), heavy lysine (+8 Da), medium arginine (+6 Da) and heavy arginine (+10 Da) were searched for as variable modifications. The database search criteria were held at 1% FDR on both protein and on peptide levels for all output

reported data. All parameters for MaxQuant runs are supplied in the Dryad package. We used MaxQuant intensities from the evidence.txt file, not the reported ratios, which are calculated using a different method, because we noted a detection-intensity-dependent bias in ratios that was largely absent from the quotient of the intensities.

2.6.5 Statistical analysis

MaxQuant reports intensities in three channels per detection event: light (L), medium (M), and heavy (H), which in this experimental design are noisy proxies for total sample (T), 100,000 g supernatant (S), and 100,000 g pellet (P) respectively. Our goal is to estimate the proportion in supernatant (pSup), the ratio of supernatant to total, for each protein individually, which is a number between 0 and 1. This is complicated by measurement noise in the data, principally that the separate samples undergo multiple processing steps in parallel before being mixed and measured by mass spectrometry, so that the ratios measured on the machine are not stoichiometric compared to the original ratios in cell lysate. For example, directly estimating the S/T ratio from the M/L ratio produces estimates greater than 1; conversely, we can employ conservation of mass (in cells, for each protein T = S + P) to constrain models in order to fit the data accurately. We employed multiple statistical analyses to estimate pSup, finding that correcting for uneven fraction mixing, batch effects, and other measurement noise produces the most biologically coherent quantitative picture of protein aggregation across multiple biological replicates, while agreeing in outline with more naive analyses. Three alternative estimates of pSup are shown in 2.8. The first, called M/(M+H), simply takes the median across peptides of intensity ratios. The second, called model 2 (m.2), uses conservation of mass and an error model, applied to each experiment independently, to correct for uneven mixing and estimate confidence intervals. The third, called model 3 (m.3), corrects for batch effects in biochemical separation by normalizing the pSup across experiments for a subgroup of proteins. We found that all models agree in

outline and produce high correlation (Pearson's r coeffcient) between biological replicates, although model 2 successfully accounts for conservation of mass, and model 3 was better at reducing bias and root-mean-squared-error (RMSE), as shown in figure S1. In particular, model 3 reduced batch-effect variation between measurements of one biological sample with multiple treatments (30C.rep1, 46C.2min, 46C.4min, 46C.8min) and another collected at a different time and measured in less depth (30C.rep3, 37C.8min, 42C.8min). We use the output of model 3 as pSup estimates in all figures in this paper except as noted in 2.8.

2.6.6 Technical details of statistical models

The goal of the statistical analysis is to estimate proportion in supernatant (pSup), the ratio of supernatant to total. The measurement noise has three components, all acting multiplicatively. The first noise component captures the fact that the proportions of each sample (T,S,P) as mixed and measured dier from their original proportions in cell lysate, since samples are extracted, digested and labeled separately; we call these the mixing ratios, and denote them by = (T , S , P). The second noise component quantifies how distinct peptide states from a single protein may have highly variable intensities; we call this the detectability of events, and denote by ij for event j associated with protein i. The third, residual, noise component, denoted by C,ij, is considered independent across channels C = (L, M, H), and for each detection event j associated with protein i.

The list of quantities needed for an accurate statistical model is as follows: i indexes proteins ri proportion in supernatant (pSup) of protein i Ti abundance of protein i Si abundance in supernatant of protein i Pi abundance in pellet of protein i j indexes peptide detection events Lij intensity in light channel detected in event j, protein i Mij intensity in medium channel detected in event j, protein i Hij intensity in heavy channel detected in event j, protein i ij detectability for event j L,ij residual noise in L intensity for event j M,ij residual noise in M intensity for event j H,ij residual noise in H intensity for event j T mixing ratio for total

fraction S mixing ratio for supernatant fraction P mixing ratio for pellet fraction where (T , S , P) 2 Simplex, ri 2 [0, 1] for each i, and the remaining quantities are non-negative. We posit multiplicative lognormal noise in each channel. The full model is as follows. Lij = T Ti j T,ij Mij = S Si j S,ij Hij = P Pi j P,ij Si = ri Ti Pi =(1ri)Ti (1a) (1b) (1c) (1d) (1e) The inferential targets are the proportions in supernatant for each protein, r . i In fig. S1, model 1 "M/(M+H)" naively estimates r = median Mij i j Mij +Hij , which does not To estimate ri, we need not estimate the absolute protein abundances. Thus we consider a account for the mixing ratios nor use data from the total protein channel. restricted model for ratios M and H in our analysis, as follows. LL Mij = S ri M/L,ij (2a) Lij T Hij =P (1ri)H/L,ij (2b) Lij T The restricted model has the advantage that both the absolute protein abundances, Ti, and the detectability parameters, ij, cancel out, and need not be estimated. We complete the specifications by positing a single noise term per ratio, M/L,ij and H/L,ij, for each event j associated with protein i. This strategy for estimating the proportions in supernatant is akin to a partial likelihood approach. To complete the model specifications, we posit the following prior distributions: iid 11 ri Beta(2,2) (2c) (2d) (T , S , P) Dirichlet(100, 100, 100) lnM:L,ijiid M2:L M:LH:L •:L Cauchy(0, 1)+ (2f) Beta(1, 1). (2g) Here we chose a Beta(1, 1) prior for ri, the Jereys prior for the binomial likelihood; after testing a 22 variety of priors we found this to be weakly informative and numerically stable. The Dirichlet prior for is a strong prior that enforces even mixing proportions; since we have thousands of observations the posterior is nevertheless dominated by the data. We chose a half-Cauchy prior distribution for the variance parameters as this is a sensible default choice for top-level variance parameters (Polson and Scott, 2012). represents the correlation of the M:L and H:L ratios (equations 2a, 2b) due to shared noise from the L channel; if all noise variances are the same in each channel then = 0.

We used equations (2a-2g) to estimate values of ri jointly with other specified parameters by Markov Chain Monte Carlo (Robert and Casella, 2005). We implemented the sampler

using the probabilistic programming language STAN, accessed using the rstan package (Stan Development Team, 2014) in the R software environment (R Core Team, 2014). This output ri is displayed as pSup, model 2 in fig. S1. All code is provided in the datadryad package. We fit model 2 to each experiment individually. Subsequently, we found discrepancies in certain datasets consistent with compression of dynamic range (fig. S1), presumably due to less ecient separation, an artifact of the mass spectrometric measurement and MaxQuant analysis, or other batch eects. To correct for this, we chose lists of proteins reliably in the supernatant (2 peptides detected in every experiment, and ri $>$ 0.9 in 30C.rep1 and 46C.8min) or reliably in the pellet (2 peptides detected in every experiment, and ri $<$ 0.1 in 30C.rep1 and 46C.8min), with median ri's FS and FP respectively across the 30C.rep1 and 46C.8min datasets. Then, we normalized so that these proteins had the same pSup across all experiments, with a linear transformation in log-odds space. Precisely, for a given experiment, fS is the median ri for reliably supernatant proteins and fP for reliably pelleted proteins, and

g(r)=log r (3) 1r is the logistic function, we transformed: ri0 =g1g(FP)+[g(ri) g(fP)]g(FS) g(FP). (4) This output ri0 is displayed as pSup, model 3 in fig. S1 and reported in the data package, along with 95% confidence intervals. As the figure shows, it is a minor adjustment in most datasets, and generally reduces the inter-dataset bias and RMSE without obscuring the signal of heat-dependent aggregation. 95% confidence intervals from model 2 were transformed by applying the same equation and parameters to the endpoints. Processing code/scripts and intermediate data are included in the data package.

2.6.7 Statistical analysis for SILAC recovery data

In the SILAC recovery assay, we again used MaxQuant Software, version 1.5.0.30 ([175]. We searched for SILAC-labeled arginine and lysine as standard, otherwise using the same variable protein modifications as above. We report median ratios of MaxQuant-estimated

intensities, correcting for deviations from even mixing by fixing the median ratio to 1 for proteins reliably found in the supernatant in the aggregation assay previously. This code is also available in the data package.

2.6.8 Sedimentation coefficients of pelleting particles

Here we estimate the particle sizes expected to sediment in our assay. Centrifugation conditions are acceleration a = 100, 000g 106ms2 for t = 20mins 103s. 0.5mL of liquid in a 1.5mL eppendorf tube is approximately d = 2cm = 2 103m high, so particles pellet if: v = d/t 2 103m = 2 106ms1 (5) 103 s since the sedimentation coefficient c = vt/a, that implies that c 106ms2 = 5 10 as a Svedberg unit S = 1013s. This rough estimate suggests that the smallest pelleting particle should be much larger than the 80S ribosomes, consistent with our observations.

2.6.9 Protein annotation

Annotation of protein groups used in figures 1 and S4, were derived from the Saccharomyces Genome Database (Cherry et al., 2012) for most groups, from the sources listed in table S2 for heat shock granule components, and from computational structure prediction for Membrane proteins. Glycolytic enzymes are: Hxk1, Hxk2, Pgi1, Pfk1, Pfk2, Fba1, Tpi1, Tdh3, Tdh2, Tdh1, Pgk1, Gpm1, Eno1, Eno2, Cdc19, Pyk2. Ribosomal proteins annotated here include only core components, whose names in yeast begin Rpl for the large subunit, Rps for the small subunit, and Rpp for the stalk. Our list of nucleolar proteins is manually curated from the gene ontology category (Cherry et al., 2012), as proteins whose principal function is nucleolar. There are 143 well-detected nucleolar proteins: Mak16, Utp20, Mak5, Enp1, Spb1, Krr1, Bud23, Pwp2, Rsa4, Csm1, Ycr087c-a, Nop1, Dbp10, Tsr1, Nop14, Sas10, Nhp2, Nop6, Fal1, Mak21, Rrp8, Arx1, Fob1, Rpa14, Hmo1, Bfr2, Ssf2, Utp4, Fcf1, Esf1, Utp5, Utp6, Snu13, Pol5, Nop16, Nug1, Utp7, Spb4, Loc1, Cdc14, Dbp3, Prp43, Rok1,

Utp22, Nop7, Utp8, Enp2, Mtr3, Nsr1, Nop19, Efg1, Pxr1, Ygr283c, Rrp3, Ssf1, Nop10, Rpf1, Gar1, Rpc10, Imp3, Dbp8, Utp9, Air1, Utp25, Rrt14, Nop9, Hca4, Mtr4, Utp18, Net1, Utp10, Rpa34, Mpp10, Urb2, Rpa12, Mrt4, Urb1, Dhr2, Rrp14, Utp11, Rrn3, Ebp2, Tof2, Dbp7, Las1, Rpf2, Srp40, Drs1, Sof1, Rix7, Noc3, Rlp24, Fcf2, Dip2, Acs2, Cbf5, Emg1, Pwp1, Nop56, Rsa3, Utp13, Ifh1, Dbp9, Utp21, Fpr4, Fpr3, Utp14, Utp15, Ecm16, Rrb1, Rrp5, Tma23, Has1, Rlp7, Imp4, Nop15, Rpc19, Kre33, Nop13, Ubp10, Rpa49, Trf5, Kri1, Dbp6, Nog2, Esf2, Rcl1, Nop12, Brx1, Pap2, Nop8, Utp23, Bud21, Pno1, Ytm1, Rrs1, Nop58, Rpa43, Rpa190, Nop4, Nog1, Nan1, Nop53, Nip7, Bms1, Dim1, Rpa135, Tif6, Mrd1, Rrp9, Rrp15, Noc4.

Our list of membrane proteins includes those with at least 2 transmembrane domains identified by TMHMM 2.0 (Krogh et al., 2001). There are 268 well-detected membrane proteins: Aus1, Ccc1, Drs2, Rcf2, Erg11, Sna2, Yro2, Gup1, Ftr1, Eos1, Gaa1, Rsn1, Tda5, Csg2, Sft2, Tvp38, Chs2, Alg9, Adp1, Nce102, Gpi11, Erp2, Sal1, Spf1, Dip5, Nsg1, Pmt7, Ecm3, Dfm1, Ssh1, Pmt3, Dnf1, Cst26, Sly41, Izh2, Erg3, Ale1, Pam17, Yip3, Gpi14, Tul1, Mal11, Neo1, Mdl1, Alg12, Dpp1, Ste24, Pdr15, Vma3, Erp5, Fat1, Tcb1, Hip1, Rtn1, Tsc13, Avt3, Ymd8, Aim26, Ost2, Ste2, Qdr2, Fre1, Vtc2, Vcx1, Lnp1, Shy1, Atg33, Kha1, Lac1, Sec61, Fth1, Dfg10, Atm1, Nnf2, Zrt2, Yor1, Zrt1, Flc1, Sam3, Cds1, Nte1, Pmc1, Ncr1, Gpt2, Pma1, Vtc3, Lem3, Ndc1, Cpt1, Fks1, Brl1, Hmg2, Lyp1, Atr1, Mup1, Cox15, Usa1, Tat1, Ena1, Sec62, Ypk9, Sey1, Tna1, Ost5, Aur1, Itr1, Ost3, Ssm4, Gdt1, Bap2, Zrc1, Ptr2, Sac1, Pmr1, Pom152, Hmg1, Pdr5, Fre7, Alr2, Pmt1, Enb1, Agp1, Emc4, Cho2, Sur2, Fks3, Emp24, Chs1, Ybt1, Gpi17, Yos1, Erv29, Ecm33, Hxt5, Dnf3, Gex2, Chs3, Tvp18, Svp26, Vma9, Cwh43, Pma2, Cos10, Alg2, Scs7, Gtt3, Rer1, Aac1, Cdc50, Stt3, Bi4, Ctr1, Spo75, Die2, Alg3, Pom33, Pmt5, Arn2, Pmt6, Tpo1, Hxt1, Cox1, Cox10, Erg4, Vph2, Rcf1, Pdr12, Vtc4, Bpt1, Sur4, Get2, Uip3, Mal31, Cpr8, Pho87, Rax1, Sec63, Hxt16, Mrl1, Swp1, Vmr1, Sdh3, Erg28, Pis1, Fmp37, Nsg2, Erg1, Avt7, Fsf1, Lag1, Sct1, Fun26, Ato3, Avt1, Bap3, Mrh1, Yip4, Gpi1, Erv41, Thi72, Lcb3, Pho91, Erp1, Cox2, Crd1, Trk1, Akr1, Ptm1, Mnr2,

Hxt6, Gsc2, Pmt2, Emc1, Ist2, Ycf1, Pet9, Vph1, Yip5, Yif1, Smf3, Emp70, Fen1, Fcy21, Ost6, Flc2, Yet1, Tpo4, Aim14, Pga3, Erj5, Ypq1, Ole1, Erd2, Rbd2, Aac3, Stv1, Pex31, Yct1, Sur7, Vba4, Mcd4, Dnf2, Gup2, Tpo3, Gab1, Pmt4, Syg1, Ste6, Hxt10, Tmn3, Mtc7, Gnp1, Spc1, Yop1, Rim21, Snq2, Cdc1, Cho1, Yet3, Elo1, Erv14, Mdl2, Hxt3, Flc3, Pho86, Msc2, Spc2, Dal4. Our list of molecular chaperones is: Ssa1, Ssa2, Ssa3, Ssa4, Ssb1, Ssb2, Sse1, Ssz1, Hsp26, Hsp42, Hsp82, Hsc82, Hsp104, Zuo1, Sse2, Fes1, Ydj1, Sis1, Hsp78, Ssc1, Kar2, Sil1, Hch1, Aha1, Sba1, Sti1.

2.6.10 Strains

To construct fluorescently tagged strains for microscopy, plasmids pJLS033 and pJLS035 were constructed for C-terminal Clover and mRuby2 labeling at the native locus. Clover/ mRuby2 KanMX cassette PCR fragments were transformed into BY4741 and BY4742 according to standard lithium acetate protocol and selected using G418. Diploids were generated by crossing PCR- confirmed positives for 4 hours at RT, then overnight at 30C on YPD, followed by selection on SC –cys –met –lys plates. All strains used are listed in Table S6.

2.6.11 Spinning-disk confocal fluorescence microscopy

Cells were grown to mid-log phase (3 107 cells/mL) in non-fluorescent synthetic yeast growth medium (NSD; per 1 L: 20 g glucose, 5 g ammonium sulfate, 0.79 g CSM [Sunrise Science Products 1001-100], 1.7 g YNB trace elements [US Biological Y2035-01], 2 mL 500x non-fluorescent vitamin mix [500 mg calcium pantothenate, 2.5 g myo-inositol, 100 mg niacin, 50 mg p-aminobenzoic acid, 100 mg pyridoxine hydrochloride, 100 mg thiamine hydrochloride, dH2O to 500 mL, filter sterilized], 2 mL 500x biotin (0.2 g/L), 2 mL 500 CoCl2-6H2O (0.1 g/L), 20 mg adenine sulfate). 25 L aliquots were heat-treated for 8 minutes at 30C or 46C in an Eppendorf Thermomixer. To reduce live cell motion while imaging, coverslips coated with

concanavalin-A were applied to base-washed slides to prepare flow-chambers using melted Parafilm ([176]). Heat-treated cells were applied to the flow-chamber and allowed to settle before rinsing unbound cells with NSD mounting media and sealing with VALAP (equal parts Vaseline, lanolin, and paran wax mixed to homogeneity by gentle heating and applied using a cotton-tipped applicator) to decrease evaporation of mounting medium. Images were captured with a 100/1.45 oil objective on Olympus DSU spinning disk confocal microscope (Olympus Corporation of the Americas, Center Valley, PA) with a Hamamatsu model C9100 EM-CCD camera (Hamamatsu Photonics, Skokie, IL) controlled by SlideBook v5.0 software (Intelligent Imaging Innovations, Denver, CO). Filter sets were FITC/Cy2 (excitation 490/20 nm, emission 528/38 nm) for Clover and DsRed (excitation 565/25 nm, emission 624/40 nm) for mRuby2. 20 plane z-stacks were collected over a range of 4.94 m (step size 0.26 m). Fluorescence images were deconvolved in Fiji software ([177]) using the deconvolution lab plugin ([178]) to perform 10 iterations of the Richardson-Lucy algorithm, subtracting minimal intensity background and using point-spread functions generated for the Olympus DSU microscope by PSF generator software ([179]). Then, using Fiji, a single slice from the deconvolved stack was selected, a 20m 20m square selected, and intensity automatically adjusted (ImageJ macro provided upon request); the corresponding single-slice square from the DIC images was selected alongside.

2.6.12 Protein gel electrophoresis

Samples were first boiled in Laemmli buer (BioRad 161-0737), and aliquots (5L unless otherwise noted) were loaded onto 4-15 % Criterion TGX (BioRad 567-1084). Gels were run at 200V for 40 minutes in a Bio-Rad Criterion system. Coomassie staining was performed using Gelcode Blue (Thermo 24592) according to manufacturer's instructions. Gels were imaged using a Chemidoc- MP (Bio-Rad).

2.6.13 Western blotting

Proteins were transferred to 0.2m nitrocellulose membranes (BioRad 9004-70-0) in Towbin buer using the Criterion blotter system (Bio-Rad). Protein was detected using 2.5 g anti-Pab1 antibody (EnCor; Gainesville, FL; MCA-1G1) , or 5 g anti-Ssz1 antibody ([180]), along with the ONE-HOUR WesternTM Basic Kit (Mouse; GenScript L00205) according to manufacturer's instructions, and imaged on a Chemidoc-MP (Bio-Rad).

2.6.14 Purification of multisynthetase complex components

Unless otherwise stated, cells of E. coli strain BL21 (DE3) were grown in LB at 37C.

Arc1

The full-length Arc1 gene from S. cerevisiae was cloned into the pET28a vector using standard cloning methodology, and subsequently transformed into BL21 cells for expression as a fusion with an N-terminal 6-His tag. A single colony was used to inoculate 50 mL LB supplemented with kanamycin (50 g/mL), and culture was grown to mid-log phase at 37C prior to 2% inoculation of 1 L fresh LB + kanamycin. IPTG was added to a final concentration of 1 mM when the culture reached OD600 = 0.75, at which time the flask was transferred to 30C incubator with shaking at 200 RPM for 4 hours. Cells were pelleted at 5000g for 10 minutes at 4C, then resuspended in 20 mM HEPES (pH 7.4), 120 mM KCl, 5 mM imidazole, 0.2% Triton X-100, 0.5 mM -mercaptoethanol, and EDTA-free complete protease inhibitor tablets (Roche 05 056 489 001), then lysed on ice/water bath with sonication 7 seconds ON/7 seconds OFF cycles for 20 minutes at 60% amplitude. Cell debris and insoluble material was removed via centrifugation for 20 minutes at 18, 000 g, 4C. Clarified lysate was loaded onto a buer-equilibrated 5 mL HiTrap Chelating HP column (GE Healthcare Life Sciences 17-0409) on an A KTAprime system (GE Healthcare Life Sciences) with automated fraction collector. The column was washed with 5 column volumes (CV) of buer containing 20 mM HEPES, 120 mM KCl, 30 mM imidazole, then bound proteins were eluted over a 40

mL gradient (0-100%) to buer containing 20 mM HEPES, 120 mM KCl, 300 mM imidazole. Fractions containing Arc1 were pooled and buer exchanged to 50 mM Na2HPO4, pH 6.7, prior to loading onto a 5 mL HiTrap SP HP column (GE Healthcare Life Sciences 17-1151-01). The column was washed with 5 CV of buer containing 50 mM Na2HPO4, pH 6.7, and Arc1 was eluted over a 35 mL gradient (0-100%) to buer containing 50 mM Na2HPO4, 1M NaCl, pH 6.7. Fractions containing Arc1 were pooled, buer exchanged to buer A [20 mM HEPES, 150 mM KCl, , pH 7.4], concentrated and further purified on Superose 6 10/300 GL column (GE Healthcare Life Sciences) equilibrated with buer A using A KTApurifier FPLC system (FPLC; GE Life Sciences). Arc1 was eluted at 15.8 ml and 0.5 ml peak fraction was divided into aliquots, frozen, and stored at 80C until used.

Mes1 The protocol is the same as for Arc1, with the following exceptions. Culture was grown in TB medium [1.2% peptone, 2.4% yeast extract, 0.4% glycerol, 72 mM K2HPO4, 17 mM KH2PO4] and induced at OD600 = 0.4 with 1 mM IPTG at 20C for 5 hours. Cells were lysed in buer containing 20 mM HEPES, 250 mM KCl, 20 mM imidazole, 0.5 mM -mercaptoethanol, 0.5% Chaps detergent and EDTA-free complete protease inhibitor tablets, pH 7.4]. HiTrap Chelating HP column was washed with buer containing 20 mM HEPES, 250 mM KCl, 20 mM imidazole, pH 7.4 and bound protein was eluted using buer containing 20 mM HEPES, 250 mM KCl, and 400 mM imidazole, pH 7.4]. Fractions containing Mes1 were pooled, buer exchanged to 20 mM HEPES (pH 7.4), 80 mM KCl, applied to monoQ 5/50 GL column and fractions were collected across a 10 ml 80-600 mM KCl gradient by FPLC. Mes1 containing fraction (eluted between 300 and 400 mM KCl) was then applied to Superdex 200 10/300 GL equilibrated with buer A and 0.5 ml fractions were collected following elution by FPLC. Mes1 was eluted at 14.0 ml and peak fractions were concentrated, divided into aliquots, frozen, and stored at 80C until used.

Gus1 The protocol is the same as for Arc1, with the following exceptions. Cells were induced at OD600 = 0.75 with 1 mM IPTG at 20C for 5 hours. Cells were lysed in buer

containing 20 mM HEPES, 140 mM KCl, 20 mM imidazole, 0.5 mM -mercaptoethanol, 0.2% Triton X-100 and EDTA-free complete protease inhibitor tablets, pH 7.4]. HiTrap Chelating HP column was washed with buer containing 20 mM HEPES, 140 mM KCl, and 20 mM imidazole, pH 7.4 and bound protein was eluted using buer containing 20 mM HEPES, 140 mM KCl, and 400 mM imidazole, pH 7.4]. Fractions containing Gus1 were pooled and buer exchanged to 20 mM bis-tris propane, pH 7.1, then loaded onto a 5 mL HiTrap Q HP column (GE Healthcare Life Sciences 17-1154-01). Column was washed with buer containing 20 mM bis-tris propane, pH 7.1, and eluted using 20 mM bis-tris propane, 1 M NaCl, pH 7.1. Fractions containing Gus1 were pooled, buer exchanged to buer A, concentrated and further purified on Superose 6 10/300 GL column using FPLC. Gus1 was eluted at 16.2 ml and 0.5 mL peak fraction was divided into aliquots, frozen, and stored at 80C until used.

2.6.15 Isolation and heat-assembly of AME multisynthetase complex

Purified Mes1, Arc1, Gus1 were mixed in a 1:1:1 molar ratio in a total volume of 0.5 mL in a buer containing 20 mM HEPES (pH 7.4), 150 mM KCl, 5 mM MgCl2, incubated for 12 hours at 4C, then spun down at 10, 000 g for 10 minutes at 4C prior to loading on a Superdex200 column equilibrated with buer B (20 mM HEPES [pH 7.0], 150 mM KCl, 0.1 mM MgCl2). AME complex was collected upon elution from the column at 11.3 mL and subsequently concentrated and stored at 4C. All reactions were assembled to contain 4 M AME (or 2M Mes1) in buer 20 mM HEPES (pH=7.0), 150 mM KCl, 2 mM MgCl2 and incubated 15 min at either 30C or 46C followed by dilution (when indicated) and further 1 hr incubation at indicated temperature. Reactions were centrifuged at 100,000 g for 20 min and supernatant transferred to a clean tube. The pellets were washed once with 200 L of 20 mM HEPES (pH=7.0), 150 mM KCl, 2 mM MgCl2 and centrifuged again. Pellets were resolubilized in Laemmli buer and proportional amounts of T and S material diluted with 2 Laemmli were subjected to PAGE and staining. Heated samples wer diluted 40 with 20 mM

HEPES (pH=7.0), 150 mM KCl, 2 mM MgCl2 followed by 1 hr incubation at 30C, and in a separate sample additionally supplemented with (cold) methionine and yeast total tRNA as in aminoacylation reactions followed by 1 hr incubation at 30C.

2.6.16 Dynamic light scattering

Dynamic light scattering (DLS) measurements were performed using a DynaPro Nanostar (Wyatt Technology). Protein samples at 5–6 M in aggregation buffer were incubated at 20C and centrifuged at 21,000 g for 30min prior to the measurements, equilibrated and verified for stability in DLS at 25C, and then the temperature was ramped to 50C at 0.25C per minute. Each timepoint was measured five times, with an acquisition time of 6s, filtered for only those runs with a baseline deviation of less than 0.003 to remove spurious readings. The apparent hydration radii reported are cumulant radii calculated using Dynamics software (Wyatt Technology).

2.6.17 Absorbance

For aggregation studies, absorbance data was collected on a Jasco J-715 spectropolarimeter equipped with Jasco PFD-425S temperature control unit. Proteins were dialyzed into assay buer (20mM HEPES, 175mM KCl, pH 7.4) and this buer alone was preheated to the desired temperature in a 1cm quartz cuvette, with a magnetic stir bar at full speed to prevent settling of large particles during the experiment. Protein sample at the desired concentration was added after temperature equilibration, and 550nm absorbance readings were collected at 1-second intervals. Absorbance dierences were calculated by subtracting the minimum of the first five readings.

2.6.18 Supernatant/pellet fractionation of AME Aminoacylation assay

Filter-based aminoacylation reactions were performed at 30C in 20mM HEPES-KOH, 150mM NH4Cl, 100uM cold Met, 10mM MgCl2, 0.1mM EDTA, 5mM DTT, 4mM ATP, 0.5 Ci/L 35S- methionine, 40 M total yeast tRNA and AME or Mes1 enzyme. Heat shock was performed on enzymes at 4M at 46C for 15 minutes or 95C for 5 minutes immediately prior to the aminoacylation reaction, then diluted to 10 the reaction concentration. Reactions were run for 10 minutes and quenched in cold 10 % trichloroacetic acid (TCA) before spotting on filter disks in a vacuum apparatus. Filters were washed with 2 mL cold 10 % TCA and 1 mL cold ethanol, dried, and exposed to a phosphorimager screen for quantification with ImageLab software (BioRad). Aminoacylation reactions for tRNA microarray analysis were performed at 30C in 50 mM HEPES KOH (pH 7.5), 100 mM potassium glutamate, 10 mM magnesium acetate, 1 mM DTT, 2 mM ATP, 2.5 Ci/L 35S-methionine, 40 M total yeast tRNA and 1 M AME enzyme prepared as above. Microarray analysis of tRNA charging was performed as previously described ([181, 182]).

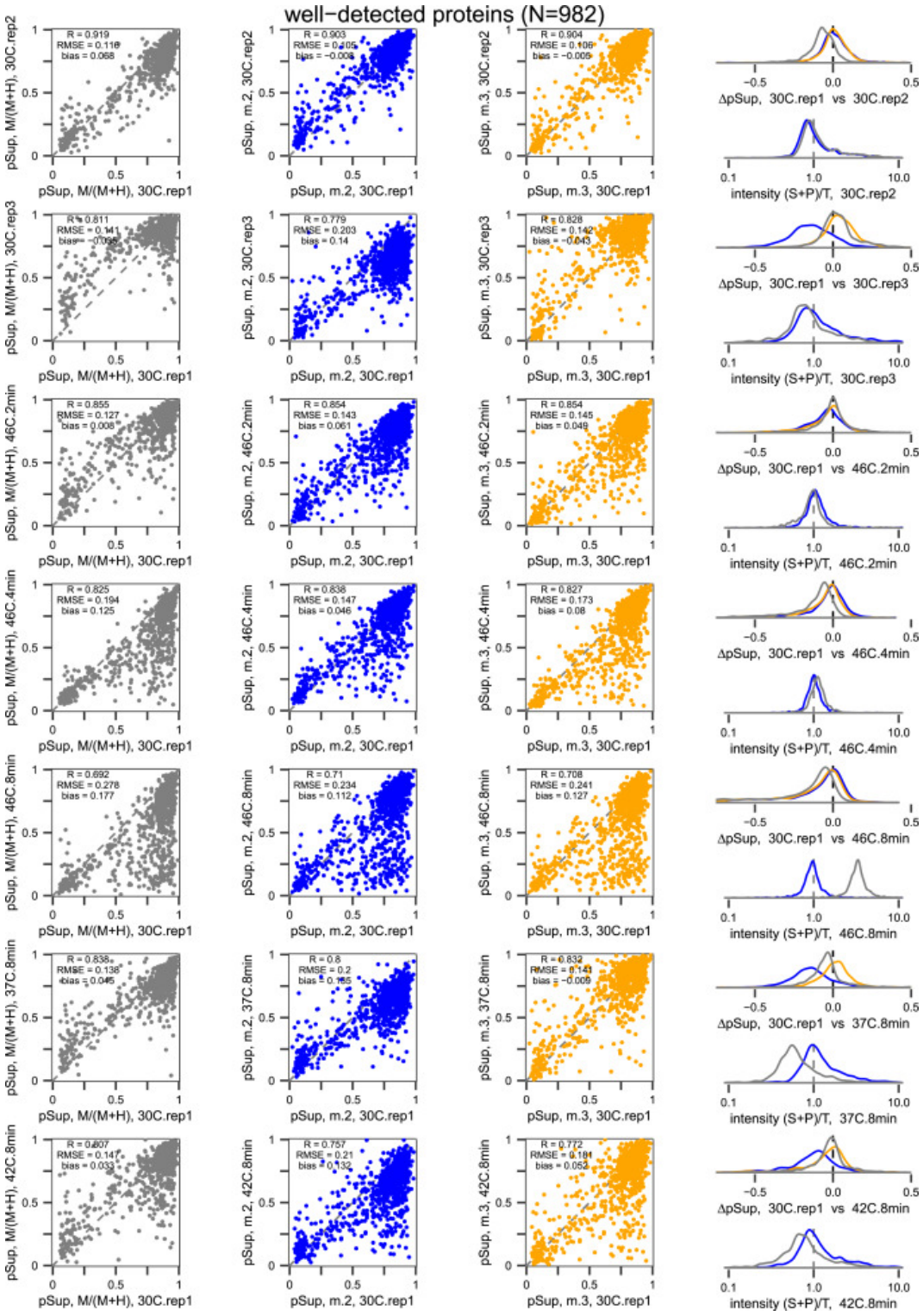

Figure 2.8: **Statistical Models Estimate Proportion in Supernatant Reproducibly between Biological Replicates, Related to Experimental Procedures and 2.1**
Continued on the next page.

Figure 2.8: 2.8 continued. For the scatter plots, each dot represents a well-detected protein, x-axes are estimates of proportion in supernatant (pSup) from unshocked (30°C) replicate 1, and y-axes are pSup estimates from other conditions and replicates. R is Pearson's correlation coefficient, RMSE is root mean squared error, bias is mean difference, in pSup between condition (as y axis) and control (30°C, rep 1). Left column (gray) naively estimates pSup as the median of the ratios M/(M+H) across peptides (M, medium intensity; H, heavy intensity). Middle column (blue) estimates pSup with the Bayesian model correcting for noise and mixing variability. Right column (gold) further normalizes for dynamic range, applied to output of the Bayesian model. See Supplemental Experimental Procedures for details. Distribution plots of difference (D) in pSup use the same colors and data as the scatter plots. Distributions of (S+P)/T compare proteinwise summed intensity on a log-scale, before (gray) or after (blue) correcting for mixing ratio using estimates from the Bayesian model.

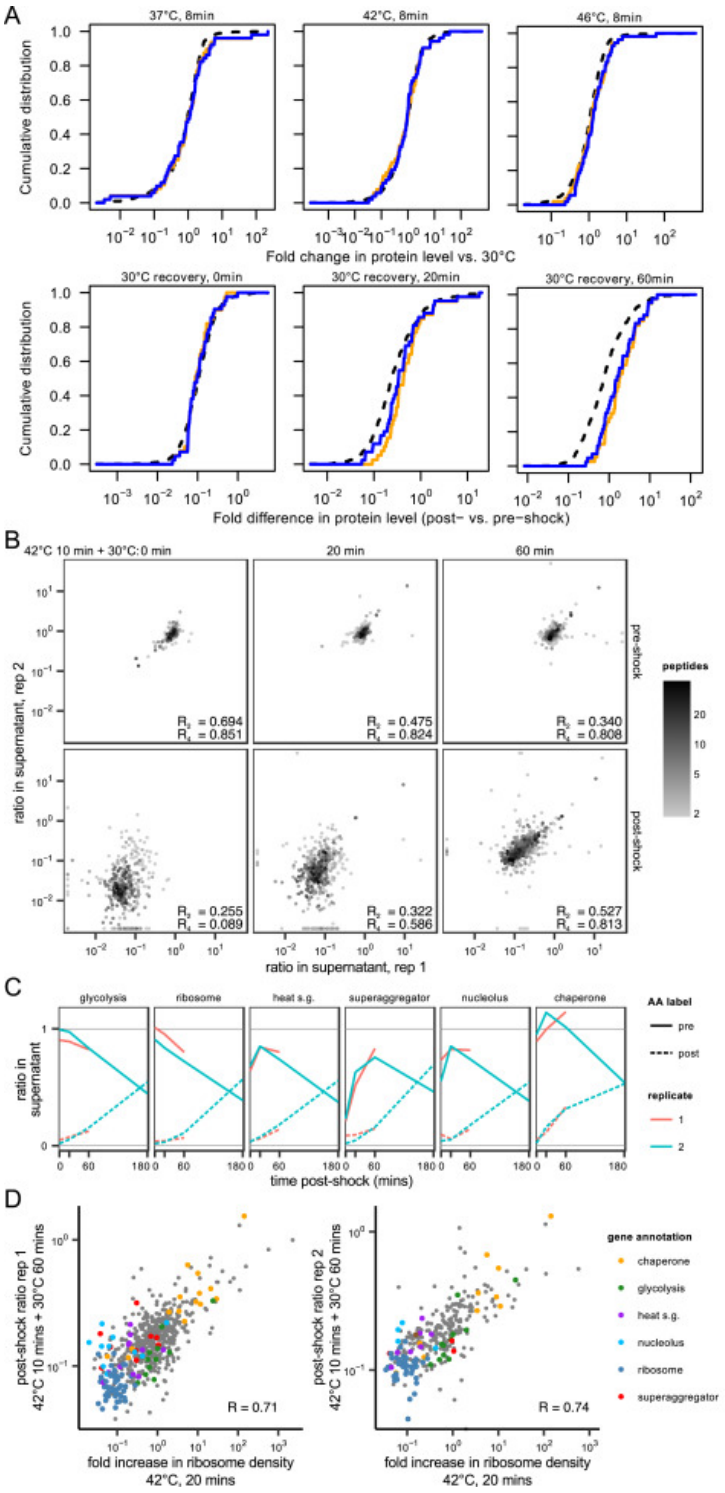

Figure 2.9: **No Detectable Protein-Level Heat-Shock Response during 8 min Heat Shocks; Detectable Responsed uring Recovery, Related to 2.1 2.6**
Continued on next page.

Figure 2.9: 2.9 continued. (A) Top, fold change in protein levels during 8 min treatments relative to the 30°C control. Bottom, fold difference in protein levels, comparing new synthesis to pre-shock levels, during recovery from a 10 min, 42°C shock. All comparisons show ratios of protein LC-MS/MS intensities. Dashed black line shows all well-detected proteins, orange line shows proteins from genes with at least 5-fold induced mRNAs after a 42°C, 10 min shock [169], and blue line shows proteins from genes whose translational induction, assessed by ribosome profiling, increases by at least 5-fold after a 42°C, 20 min shock [161]. By Wilcoxon signed-rank test, all differences are insignificant ($p > 0.02$ with no multiple-testing correction) with the exception of the 60 min recovery time point, where both transcriptional and translationally upregulated genes are also induced at the protein level in our study ($p < 10\text{-}4$). (B) Ratios in supernatant for pre-shock and post-shock labeled amino acids at all time points measured in both datasets; Pearson correlation coefficients (R) are shown filtered by minimum number of peptides detected per protein (2 or 4), and points are shaded by minimum number of peptides detected, starting with 2. The higher dispersion and lower correlation for proteins with fewer detected peptides indicates that much of the dispersion is due to measurement noise in peptide detections. (C) Median trajectories of ratios for protein groups in replicates of recovery dataset. (D) New protein synthesis, as measured by post-shock:unshocked amino acid ratio in supernatant, correlates with increased ribosome occupancy measured by Gerashchenko and Gladyshev (2014), for both replicates. Proteins are filtered to be well-detected in the recovery dataset (2 or more unique peptides detected per protein) and in the ribosome occupancy dataset (rpkm R 10 in shocked and unshocked samples), and outliers Nnt1 and Vps4 are excluded from the plots, but included in the correlation coefficient.

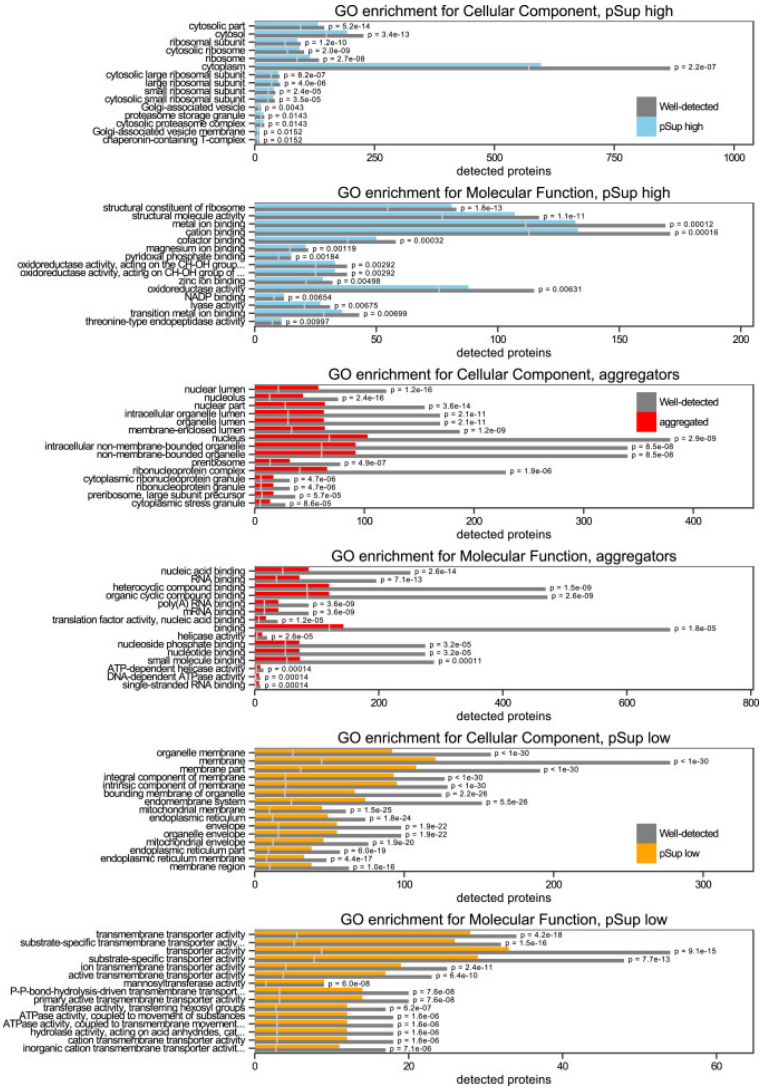

Figure 2.10: **Gene Ontology Terms Enriched in High and Low pSup Proteins and Heat-Aggregating Proteins, Related to 2.1** Enrichment analyses were performed to test, which gene ontology (GO) terms were enriched in proteins with high and low pSup, compared to the null expectation of random binomial assignment (gray vertical line). High pSup are those well-detected proteins with mean pSup > 0.5, and low pSup those with mean pSup < 0.5, excluding aggregating proteins. GO terms were taken from SGD [148], and calculations were done using Fisher's exact test, with the topGO package [170]. Aggregating proteins were identified as described in experimental procedures.

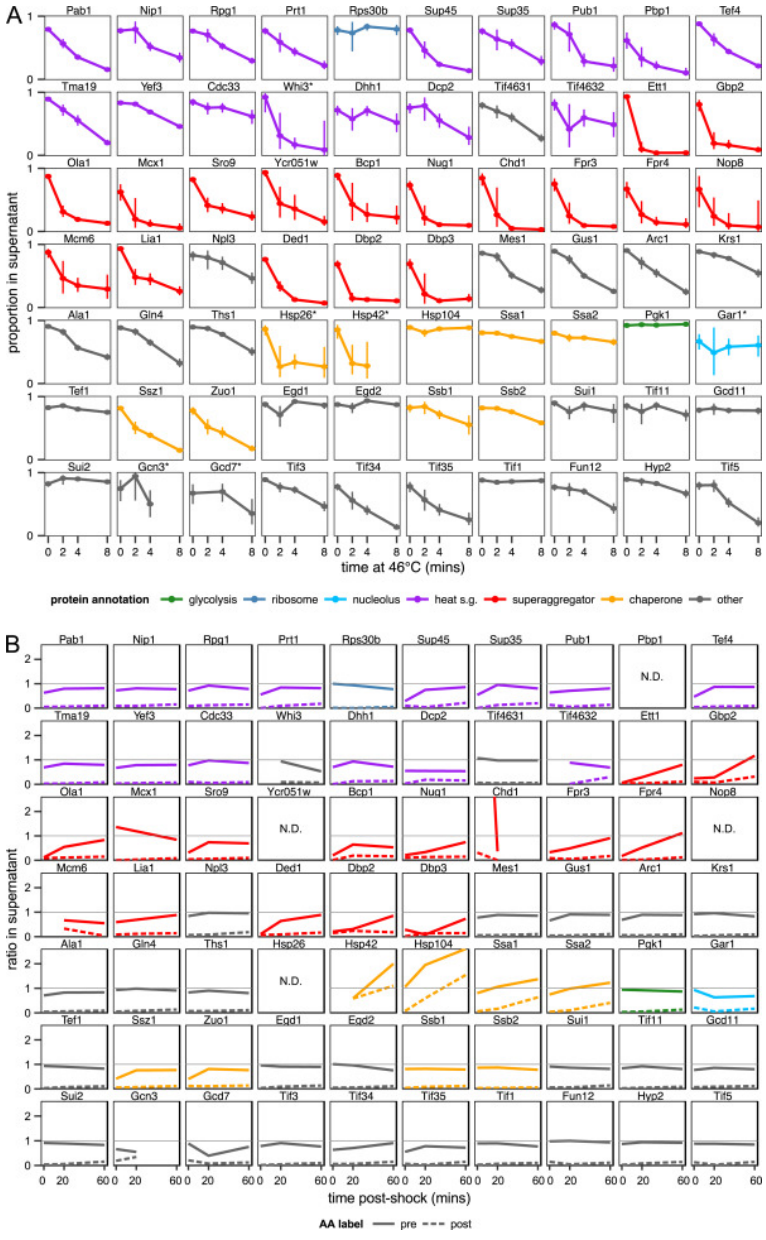

Figure 2.11: **Heat Aggregation and Disaggregation of Select Proteins, Related to 2.1**

Continued on next page.

Figure 2.11: 2.11 continued. (A) Proportion in supernatant (pSup) during 46°C time course is shown for proteins mentioned in the text, including heat shock granule components, superaggregators, molecular chaperones, tRNA synthetases and translation factors. Median estimate (point) and central 95% Bayesian credible interval (vertical interval) are displayed. Genes indicated by asterisk (*) are not well-detected. Fpr3 and Fpr4 are nucleolar proteins and superaggregators, here colored as superaggregators. (B) Ratios in supernatant of select proteins during recovery from heat shock. Replicate 1 is shown; data from all detected proteins, in both replicates, are included in supplemental data and are visualizable online at http://drummondlab.org/endogenous-aggregates. Ratio in supernatant is shown for all proteins mentioned in the results section, and all superaggregators; some proteins (e.g., Tif4632) are detected at only some time points and others (e.g., Pbp1) are not detected. The value at 0 min for Chd1 lies above the y axis limits. Fpr3 and Fpr4 are nucleolar proteins also classified as superaggregators.

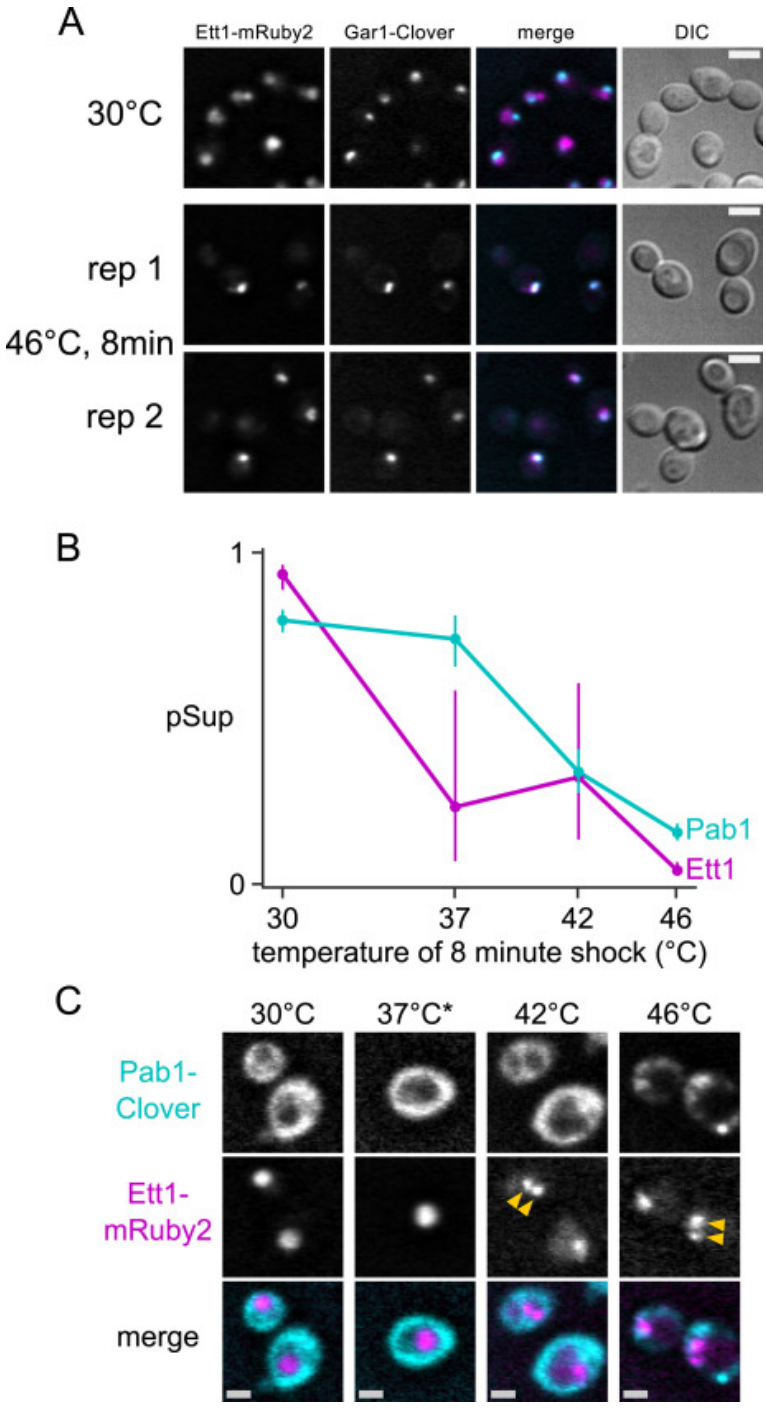

Figure 2.12: **Ett1 Relocalizes to the Nucleolar Periphery during Heat Shock, and Its Rapid Aggregation Is Detectable without Formation of Fluorescent Foci, Related to 2.2 and 2.3**

Continued on next page.

Figure 2.12: 2.12 continued. (A) Ett1 and Gar1 localization converge upon heat shock. Gar1 is a nucleolar marker that does not aggregate during heat shock. Ett1-mRuby2 and Gar1-Clover fusions show distinct nuclear localization of the two proteins at 30°C, with closer association after 8 min heat shock at 46°C. Scale bar represents 5 mm in all panels. (B) Proportion in supernatant (pSup) for Pab1 and Ett1 after an 8 min heat shock at varying temperatures; 95% credible intervals are shown. (C) Microscopy of fluorescently tagged Pab1 and Ett1 at 30°C, after 10 min (noted by *) treatment at 37°C, or 8 min treatment at 42°C or 46°C. Formation of pelletable aggregates is detected in conditions where no foci are visible, for Ett1 at 37°C, and for Pab1 at 42°C. Arrows indicate instances of multiple nuclear Ett1 foci.

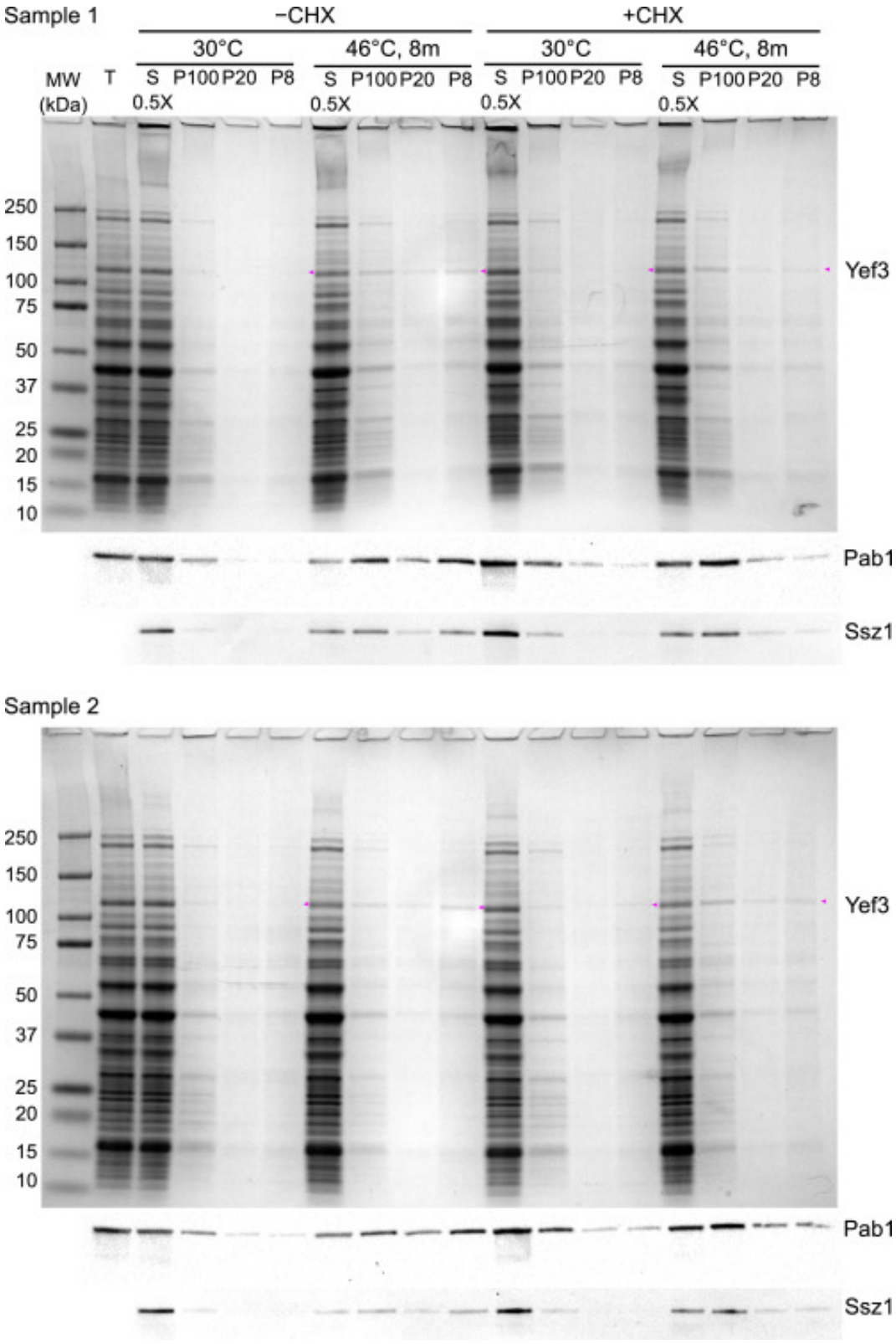

Figure 2.13: **Heat-Triggered Protein Aggregation Does Not Require Ongoing Translation, Related to 2.3**

Continued on next page.

Figure 2.13: 2.13 continued. After 8 min at 46°C some proteins, indicated by arrows, aggregate in response to heat, regardless of cycloheximide treatment. Two biological replicates are shown of denaturing protein gel (SDS-PAGE, Coomassie stained) analysis of fractionated cell lysate, with and without heat shock, with and without 100 mg/ml cycloheximide treatment (see methods), and anti-Pab1 and anti-Ssz1 western blots from identically loaded gels (total protein sample was not loaded for Ssz1 gels). Quantification of the blots is shown in 2.3.

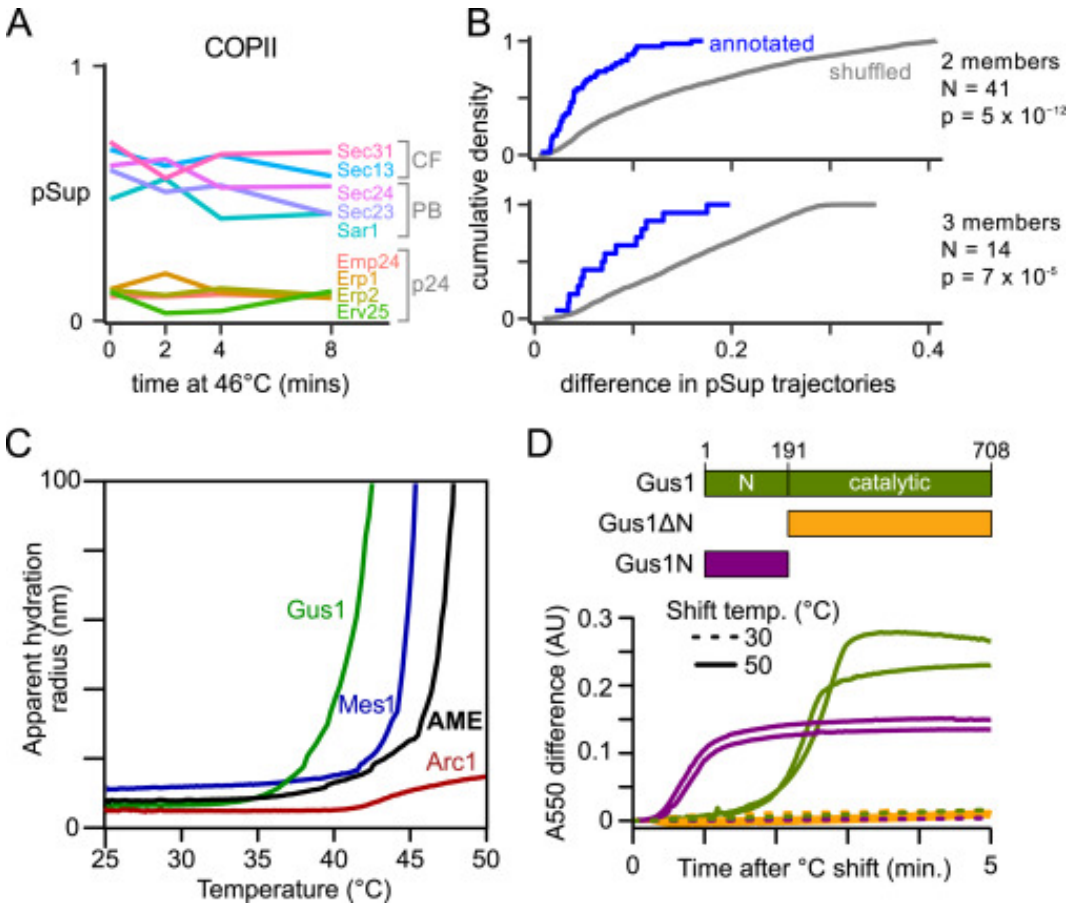

Figure 2.14: **Complexes Coherently Aggregate and Show Component- and Domain-Specific Aggregation Propensity, Related to 2.4**
Continued on the next page.

Figure 2.14: 2.14 continued. (A) The COPII coat protein complex consists of three subcomplexes, whose proportion in supernatant (pSup) tracks their degree of membrane association. The COPII complex, which transports proteins from the ER to the Golgi, consists of a constitutively membrane-associated p24 complex (Erp1, Erp2, Emp24, and Erv25), the prebudding complex (PB; Sec23/Sec24 dimer, Sar1), which initially binds the ER membrane to form a vesicle, and the remaining vesicle coat-forming (CF) Sec13/Sec31 tetramer. Across all heat shock treatments, we observed the p24 complex pelleted and the other vesicle coat proteins partially pelleted; the prebudding complex has lower pSup than the late-binding coat-forming components. (B) Proteins annotated to the same complex have similar pSups across heatshock time points. For each complex annotated in CYC2008 [158] with 2 or 3 well-detected proteins, we compute the intracomplex mean-squared distance in pSup across time points, and plot the cumulative density (blue line). As a null distribution, we sampled 2000 pairs or triplets of well detected proteins and estimate intracomplex distance in pSup (gray line). We present p-vales for a one-sided Wilcoxon rank test of the hypothesis that the intracomplex distance for annotated complex is less than for randomly sampled complexes. These distributions are clearly different, despite some annotated complexes consisting of stable subcomplexes, each of which has pSup more similar that the supercomplex, as for COPII. (C) Particle size versus temperature for recombinant AME components (Arc1, A; Mes1, M; Gus1, E) and reconstituted AME complex measured by dynamic light scattering (DLS). (D) Aggregation of full-length Gus1 and subdomains measured by absorbance at 550nm (A550).

CHAPTER 3

CHARACTERIZATION OF POLY(A)-BINDING PROTEIN PHASE SEPARATION (RIBACK AND KATANSKI ET AL. 2017)

The material presented in this chapter appears as published work, followed by related unpublished results. While this work was not among the first examples of phase separation in biology it was an important contribution to the field for several reasons. In addition to establishing a new experimental system, poly(A)-binding protein (Pab1), we also were able to finely tune the phase separation properties of Pab1 and show that these changes had an effect on cellular fitness.

Josh Riback, co-first author, pioneered use of dynamic light scattering and SAXS here, in the study of phase separation and intrinsically disordered domains. Jamie Kear-Scott performed microscopy on both live cells and on purified Pab1 assemblies. Jamie also performed *in vitro* pelleting experiments of Pab1 characterizing bulk aggregation properties. Evgeny Pilipenko performed size-exclusion chromatography experiments to understand the size of Pab1 assemblies and the behavior of associated RNA. Alexandra Rojek performed initial experiments detecting the heat-triggered demixing of purified Pab1.

I generated and characterized yeast strains, including finding growth conditions, testing RNase sensitivity of assembles, and characterizing differences in assembly dynamics. Specifically, I generated the biological samples and performed western blotting for figure 3.1B, establishing RNase insensitivity for Pab1 assemblies *in vivo*. Next, I generate yeast strains with modified P-domains. Since Pab1 is an essential gene it can't be simply deleted then replaced. Preliminary work also revealed that the 3' UTR is empirically important for regulating protein expression levels. For these reasons, I had to design a scheme to modify this protein domain, and leave the endogenous 3' UTR. The strains generated using this technique were used for western blotting and phenotypic characterization in 3.6D, F, H, 3.16, and 3.17.

Additional data included here explore other phenotypes associated with the hydrophobicity of the Pab1 P domain. Results exploring the detection of starvation induced assemblies are presented, followed by a brief exploration into cell-sized assemblies and the effects of RNase and intracellular pH on Pab1 demixing *in vivo*.

3.1 Summary

Stress-Triggered Phase Separation Is an Adaptive, Evolutionary Tuned Response

Authors:

Joshua A. Riback, Christopher D. Katanski, Jamie L. Kear-Scott, Evgeny V. Pilipenko, Alexandra E. Rojek, Tobin R. Sosnick, D. Allan Drummond (2017) Cell 168 (10281040)

In eukaryotic cells, diverse stresses trigger coalescence of RNA-binding proteins into stress granules. *In vitro*, stress-granule-associated proteins can demix to form liquids, hydrogels, and other assemblies lacking fixed stoichiometry. Observing these phenomena has generally required conditions far removed from physiological stresses. We show that poly(A)-binding protein (Pab1 in yeast), a defining marker of stress granules, phase separates and forms hydrogels *in vitro* upon exposure to physiological stress conditions. Other RNA-binding proteins depend upon low-complexity regions (LCRs) or RNA for phase separation, whereas Pab1's LCR is not required for demixing, and RNA inhibits it. Based on unique evolutionary patterns, we create LCR mutations, which systematically tune its biophysical properties and Pab1 phase separation *in vitro* and *in vivo*. Mutations that impede phase separation reduce organism fitness during prolonged stress. Poly(A)-binding protein thus acts as a physiological stress sensor, exploiting phase separation to precisely mark stress onset, a broadly generalizable mechanism.

3.2 Introduciton

Eukaryotic cells react to a wide range of stresses with a consistent set of responses: transcribing genes encoding stress-responsive proteins, slowing translation of most mRNAs, and assembling hundreds of proteins and mRNAs into massive ribonucleoprotein (RNP or mRNP) stress granules [183, 19, 35]. Heat stress, starvation, hypoxia, treatment with metabolic inhibitors, and other unfavorable changes trigger stress granule formation across a wide array of organisms [19, 35, 184, 54]. Although stress granule composition varies somewhat by stress [144, 64], certain proteins are consistently recruited, such as poly(A)-binding protein (PABP; Pab1 in budding yeast) [183], an abundant RNA-binding protein, which plays key roles in mRNA polyadenylation, stability, and translational control.

Stress granules fall into a large class of protein- and RNA-rich cellular structures, including germline P granules, P bodies, and nucleoli, which do not rely on membranes for their physical coherence [76, 80, 54, 67]. In groundbreaking work, multiple groups have reported purified proteins (including stress-granule-associated proteins FUS, hnRNPA1/2, Whi3, and others) forming physically coherent hydrogel and phase-separated liquid states *in vitro* [66, 88, 65, 67, 185, 68].

Liquids, hydrogels, dynamic fibers, colloids, and related massive networks of interacting molecules share, as a defining feature, a lack of fixed stoichiometry, unlike typical quaternary structures. Consequently, they have been termed quinary structures [62, 63, 64]. Formation of quinary structures often involves multivalent interactions between groups of binding partners [165]. Quinary interactions and colocalization into cellular-scale structures are, in certain cases, distinct processes. For example, stress-triggered quinary assemblies form during mild stress conditions, where stress granule formation does not occur, and when stress granules are pharmacologically blocked [64].

Many studies of quinary behaviors have focused on the role of so-called low-complexity regions (LCRs), protein sequences consisting of a biased subset of amino acids. Multiva-

lent interactions between LCRs can suffice to cause liquid-liquid phase separation, amyloid formation, and other demixing phenomena *in vitro* [69, 66, 65, 67, 68].

Phase separation by stress-granule-associated proteins *in vitro* has generally required conditions unrelated to stress-granule formation. Temperatures well below physiological range have been used to stimulate phase separation [67, 185]. Hydrogel formation by RNA binding proteins [66, 67] requires high concentrations and low temperatures. These studies illuminate a range of achievable material states. However, the link between these states and physiological stresses including heat, respiratory chain inhibition, and starvation is not readily apparent.

Moreover, stress-related fitness effects arising from disrupting the quinary behavior of stress-granule-associated proteins have remained elusive. A major challenge is to identify whether and how demixing by RNA-binding proteins relates to an organism's stress tolerance.

Toward that end, we have turned our attention to the core stress-granule marker poly(A)-binding protein itself. Like its orthologs across eukaryotes, poly(A)-binding protein (Pab1) in budding yeast consists of a short N-terminal leader sequence; four RNA-recognition motifs (RRMs); a proline-rich LCR termed the P domain, which is predicted to be intrinsically disordered; and a C-terminal peptide binding domain. Pab1 is known to self-interact [119], although this behavior has not been linked to stress or to phase separation. We show that Pab1 phase separates and gels in response to physiological thermal and pH stresses, a demixing process, which is modulated by the P domain but does not require it. Extracting information from unusual evolutionary patterns, we make mutational perturbations, which systematically alter the temperature onset of phase separation *in vitro* and demixing *in vivo*. Mutations that reduce the thermal and pH sensitivity of Pab1's demixing reduce fitness during growth at high temperature and during energy depletion, indicating that demixing is adaptive. Together, our results illuminate a uniquely complete path from evolved sequence features, to phase separation, to stress-triggered demixing, and finally to organism fitness

during stress.

3.3 Results

3.3.1 Pab1 Forms RNase-Resistant Quinary Assemblies in vivo during Heat Stress

Pab1 shows diffuse localization under favorable growth conditions (near 30°C) and localizes to stress granules—large cytosolic foci—within minutes of a shift to 46C (3.1 A). At 42°C, Pab1 is not recruited to stress granules detectable by standard fluorescence microscopy (3.1 A [[19, 64]]).

Consistent with these results, after 10 min at 42°C, pelletable quinary assemblies of Pab1 formed in the absence of Pab1-marked stress granules (3.1). After a more severe shock at 46°C, a greater proportion of Pab1 is recruited into small and large sedimentable assemblies (3.1) coincident with stress-granule formation.

Pab1 may form quinary assemblies by binding to RNA or through protein-protein interactions. To distinguish between these, we measured Pab1 pelleting after RNase treatment (3.1 B). Pelletable Pab1 from cells grown at 30°C was largely liberated by RNase (3.1 B and C). By contrast, RNase had little effect on assemblies formed at 42°C and no effect after 46°C shock (3.1 D). Mirroring RNase-resistance observed in yeast and mammalian stress granules ex vivo ([184]), our data indicate that both pre-granular quinary assemblies and stress-granule-associated Pab1 are RNase resistant.

Either the quinary assemblies of Pab1 *in vivo* do not depend on RNA for their integrity, or stabilizing RNAs are efficiently protected from RNase cleavage. We therefore asked how Pab1 demixing depended upon RNA *in vitro*.

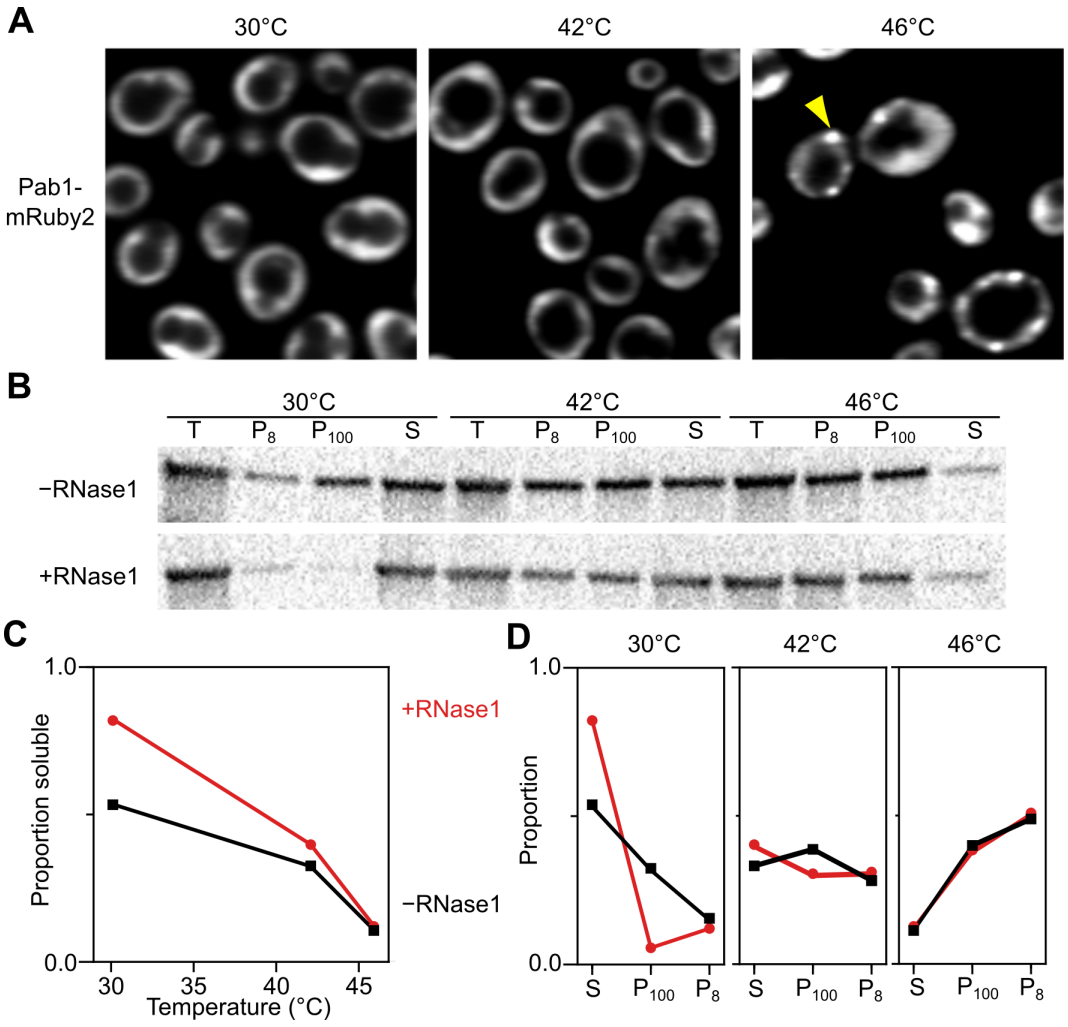

Figure 3.1: **Heat Stress Triggers Formation of RNase-Insensitive Pab1 Quinary Assemblies, Separable from Stress Granule Formation** (A) Confocal fluorescent microscopy images of diploid strains, containing Pab1-mRuby2 and Pab1-Clover, showing Pab1-mRuby2 after 8 min incubation at the indicated temperatures. Arrow indicates a stress granule. (B) Pab1 western blot after 10 min heat shock of WT cells. Lysed samples were incubated with or without RNase1, then progressively fractionated at 8,000 g and 100,000 g yielding pellets (P8 and P100, respectively) and remaining supernatant (S). (C and D) Quantification of (B), where each fraction is normalized to the total intensity in all fractions. Red or black indicate RNase1 or buffer treatment, respectively.

3.3.2 Pab1 Demixing Is Promoted by Physiological Stress-Related Conditions in vitro and Inhibited by RNA

We purified recombinant yeast Pab1 from E. coli and assessed Pab1 demixing *in vitro* under physiological conditions (see Methods). We first asked how Pab1 responded to heat stress with and without polyadenylate RNA, monitoring the soluble fraction by gel filtration and the insoluble fraction on a denaturing gel. We found that 15 μM Pab1 (physiological 20 μM, see Methods) was soluble at 30°C but demixed to form large particles after a 46°C, 30 min treatment (3.2 A and B). Pab1 binds 12 nucleotides of poly(A) RNA with full affinity and protects a footprint of roughly 25 nucleotides [105]. To promote 1:1 binding, we incubated Pab1 with a small excess of 19-mer polyadenylate RNA (A_{19}). After shifting to 46°C for 30 min, Pab1:RNA complexes partially dissociated, with the free protein demixing into large particles and the released A_{19} returning to the free pool (3.2 A and B). These results indicate that Pab1 releases RNA and demixes, forming particles stabilized by protein-protein interactions, consistent with its behavior *in vivo* (3.1).

To obtain more-sensitive measurements, we used dynamic light scattering (DLS) and monitored the apparent hydration radius (Rh) of a 15 μM Pab1 solution during a slow (0.25°C/min) temperature ramp in the presence of increasing amounts of A_{19}. Rapid particle growth in a narrow temperature window indicated the onset of demixing. We define the demixing temperature (T_{demix}) as the temperature at which the apparent hydration radius doubles relative to its baseline value. Anticipating results below, T_{demix} represents a measure of the lower critical solution temperature (LCST), above which the solution separates into protein-rich and protein-depleted phases. Adding RNA increasingly inhibited Pab1 demixing (3.2 C and D).

Alone, Pab1 remained monomeric in shifts up to 33°C (3.2 E); at these temperatures, *S. cerevisiae* grows robustly. When shifted to 36°C and above, the onset of the heat-shock response, Pab1 demixed at increasing rates such that by 42°C, where Pab1 *in vivo* assemblies

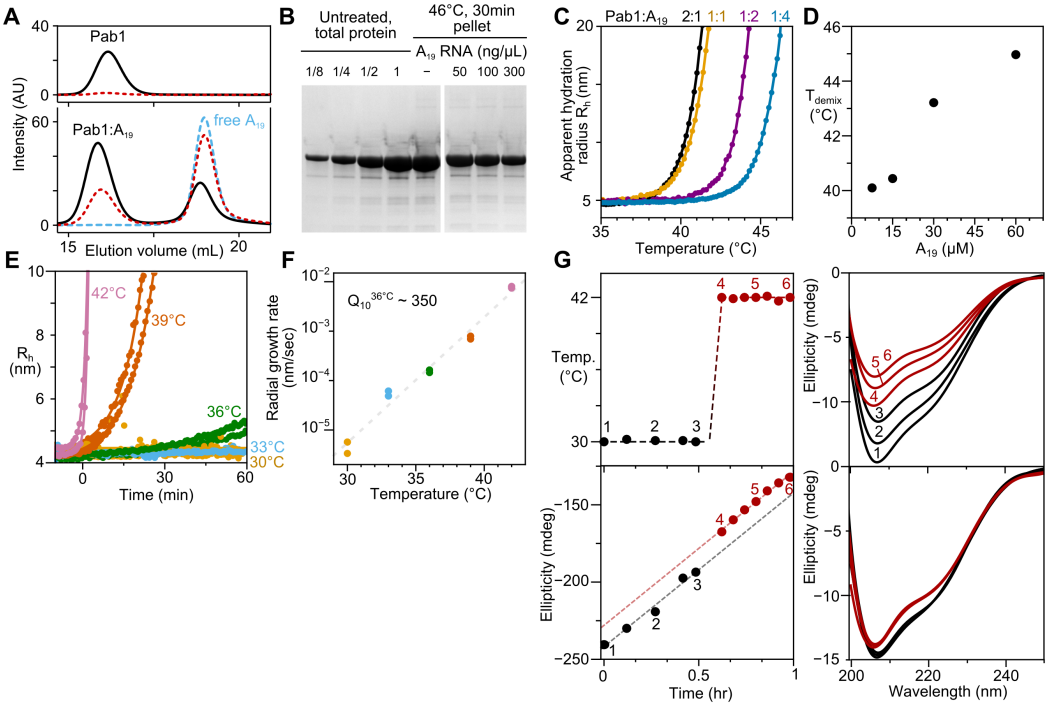

Figure 3.2: **Purified Pab1 Demixes in Response to Thermal Shock, Releasing RNA with Small Changes in Secondary Structure** (A) Top, size-exclusion chromatography trace of Pab1 after 30°C incubation (black) and after heating at 46°C for 30 min (red). Below, Pab1 with 2:1 excess of A_{19} RNA treated identically. Blue trace shows A_{19} alone. (B) Pab1 total-protein dilution for calibration (left) and pelleted material after heating with and without RNA (right), Coomassie-stained. (C) DLS temperature ramp experiments of Pab1 with indicated protein to RNA ratios. (D) T_{demix} at RNA concentrations from (C). (E) Kinetics of Pab1 assembly monitored by DLS after a temperature jump (see also 3.12). (F) Rate of hydration radius growth from (E) with the accompanying average $Q_{10}{}^{36°C}$ value. (G) Temperature jump of 0.2 μM Pab1 (top left, with numbered full-scan time points indicated) and accompanying CD spectra (top right). Total ellipticity between 210 and 250nm (bottom) shows linear temperature-independent signal attenuation used to scale scans to time zero (bottom right) (3.13).

are detectable after 10 min (3.1 B), *in vitro* demixing occurs within seconds (3.2 E). Demixing halted, but did not reverse, when the temperature was returned to 30°C, indicating lack of self-propagation of quinary assemblies and undetectable reversibility at these timescales (3.12).

The remarkable acceleration in Pab1 demixing over a few degrees can be quantified by the temperature coefficient, Q_{10}, the ratio of biological properties measured 10°C apart (see Methods) ([8, 167]). Typical biological processes have a Q_{10} of 2–4. The radial growth rate of Pab1 assemblies shows a ${Q_{10}}^{36°C}$ of 350 (3.2 F), placing a conservative lower bound on the volume growth rate.

3.3.3 Pab1 Does Not Thermally Denature Prior to Heat-Induced Demixing in vitro

To monitor temperature-dependent structural changes of Pab1 *in vitro*, we used far-UV circular dichroism (CD) spectroscopy. A dilute sample (0.2 μM, to inhibit demixing) was scanned at 30°C for 30 min, shifted to 42°C, and scanned for a further 30 min (3.2 G). The CD signal linearly decreased with time at both temperatures following similar kinetics, consistent with adsorption to the cuvette (3.2 2G). To account for this effect, we linearly extrapolated each scan to time zero, yielding scaled spectra (3.2 G, bottom right). At both 30°C and 42°C, the CD spectrum has a broad negative signal between 200 and 230 nm, consistent with a largely α/β protein. The spectrum at 42°C shows slightly reduced signal between 205 and 230 nm, inconsistent with global denaturation but compatible with a limited conformational change. A similar decrease is seen in the corresponding measurement for RRM1-3, which also undergoes phase separation (3.13 A and B). *In vitro* demixing does not involve a cooperative global unfolding transition by the bulk of the Pab1 molecules, although different effects may occur *in vivo*.

3.3.4 Pab1 Quinary Assemblies Form by Phase Separation and Gel Formation

To examine the physical forces contributing to Pab1 demixing, we asked how changes in ionic strength and pH affected demixing. At or below physiological ionic strength, Pab1 demixed readily at 46°C. At higher salt concentrations, however, demixing was almost completely inhibited (3.3 A and 3.14 A–C), suggesting an electrostatically mediated process. Demixing was also pH dependent, with demixing inhibited above physiological pH values (pH 7 during exponential growth, 6.5 or lower following heat shock). Below pH 5.5, normal growth temperature (30°C) sufficed to induce demixing (3.3 A).

To visualize Pab1 quinary assemblies, we doped a fluorescent Pab1-mRuby2 fusion at 1:20 ratio into a solution of unlabeled Pab1, triggered demixing, and imaged the sample at room temperature within 1–2 min. Examination of the resulting assemblies revealed branched clusters of micron-scale spherical droplets after heat-induced demixing (3.3 B), which varied in size in untagged samples (3.14 D), and spherical droplets after pH-induced demixing (3.3 B). Denaturation of Pab1 at low pH produced grainy, amorphous particles rather than droplets (3.14 E). Spherical droplets and the appearance of droplets wetting the microscope slide (3.14 F) revealed the existence of a liquid phase at some time, indicating an initial phase separation.

The persistence of clusters indicated that droplets did not coalesce even when in contact, similar to behavior observed in other studies ([65, 67]). To measure the internal dynamics of pH-induced Pab1 droplets, we performed fluorescence recovery after photobleaching (FRAP) experiments. No significant recovery occurred over nearly 7 min (3.3 C). To examine longer timescales, we triggered phase separation in a 1:20 Clover (green):unlabeled Pab1 solution, waited 5 min, then added 1:20 mRuby2 (red):unlabeled Pab1 solution, forming two-layer droplets. Layers remained intact over 24 hr, indicating little or no mixing (3.3 D).

Plotting Pab1 demixing temperatures observed in temperature-ramp light-scattering ex-

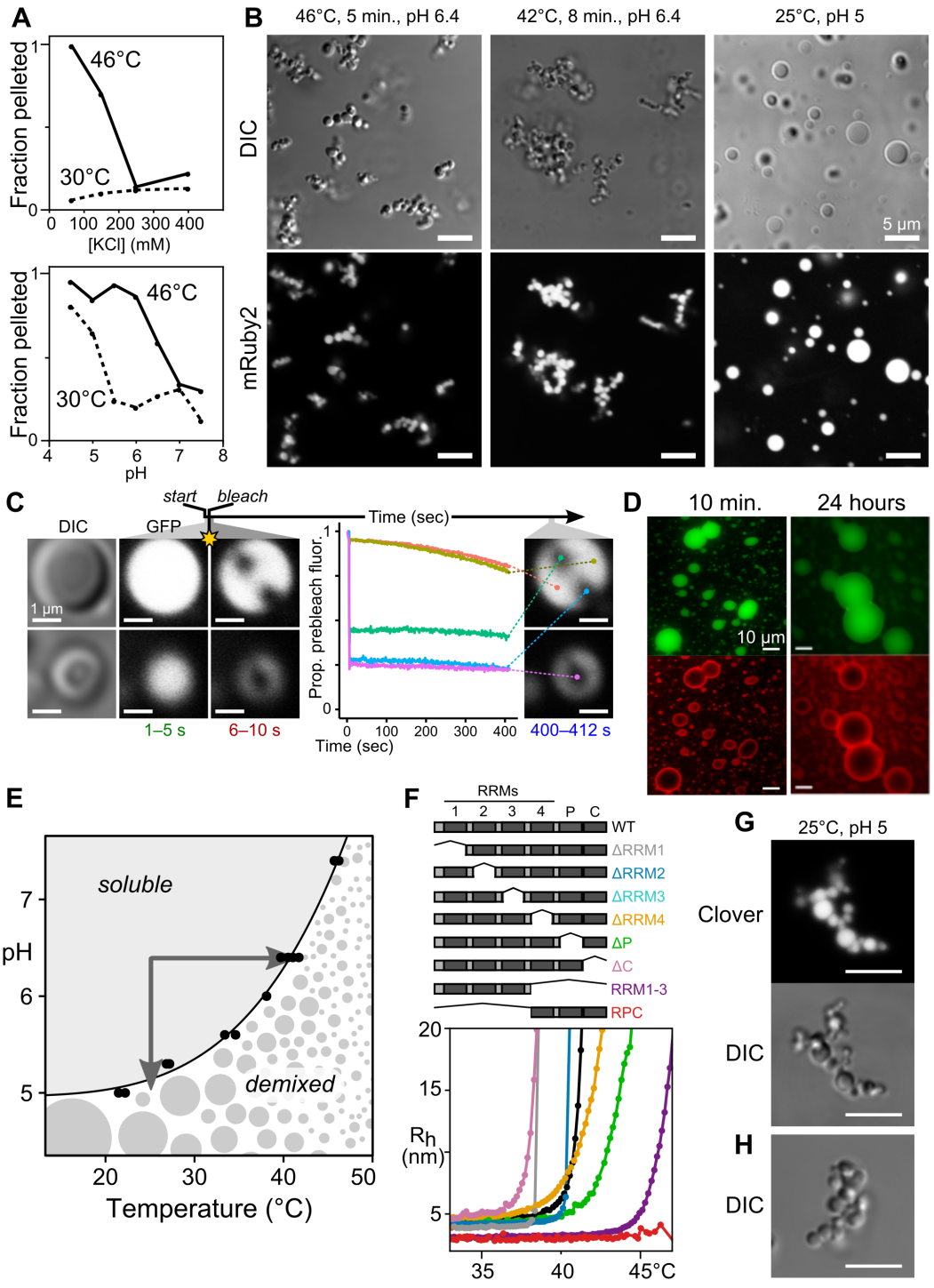

Figure 3.3: **Pab1 Demixing Proceeds via Liquid-Liquid Phase Separation and Gel Formation, Modulated, but Not Caused, by its Low-Complexity Region**
Continued on the next page.

Figure 3.3: 3.3 continued. (A) Demixing of purified Pab1 is sensitive to ionic strength and pH (3.14). (B) Morphology of 15 μM Pab1-mRuby2 assemblies. (C) Fluorescence recovery after photobleaching of Pab1 droplets. (D) Sequentially assembled two-color droplets remain unmixed after 24 hr. (E) The T_{demix} of Pab1 measured at different pH values defines a phase boundary. (F) Pab1 domain deletions and corresponding DLS temperature ramps (see online publication [61] table S1). (G and H) Morphology of Pab1ΔP quinary assemblies. (G) 15 μM 100:3 Pab1DP:Pab1-Clover. (H) 15 μM Pab1ΔP alone.

periments at varying pH reveals a continuous phase boundary passing through the physiological ranges of these parameters. Crossing this boundary either by raising temperature or lowering pH (3.3 E, arrows) causes demixing.

3.3.5 Deletion of the Proline-Rich LCR Reduces Pab1 Phase Separation in vitro

We then probed the contributions of each of Pab1's six domains to phase separation by purifying deletion variants (3.3 F, see online publication [61] table S1). DLS temperature-ramp experiments revealed that each construct self-associated in a narrow (1°C) temperature range, consistent with phase separation. All single-domain-deletion mutants still demixed by 50°C (3.3 F and 3.13 C). Nevertheless, the deletion of the P domain had the greatest positive effect on T_{demix} (3.3 E). We split Pab1 into its N- and C-terminal halves, RRM1-3 and RRM4-P-C (RPC). RRM1-3 demixed, whereas RPC did not up to 50°C (3.3 E and 3.13 B). These observations reinforce the finding that the P domain is not required for phase separation.

Because the Pab1ΔP lacks an LCR yet retains the ability to phase separate, we examined its assembly morphology by microscopy. Pab1ΔP assemblies largely retained the droplet-cluster morphology of full-length Pab1 quinary assemblies (3.3 G and H). Together, these results point to an electrostatically driven phase separation dependent on molecular determinants in the RRM regions, which is enhanced, but not solely caused, by the P domain.

3.3.6 Natural Selection Shapes Usage of Hydrophobic Residues in Pab1's Low-Complexity Region

To identify the features of the P domain that might enhance demixing, we examined its sequence (3.4 A). As the P domain's name implies, this LCR is rich in proline (19% versus a yeast-proteome-average 4%), along with methionine (10% versus 2%) and glycine (14% versus 5%), and depleted in charged amino acids (3.4 B and 3.15 A). The rest of Pab1 (Pab1ΔP) exhibits similar amino acid frequencies to the proteome average, as did a set of intrinsically disordered regions (IDR) from DisProt ([186]) (minimum pairwise rank correlation $r = 0.72$, $p < 103$ between each of these three sets versus maximum $r = 0.19$, $p = 0.41$ between these and P domain). IDRs tend to be proline-rich (3.4 B). Methionine enrichment, by contrast, we found surprising. The P domain's fractional methionine conent is 5.5-fold higher than the median IDR and greater than 97.5% of these regions.

We turned to an evolutionary analysis, first asking whether these methionines are conserved across species. We constructed a diverse alignment of 351 poly(A)-binding protein orthologs. All but one possess a proline-enriched region, indicating that the P domain's existence is highly conserved (3.4 C, 3.15 B, and C). While profound length variation in these orthologous regions (3.15 B) renders them unalignable, within groups of closely related species where many sites show perfect conservation, no methionine residues are conserved; instead, medium- and long-chain aliphatic residues (M, V, I, L) frequently replace each other (3.4 D).

Rapid yet restricted exchange of aliphatic residues over evolutionary time is consistent with natural selection acting on the hydrophobicity associated with aliphatic composition rather than site-specific residue identities. To look for a signature of selection, we examined the relationship between aliphatic amino acid frequency and hydrophobicity for the P domain, finding strikingly strong log-linear negative correlation in P domains (3.4 E), which was consistent (3.15 D and E, median $r = 0.82$; 98% of PABP LCRs show $r < 0.25$) and not

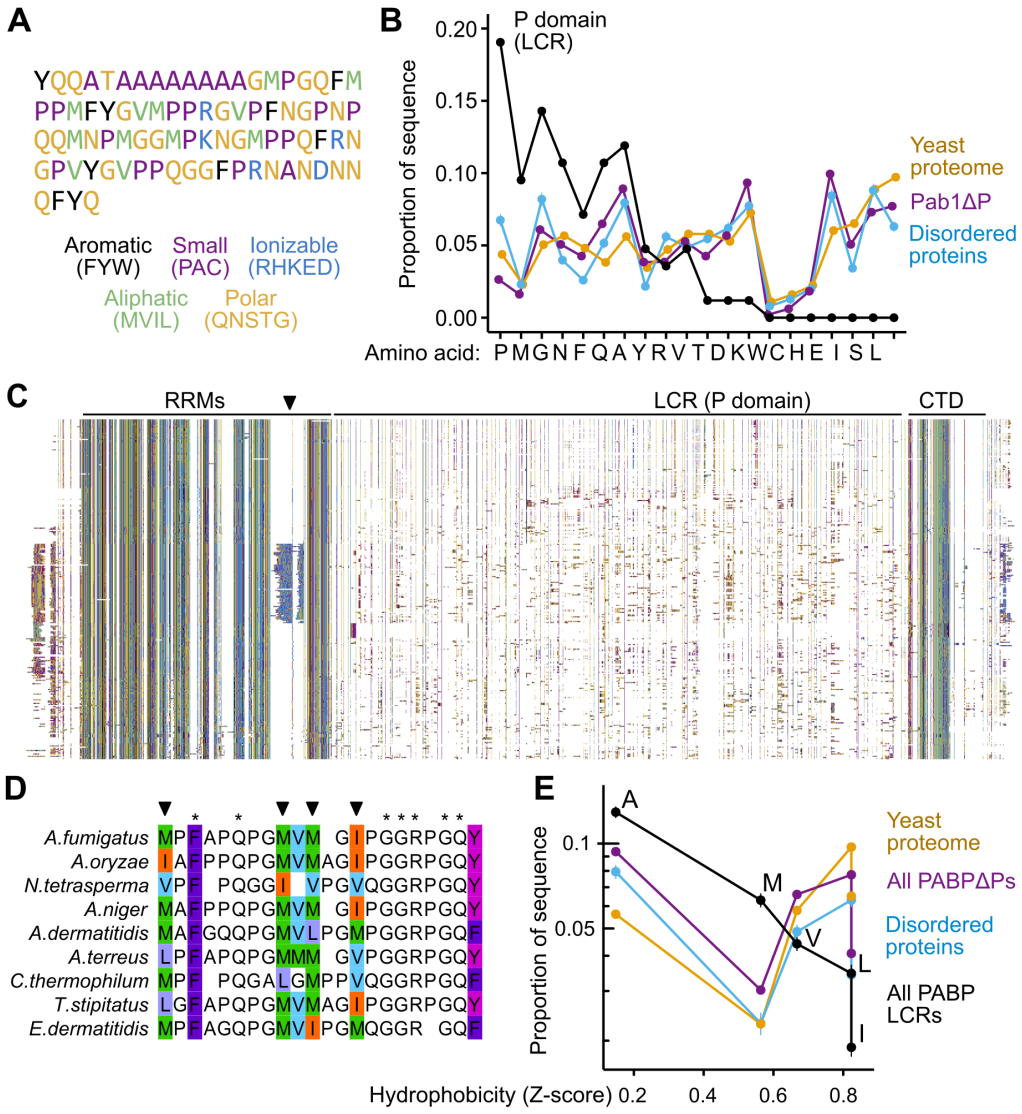

Figure 3.4: **Evolutionary Analysis Reveals Rapid Exchange between Aliphatic Residues in Poly(A)-Binding Protein's Proline-Rich Low-Complexity Region**
Continued on the next page.

Figure 3.4: 3.4 continued. (A) The low-complexity P domain of *S. cerevisiae* Pab1 colored by amino acid types. (B) Amino acid usage in the P domain, ordered by enrichment relative to the rest of Pab1 (Pab1ΔP). Usage for all yeast proteins, and for disordered sequences curated by DisProt, are shown for comparison. (C) A diverse alignment of 295 PABPs (pruned for clarity of display from 351) indicating locations of the RRMs, P domain, and CTD, where each column is a residue, colored as in (A), and each row is a species. White spaces are alignment gaps. The figure contains no text. A black triangle marks a clade-specific insertion in RRM4. (D) A subset of fungal species and a portion of the P domain from the alignment in (C) containing multiple sites where aliphatic residues (colored to show differences) exchange rapidly, while nearby positions (starred) remain invariant. (E) In the P domain, but not in general, aliphatic residue frequency negatively correlates with residue hydrophobicity. The mean aliphatic residue usage in the aligned set of P domains, remainder of PABP, disordered sequences from DisProt, and the yeast proteome are shown, colored as in B. See also 3.15. Error bars throughout show standard error on the mean.

reflected in the rest of the polypeptide (r = 0.36; 69%), the yeast proteome (r = 0.32; 6%), or in DisProt disordered regions (r = 0.06; 31%). The correlation was reliably stronger than in any of the alternative sets (3.15 E, pairwise Wilcoxon rank sum tests $p < 10^{-6}$). These controls indicated that neither local or global biases in sequence composition, nor unusual pressures on disordered domains in general, explain the above observations. We conclude that natural selection has shaped the relationship between residue hydrophobicity and usage among aliphatic residues in the P domain, implying an accompanying fitness advantage.

3.3.7 Hydrophobic Forces Drive Collapse of the Proline-Rich Low-Complexity Region

The results of the evolutionary analysis above led us to ask how altering the evolutionarily conserved features of the proline-rich LCR alters its biophysical and biological properties. To systematically alter the P domain's hydrophobic composition, we made mutant sequences in which all instances of a residue were replaced with another, such as MV/X, where all eight methionines and four valines were replaced with X = I (most hydrophobic), L, V, M, and A (least hydrophobic).

We purified the P domain in isolation and, for the wild-type (WT) and mutants, as

a fusion to a small expression tag, a highly stable variant of protein G ([187]). The CD spectrum of the unfused WT P domain is typical of a denatured protein (3.5 A), and we observe no cooperative thermal unfolding transition from 4–80°C. We conclude that, like many LCRs, the P domain is disordered and lacks stable secondary structure.

Using small-angle X-ray scattering (SAXS), we then probed the size and shape of the P domain. The estimated radius of gyration (Rg) in water is roughly half that of the chain in high levels of denaturant, 2 M guanidinium chloride (GdnHCl) (3.5 B). The expression-tag fusion had a larger Rg than the P domain alone (3.5 C). To extract information about the shape of the P domain from the SAXS data, we built models of the fusion with three different P domain conformations: extended, compact, or contacting the expression tag (3.5 D). The SAXS data are best described by the middle option, where the P domain is largely non-interacting with the expression tag but compact. The tagged P domain has an Rg of 20A (3.5 D), matching the value for the isolated P domain. We conclude that this LCR adopts a compact conformation.

The intramolecular interactions that cause P domain compaction may also contribute to intermolecular interactions that influence phase separation. We therefore examined the influence of aliphatic composition on the degree of compaction. Reducing hydrophobicity with MV/A substitutions increased the domain's Rg, while increasing hydrophobicity with MV/I substitutions decreased Rg (3.5 C). Corresponding hydrophobicity-dependent compaction is apparent in the shape of the domains (3.5 E).

To examine how non-aliphatic hydrophobic residues, the aromatic residues F and Y, contribute to collapse, we mutated all hydrophobic and aromatic residues to a selection of polar groups, MVFY/AGPNQ. This polar mutant had an Rg that was indistinguishable from that of the denaturant-treated WT P domain (3.5 F). An FY/L mutant showed only a small expansion entirely consistent with the small reduction in hydrophobicity in this mutant (3.5 F), ruling out strong aromatic-specific effects on compaction. Indeed, with the exception

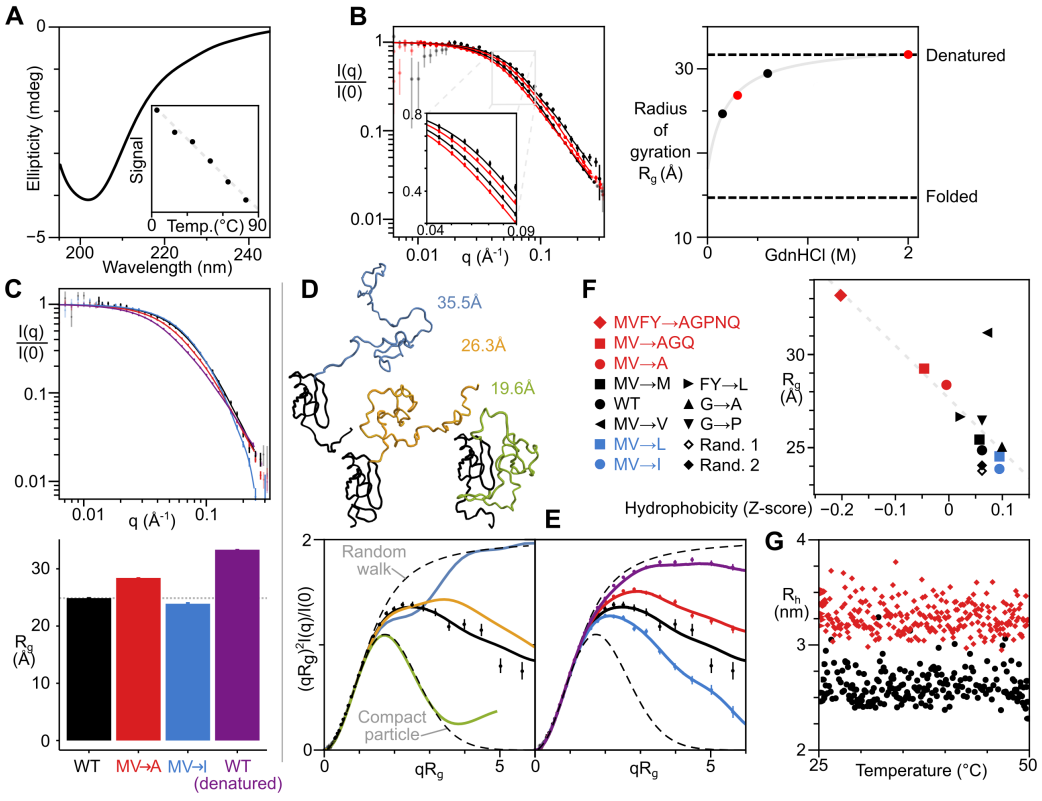

Figure 3.5: **The P Domain Is Unstructured and Displays Hydrophobicity-Dependent Compaction** (A) CD spectrum of the P domain (without His8 tag) at 1 μM, 20°C. Inset, the temperature dependence of the average CD signal from 215–235 nm. (B) SAXS of P domain (with His8 tag) at denaturant (GdnHCl) concentrations shown at right. Inset highlights the mid-q region. Corresponding Rg values are plotted; gray line shows extrapolation to zero denaturant (see STAR Methods). Dashed lines correspond to approximate values for denatured proteins and folded proteins. (C) SAXS of tagged P domain for WT (black), MV/I (blue), MV/A (red), and WT in 2 M GdnHCl (purple) (the hyperstable expression tag remains folded) with corresponding Rg values below. (D) Top, model fusion conformations where the P domain is extended, (self-)collapsed, or collapsed around the expression tag (black), with corresponding P domain models highlighted in blue, yellow, and green, respectively. Dashed lines show profiles expected for a random walk and compact (Guinier) particle. The Rg for the fusion is indicated. Bottom, dimensionless Kratky plots for the three models. (E) Dimensionless Kratky plots for SAXS curves shown in (C). (F) Correlation between hydrophobicity and Rg for all P domain mutant constructs. (G) DLS of WT and MVFY/AGPNQ fusion variants in black circles and red diamonds, respectively. For SAXS plots in (B)–(E), error bars show standard error on the mean within bins spaced equally on a log (B and C) or linear scale (D and E).

of the M/V mutant, altering the net hydrophobicity produced well-correlated changes in domain compaction across multiple sets of mutations (3.5 F).

Domain collapse persisted after mutation of 12 glycines to bulkier, less-flexible alanines (G/A) or prolines (G/P) and after randomization of the WT sequence (3.5 F). Interactions driving compaction are not glycine dependent and are unlikely to be specific or structured.

Neither the WT P domain nor the MVFY/AGPNQ mutant showed significant change in Rh between 25°C and 50°C, and both showed no evidence of self-association (3.5 G). This supports other results (3.3 E) indicating that the P domain promotes, but does not cause, phase separation.

In summary, intramolecular hydrophobic interactions cause biophysical collapse of the low-complexity P domain, which is it-self largely temperature-insensitive. These results prompt the question of how these interactions influence stress-induced demixing.

3.3.8 P Domain Hydrophobicity Modulates Pab1's Phase Boundary and in vivo Demixing

We measured the T_{demix} of phase separation for a variety of full-length Pab1 constructs using DLS. MV/I substitutions decreased T_{demix} by 1.6°C, while MV/A changes increased it by 2.2°C, virtually equivalent to the behavior seen when the P domain is deleted (3.6 A). Demixing temperatures of full-length Pab1 variants correlate with the corresponding P domain variants' Rg (Spearman r = 0.93, 3.6 B, see online publication [61] table S1), linking monomer biophysical characteristics to demixing behavior. Measuring the demixing behavior of the MV/I and MV/A mutants as in 3.3 E revealed that evolutionarily motivated mutations systematically shifted the phase boundary relative to the WT, yielding greater and lesser thermal and pH sensitivity, respectively (3.6 C).

We next asked how Pab1 mutations, which modulate *in vitro* phase separation, alter *in vivo* demixing. After integrating P domain variants into the single chromosomal copy of the

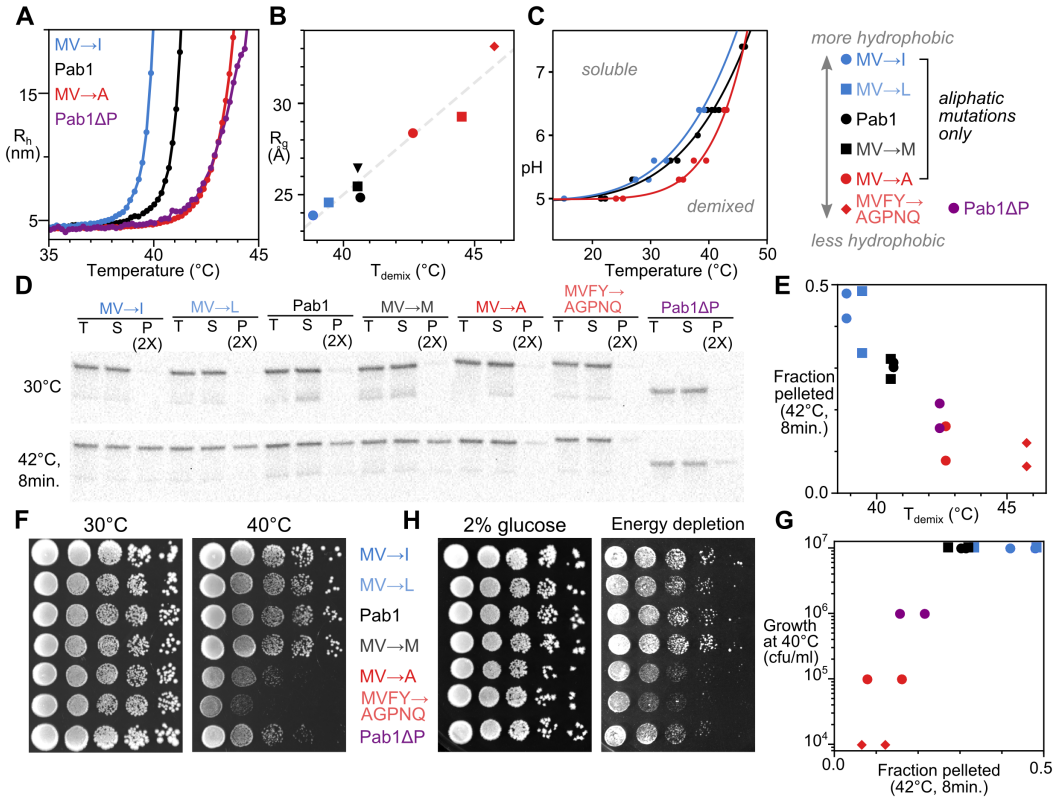

Figure 3.6: **Hydrophobicity of the P Domain Modulates Pab1 Demixing *in vitro* and *in vivo* and Alters Yeast Growth during Stress** (A) DLS temperature ramp experiments of listed P domain mutant constructs in Pab1 background, with Pab1 and Pab1ΔP, all at pH 6.4. (B) Correlation between compaction of the P domain (Rg, 3.5) and T_{demix} at pH 6.4 (see online publication [61] table S1). (C) Altering the hydrophobicity of the P domain shifts the phase boundary. (D) *in vivo* variation in Pab1 demixing between P domain mutants assess by anti-Pab1 western blot. Total (T), soluble (S), and pellet (P) lanes are shown for yeast treated as indicated. RNase A was added to to lysates before fractionation at 20,000 g. Total protein loading control and replicate in 3.16. (E) Comparison between *in vitro* T_{demix} of Pab1 at pH 6.4 and *in vivo* pellet fractions after stress as in (D) from two biological replicates. (F) Colony formation assay of yeast strains containing mutations in the P domain. Plates were incubated at 30°C and 40°C for 4 days. Columns are 10-fold dilutions. (G) Comparison between *in vivo* pelleting of Pab1 and yeast strain growth at 40°C. (H) Colony formation assay of yeast strains when challenged with energy depletion (4.2 mM 2-deoxyglucose and 0.42 mM antimycin A) grown at room temperature for 5 days (3.17).

PAB1 gene (Key Resources Table), we quantified Pab1 demixing into quinary assemblies at 30°C and after a 42°C, 8 min shock as in 3.1 (3.6 D and 3.16). T_{demix}, which quantifies the heat sensitivity of phase separation *in vitro*, correlates strongly with heat-triggered Pab1 demixing *in vivo* (3.6 E, Spearman r = 0.94). Pelleting of another assembling protein, Yef3, does not vary (3.16 A and B) ([64]). Pab1 variants with an *in vitro* T_{demix} above 42°C show negligible demixing after a 42°C heat shock *in vivo*.

Together, the tight relationships between consequences of *in vitro* and *in vivo* perturbation provide strong evidence that Pab1 phase separates *in vivo* during heat shock, with temperature sensitivity modulated by its low-complexity region.

3.3.9 Reducing Pab1 Stress-Triggered Phase Separation Reduces Yeast Fitness during Stress

We next examined the relationship between demixing and yeast stress tolerance using our battery of P domain variants. Yeast were grown under normal (30°C) and heat-shock conditions (40°C). All six variants studied display growth behavior at 30°C equivalent to the WT, despite Pab1's essential role (3.6 F). Strikingly, only the three variants whose phase separation occurs at temperatures substantially above that of the WT (MV/A, MVFY/AGPNQ, and ΔP) showed reduced fitness under heat-shock conditions (3.6 G). The unperturbed behavior of MV/I and MV/L variants indicates that changing the identity of these 12 aliphatic residues is both tolerable and has no apparent stress-dependent phenotype. The phenotype emerges when these residues are mutated to reduce their hydrophobicity. Returning plates to 30°C caused all strains to resume growth, indicating that mutant cells suffer a reversible fitness defect rather than death (3.17 A). The mutant effects are genetically dominant (3.17 B).

To determine whether this effect would generalize to a non-thermal stress, we challenged cells with energy depletion by treating them with the glycolysis inhibitor 2-deoxyglucose

(2-DG) and the respiratory chain inhibitor antimycin A. Dual treatment or 2-DG alone induces a cytosolic pH drop ([188, 189]), and glucose deprivation triggers formation of Pab1-marked stress granules in yeast ([144, 190]). Phase-separation-defective strains again showed stress-induced growth defects (3.6 H) in an inhibitor-concentration-dependent manner (3.17 C).

We conclude that Pab1's phase separation during stress is an adaptive response. Altered stress tolerance correlates with altered quinary assembly formation *in vivo*, phase separation *in vitro*, P domain hydrophobicity, and P domain compaction in the monomer, revealing connections between each phenomenon.

3.4 Discussion

How do cells sense stress? What are the relationships between phase separation of individual proteins, stress granule formation, and the ability to tolerate stress? How do intrinsically disordered regions promote phase separation? We have discovered that yeast's poly(A)-binding protein, Pab1, senses stressful temperatures and stress-associated pH changes autonomously, phase-separating in a way that helps yeast cells grow during stress. Evolutionarily tuned hydrophobic interactions in Pab1's proline-rich, intrinsically disordered low-complexity region modulate the phase boundary rather than causing demixing.

Phase-separated Pab1 rapidly gels, mirroring the solid-like, non-amyloid character of stress granules in yeast ([54]). Pab1 hydrogels, however, are distinct from previously reported RNA-binding-protein hydrogels ([66, 67]) in that they form at physiological concentrations and do not require a low-complexity region. Slow solidification of liquid phases over hours has been reported ([65, 68]), again distinct from the rapidly forming hydrogels we observe.

That a core marker of stress granules phase-separates in response to physiological stress cues provides compelling support for the broader hypothesis that phase-separation phenomena underlie adaptive reorganization of cellular matter in response to environmental change.

Groundbreaking work has focused on phase separation as a mechanism to compartmentalize an otherwise-well-mixed milieu ([80, 191, 165, 192]). The sharp spatial boundaries delineated by phase separation serve to localize and partition molecules that may collaborate functionally, as in the case of membraneless organelles ([80]) or compartmentalized signaling molecules ([192]).

Pab1's phase separation is distinct from its coalescence into well-defined cellular bodies (stress granules). In yeast, evidence *in vitro* (here) and *in vivo* ([54]) indicates that Pab1 does not form sustainably fluid compartments under physiological conditions. Rather than defining key spatial boundaries, we find that Pab1's phase separation delineates sharp thermal and pH boundaries of profound biological importance to the organism.

3.4.1 Stress Sensing by Phase Separation of an RNA-Binding Protein

We find that Pab1's phase boundary depends strongly on temperature and pH in the physiological ranges of these parameters. Temperature is an environmental stress, which Pab1 can sense directly. pH is a second messenger for glucose starvation ([188, 189]), and drops in cytosolic pH reliably follow a wide range of cellular stresses ([193]). Pab1 LCR variants with reduced thermal and pH-dependent demixing *in vitro*, and reduced thermally induced demixing *in vivo*, show compromised growth during thermal and energy depletion stress; we speculate, but have not demonstrated, that these mutants will show differential demixing in energy-depleted cells. Using phase separation, Pab1 synthesizes varying thermal and pH signals into a unified quinary response.

The molecular processes by which eukaryotic cells sense temperature remain surprisingly murky ([167]). In budding yeast, which lack the thermosensing channels found in animals, a long-standing model mechanism has been that a molecular chaperone represses the heat-shock transcription factor under non-shock conditions, and misfolded proteins titrate away this repressor, activating a response ([194]). Notably, misfolded proteins act as the temper-

ature sensors in this model. However, no specific misfolded protein has been identified in eukaryotes. Stress-triggered phase separation of Pab1 and other proteins can substitute for misfolded proteins in this model.

Pab1's thermally induced, adaptive phase separation shows temperature-sensitivity unmatched by other systems. The most sensitive previously described ratiometric change in a biological property over a 10°C range (Q_{10}) for a thermosensing-relevant molecular process is 200, observed for the conductance change in the *Anopheles gambiae* mosquito's AgTRPA1(B) thermosensing cation channel ([8]). By comparison, the Q_{10} of 350 for growth rate of Pab1 quinary assemblies at the onset of heat stress is remarkable. We speculate that phase-separation-based environmental sensing may be broadly exploited by cellular life.

Discovery of quinary stress sensing may also help catalyze an ongoing conceptual shift in the study of proteotoxic stresses. The standard model holds that such stresses disrupt protein folding, producing toxic aggregates of misfolded, non-functional proteins in need of refolding or destruction ([139]). Alternatively, apparent "aggregation" may reflect the evolved, stress-responsive demixing of a wide range of cellular proteins ([19, 64]). We have argued that the key method to distinguish misfolding from quinary assembly formation (which may involve unfolding) lies in fitness: misfolding is deleterious, whereas evolved quinary assembly formation is adaptive ([64]). Here, the results are clear: impeding Pab1's "aggregation" during stress compromises fitness during stress. Pab1 demixing is adaptive. The implication is that the dozens of other endogenous, mature proteins that form reversible assemblies during stress constitute a vast, distributed sensory system for adaptively reorganizing cellular matter.

3.4.2 LCRs as Biophysical Modulators of Phase Separation

A fundamental principle underlying the phase separation of biological molecules is multivalency, the capacity to interact with multiple partners simultaneously ([165]). Previous work

on RNA-binding proteins has demonstrated phase separation requiring either an LCR or RNA ([66, 65, 67, 185, 68, 195]). We find that, in contrast to these systems, RNA interferes with Pab1 phase separation, and Pab1's LCR is both dispensable for phase separation and unable to cause phase separation under physiological conditions in the context of its flanking domains.

Atypically for intrinsically disordered regions, poly(A)-binding protein's LCR has few charged residues and contains many non-aromatic hydrophobic residues whose relative frequencies appear to have been shaped by natural selection. Previous work has focused on the roles of aromatic and charged-residue interactions in promoting IDR-mediated phase separation ([196]). Complementing work demonstrating cooperativity between LCR- and RNA-mediated phase separation ([65, 67]), we demonstrate the ability to tune Pab1's domain-mediated phase separation by dialing up or down the hydrophobicity of its aliphatic LCR residues. While a detailed mechanism is not yet clear, it seems plausible that temperature-dependent desolvation ([197]), charge-patch interactions ([198]) between multivalent RRMs enhanced by pH-modulated histidine protonation, and limited conformational change collaborate to cause phase separation.

How does Pab1's LCR modulate demixing? Any mechanism must incorporate both the profound links between hydrophobically mediated P domain compactness and phase separation and the lack of P domain self-association at physiological Pab1 concentrations. We propose that Pab1 phase separation brings the associated P domains to high concentration, where they swap hydrophobic intramolecular interactions for intramolecular interactions, boosting the net affinity between Pab1 molecules (3.7). Enhancing hydrophobic interactions thus boosts both domain compactness and demixing, while reducing hydrophobic interactions does the opposite.

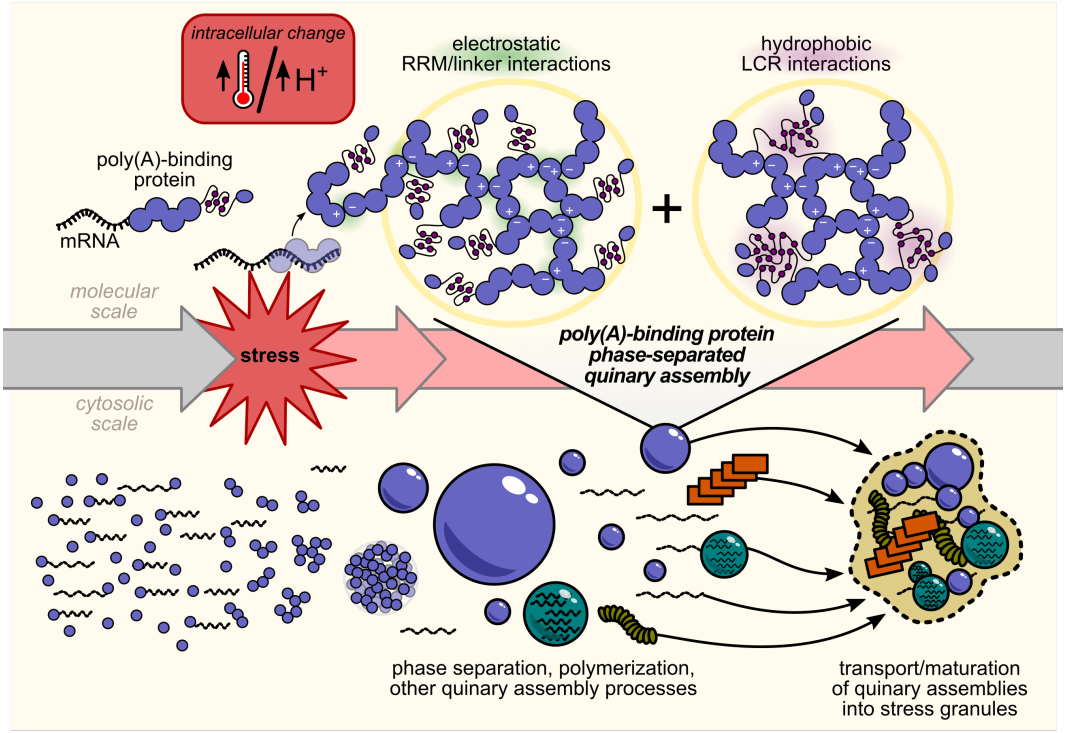

Figure 3.7: **Model for Poly(A)-Binding Protein Stress-Triggered Phase Separation** Under non-stress conditions, poly(A)-binding protein (Pab1) is bound to RNA. Either directly. through thermal shock. or indirectly. through a stress-induced cytosolic pH drop, stress triggers RNA release and phase separation by Pab1. Phase separation is mediated by electrostatic interactions between RNA-binding regions, which compete with RNA binding. Hydrophobic residues in Pab1's low-complexity region, intramolecularly engaged in the monomer, form intermolecular interactions, which promote the phase-separated state at elevated temperatures. Under conditions of severe stress, Pab1 and other quinary assemblies are localized to stress granules in a separate cell-biological process.

3.4.3 An Adaptive Role for Phase Separation in Stress Sensing

How does Pab1 phase separation promote cellular adaptation to growth during stress? Uncovering the precise mechanism will require further study. We hypothesize that Pab1 represses mRNAs contributing to stress adaptation, that stress-induced demixing relieves this repression, and that disassembly during recovery restores repression. Outlines of a specific mechanism emerge from four results. First, poly(A)-binding protein acts as a translational repressor of its own and other mRNAs by binding A-rich tracts in the 5'UTR ([130]); second, several major molecular chaperones possess evolutionarily conserved A-rich tracts in their 5'UTRs ([32]); third, these molecular chaperones are required for efficient disassembly of Pab1 quinary assemblies, which precedes resumption of translation and growth ([19, 54]); and fourth, our study reveals that Pab1's phase separation competes with RNA binding, consistent with RNA release during stress.

Synthesizing these results, we speculate that upon stress, Pab1 phase separates, releasing chaperone mRNA 5'UTRs and permitting higher levels of translation. The chaperones produced disperse Pab1 quinary assemblies. Resolubilized Pab1 rebinds 5'UTRs, represses chaperone translation, and so completes an autoregulatory circuit. If Pab1 demixing is slowed, free Pab1 continues to repress chaperone transcripts during stress, preventing dismantling of quinary assemblies of dozens of proteins required for growth. As noted above, all of these behaviors likely apply during a range of stresses, with second messengers like pH providing triggers for demixing.

Any mechanism must address an important fact: quinary assemblies of Pab1 do not observably reverse *in vitro* on physiological timescales, and stress-induced ATPases facilitate their dispersal *in vivo*. We hypothesize that facilitated dispersal will prove a common feature of stress-responsive quinary circuitry: it links resumption of normal cellular processes to the production of an effective stress response, not simply the end of stress—a crucial distinction.

3.5 Further data

Here I present unpublished data related to the above manuscript. Some of these findings are incomplete and warrant further investigation, while others offer further insight into the fitness consequences of mutating the Pab1 P domain.

3.5.1 Hydrophobicity of the P domain modulates sensitivity to caffeine

In addition to heat and starvation, a variety of other treatments stimulate Pab1-marked stress granule formation in yeast including caffeine. Caffeine is known to inhibit TOR signaling in a manner similar to rapamycin; however, it is more potent. TOR signaling supports normal cell growth; endogenous inhibition of TOR by stress like nutrient starvation leads to slowed growth and decreased cap-dependent translation [96].

P domain mutants with decreased hydrophobicity do not grow as well under stressful conditions such as high temperature or starvation. However, the cells aren't dying - they are growth arrested. This suggests that the fitness defect isn't related to a catastrophic formation of toxic species or to damage that wasn't properly corrected. One possibility is that an endogenous signaling mechanism related to Pab1 assembly is disrupted, preventing cells from growing.

When challenged with caffeine, yeast with less hydrophobic P domains are growth impaired compared to wild type cells (3.8). Moreover, yeast with a more hydrophobic P domain are more resistant to the growth inhibition of caffeine than wild type cells. It's not obvious whether caffeine treatment should deferentially influence the phase separation of Pab1, in contrast to heat or starvation stress, where the environmental change can directly stimulate phase separation. These data hint that the function of Pab1 in the stress response occurs through the TOR signaling. It is not clear whether this function is the same source as for the heat and starvation dependent phenotypes. Further, it is not clear whether Pab1 is upstream or downstream of TOR in the overall stress sensing. However, TOR1 is known to regulate

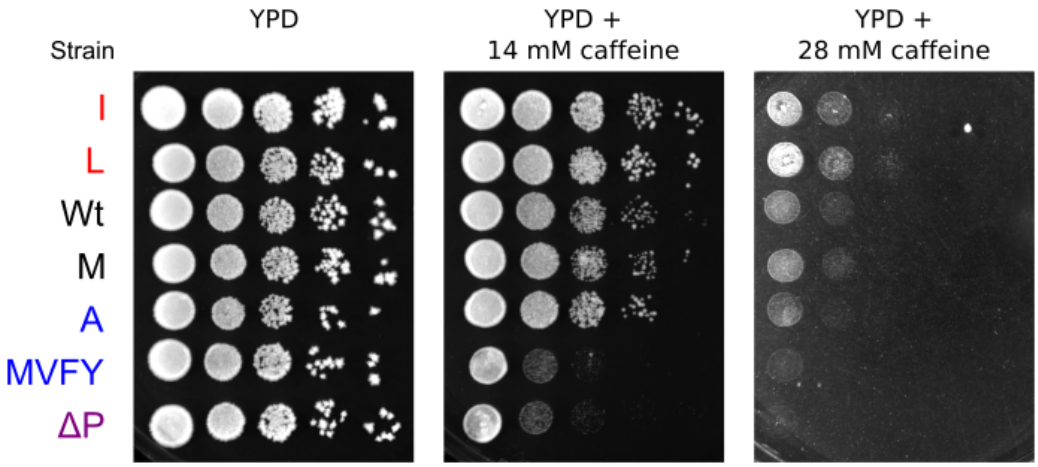

Figure 3.8: **Hydrophobicity of the P domain modulates fitness during caffeine stress** When grown on plates supplemented with caffeine, strains with impaired Pab1 demixing are more sensitive to caffeine. At high concentrations of caffeine it can be seen that increased P domain hydrophobicity makes the cells more resistant to caffeine.

disassembly of Pab1-marked stress granules during recovery from heat stress [97, 199].

3.5.2 Fitness defects resulting from extracellular pH suggest a balancing selective pressure for P domain hydrophobicity

We have seen that increased phase separation of Pab1 correlates with greater resistance to stressful environments. Why then has the P domain not naturally evolved to be more hydrophobic? One hypothesis is that there are still other environments where increased hydrophobicity of the P domain is detrimental. Thus the overall hydrophobic content of the P domain represents a balance between many selective pressures. A test of this hypothesis is to find a condition where increased hydrophobicity of the P domain is detrimental.

Increased hydrophobicity of the P domain causes Pab1 to phase separate in response to less extreme environmental changes — such as lower temperature, or more neutral pH. I hypothesized that phase separation is part of the stress response, which ultimately leads to slowed growth. I wanted to find an environment that is not actually harmful to the cells, but can trigger a phase separation-related stress response in the most sensitive strains. In

other words, find a treatment that leads to inappropriate phase separation.

Since the Pab1 variants *in vitro* show large differences in pH dependence of T_{demix} (3.6 C), I explored growth at different pHs. Cells were grown on SC complete plates supplemented with 100 mM citrate and pH'd to different values. When grown at pH 6.1, I observed the reverse phenotype — less hydrophobic P domain supports increased growth 3.9. This effect was greatly diminished at pH 5.1, and again reversed at pH 4.1, where a more hydrophobic P domain supports increased growth. This reinforces the idea that hydrophobicity of the P domain is tuned by a variety of opposing selective pressures — in this case, the pH of the extracellular environment.

Again, it is not obvious whether the growth defect at pH 6.1 is related to the phase separation of Pab1 directly. Starvation leads to intracellular acidification, due to equilibration of extracellular and intracellular pH. Thus extracellular pH plausibly affects phase separation. What is the mechanism of this phenotype? I can only speculate. However, I imagine that when growing on plates buffered to pH 6.1, when the cells slowly run out of nutrients they begin to equilibrate their pH to 6.1. This pH is sufficient to trigger phase separation in wild type and more hydrophobic variants, but not in the hydrophilic variants: A, MVFY, ΔP. Phase separation must be reversed in order for cells to continue the cell cycle, but if Pab1 phase separation never occurred, then there is less energy required to restart the cell cycle. This idea assumes the pH 6.1 is not harmful to the cellular machinery. By contrast at pH 4.1, the acidity may be harmful to the cellular machinery, and phase separation is necessary to support growth. In this model, somewhere around pH 5.1 this harm balances the cost of reversing Pab1 assemblies.

3.5.3 Starvation induced sedimentable species

We showed that hydrophobicity of the P domain affects formation of sedimentable species *in vivo* during heat stress (3.6). However, we did not demonstrate differences of Pab1

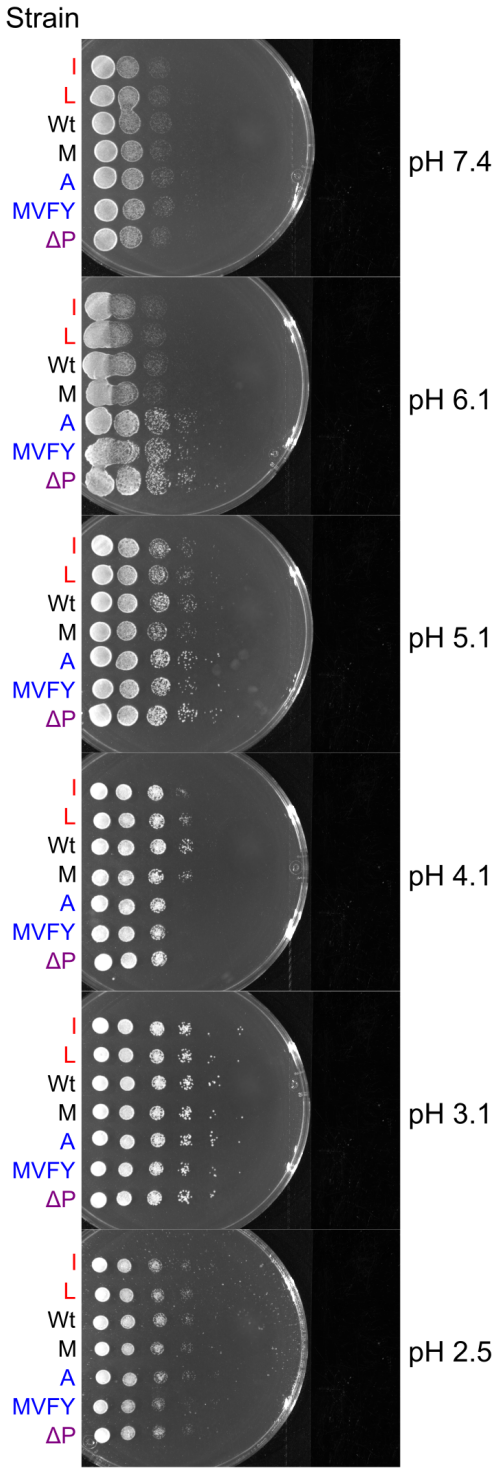

Figure 3.9: **Fitness defects in P domain mutants are sensitive to extracellular pH.** P domain mutants were grown on SC plates supplemented with 100 mM citrate and buffered to the indicated values. Plates were imaged after 72 hours of growth at room temp, 23°C.

assembly formation as a result of starvation — despite observing a growth defect. So, are there differences in starvation-induced assembly formation? To address this, I first needed to identify conditions where starvation-induced assemblies can be isolated. Starvation triggers formation of visible foci within minutes of glucose withdrawal. However, even after 2 hours of treatment with 2-deoxyglucose, to simulate starvation, I did not detect sedimentable species (3.10 A). If cells are grown to high density over two days - long enough to exit logarithmic growth - then sedimentable species are detected (3.10 A). P domain mutants were grown in YPD for 2 days, then fractionated and western blotted for Pab1 assemblies. Many degradation products of Pab1 are visible. By eye, mutant A certainly has less Pab1 in the pellet fraction, compared to wild type (3.10 B). However, a clear trend such as 3.6 D is not immediately visible.

It remains unclear why sedimentable species aren't detected during acute starvation, even when visible foci form. Several possible reasons warrant further inquiry: 1) the assemblies are liquid-like and spontaneously reversible upon lysis, similar to Pub1 aggregates [20]; 2) assemblies are large and are cleared from the lysate during the pre-clearance step that is designed to clear chromosomes and unlysed cells 3) stress treatments are either too long or too short to capture detectable assemblies *in vivo*.

3.5.4 Stress-induced assemblies may be larger than we assume

How big are sedimentable aggregates? We know that they can be much smaller than visible foci; for example, in the case of mild heat stress. However, during starvation it has been reported that the entire cytoplasm can solidify ([189]). In such a case, I expect the sedimentable species to be the size of the whole cell. This possibility exposes a possible technical oversight in the sedimentation protocol used to detect Pab1 assemblies from cell lysates.

The sedimentation procedure used [64, 61] starts with total cell lysate, then does a pre-clarification spin at 3000 g for 30 sec. The supernatant of this pre-spin is then used to

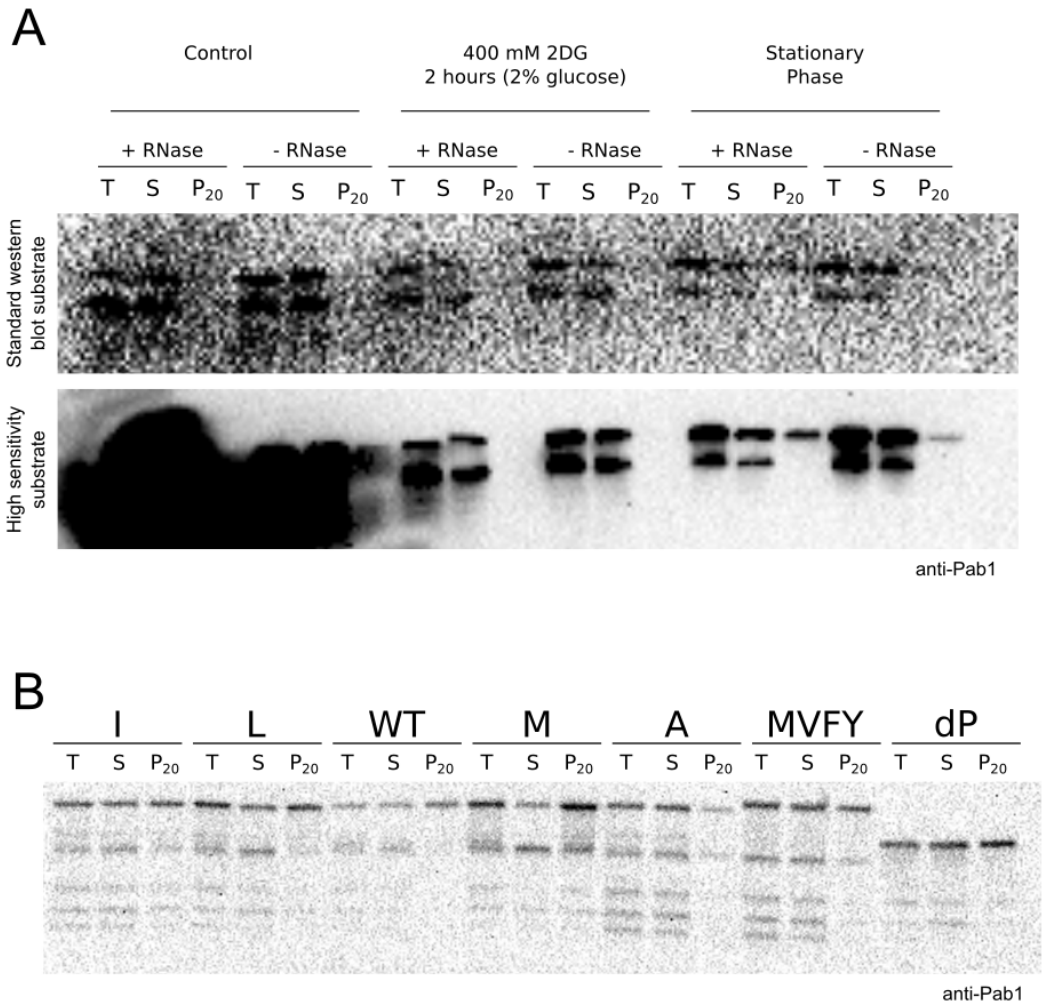

Figure 3.10: **Sedimentable Pab1 species are not detected during acute starvation, but are detected during long starvation.** (A) Cells were grown at 30°C (control), or incubated for 2 hours with a non-hydrolyzable glucose analogue (400 mM 2DG, 2 hours), or grown to high density for 2 days. Cells were then harvested, lysed, and fractionated. (B) P domain variants were grown at 30°C for 2 days. Cells were collected and fractionated. Pellets are loaded 4X.

generate the "sup" and "pellet" fractions. The pre-spin is designed to clean the lysate of unlysed cells, large chromosomes, and lipids that would otherwise contaminate the experiment and disrupt detection. However, it is possible that cell-size assemblies are also cleared during this step and never detected. This possibility seemed especially plausible when searching for starvation-induced sedimentable species.

Some evidence for cell-size assemblies during heat shock can be seen in 3.11 A. Cells were grown in SC normally. Then, cells were either mock treated in SC, or had the pH clamped to 6.8 or 7.4 using nigericin. Treated cells were split again and either left at 30°C, or stressed at 42°C for 20 min. Cells were fractionated as before. However, the P3 (3000 g 30 sec pellet) fraction was saved and analyzed. It is clear that Pab1 appears in the P3 fraction from heat stressed cells, but not in cells kept at 30°C. These data suggest that material in P3 is not the result of incomplete lysis — in which case P3 material would also be expected in 30°C treated cells. Further, Pab1 assembly can be prevented *in vitro* by raising the pH to 7.4 even at 42°C. I expected Pab1 assembly *in vivo* to be disrupted if the stress-induced acidification was blocked with ionophore as in this experiment. However, Pab1 assembly appears unperturbed in this experiment. Material in the P20 fraction appears to be slightly sensitive to RNase1 treatment.

These data are by no means definitive. Further experiments should be used to rule out incomplete cell lysis. Potentially stressed cells are resistant to cryogenic lysis in a way that unstressed cells aren't. Hemocytometry could potentially be used to count unlysed cells and distinguish them from cell debris.

Additional evidence for cell-sized sedimentable species comes from the effect of RNase treatment on how proteins move into each fraction. If proteins in P3 represent unlysed cells, then the set of proteins in the "total" fraction and "P3" fractions should be identical. Moreover, unlysed cells should not be affected by RNase treatment. However, we see that RNase treatment causes several prominent protein bands to move from the "sup" fraction

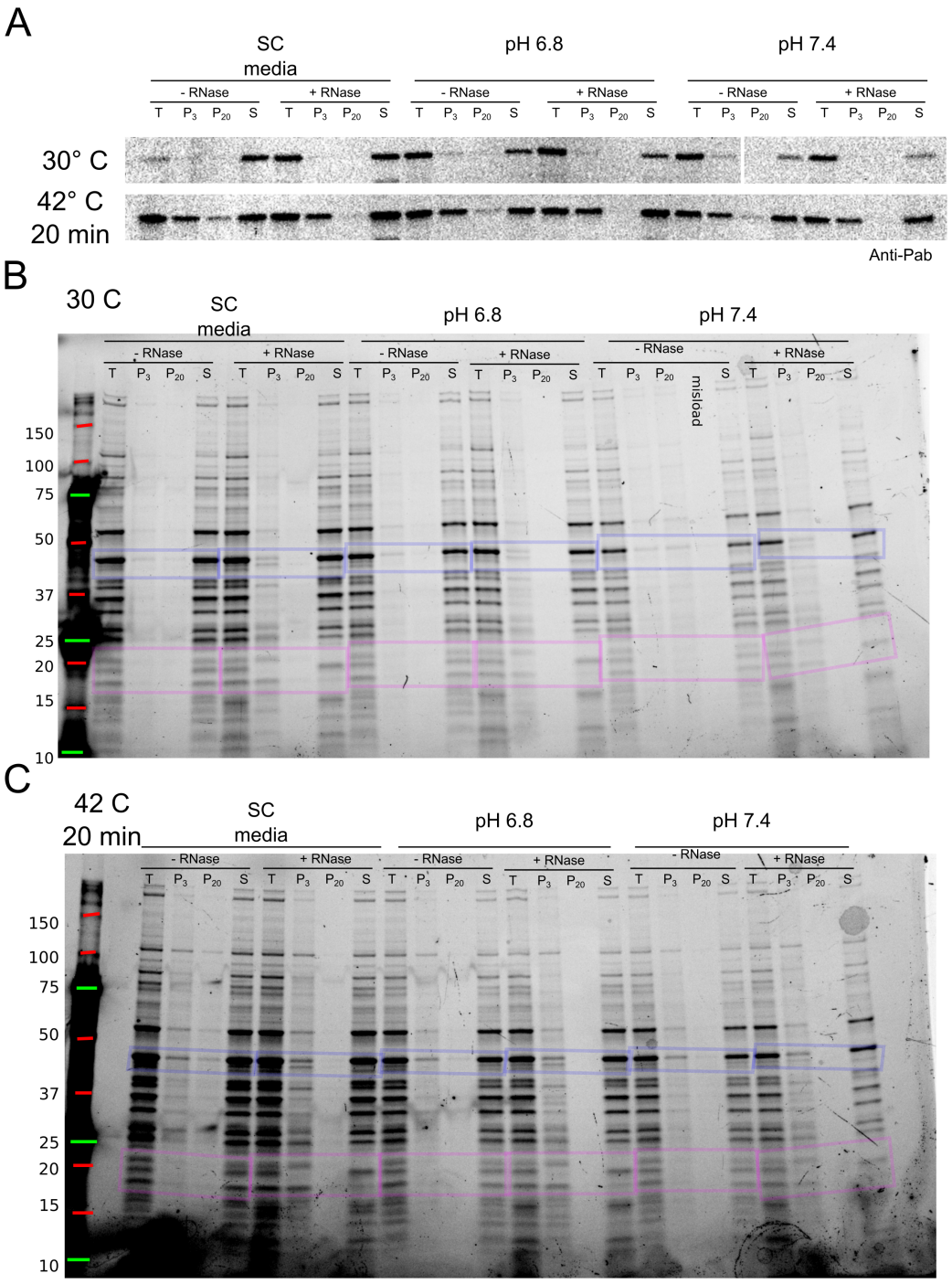

Figure 3.11: **Stress-induced species may be extremely large.** (A) Cells were grown in SC at 30°C, then split. Cells were mock treated in SC, or treated with ionophore to clamp the intracellular pH at 6.8 or 7.4. Cells were split again and either left at 30°C or stressed at 42°C for 20 min. Cells were fractionated and western blotted against Pab1. (B and C) The total protein from (A) was detected using stain-free imaging to detect abundant proteins. Pink and purple boxes highlight protein species that move from "sup" to "P3" upon RNase treatment.

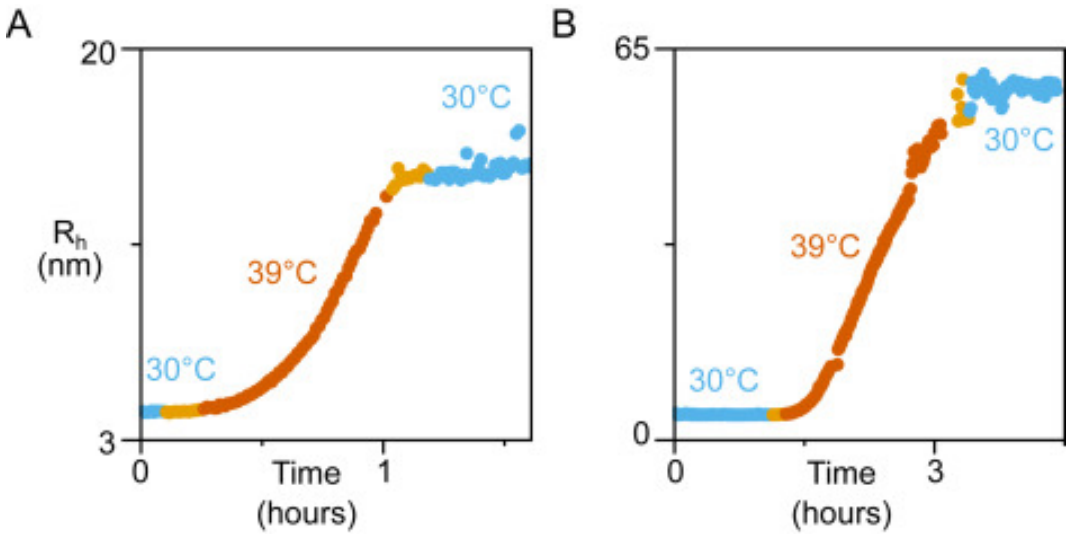

Figure 3.12: **Pab1 Requires Elevated Temperature for Ongoing Demixing Even after "Seeding," Related to 3.2 E.** Pab1 assembly followed with light scattering after temperature was shifted from 30°C (blue) to 39°C (orange), and back to 30°C (blue). Temperature equilibration period is highlighted in gold. Panels (A) and (B) differ by duration at 39°C and the extent of resulting assembly.

into "P3" (3.11 B and C). This effect is independent of stress treatment or intracellular pH manipulation. The identity of the proteins highlighted in pink and purple boxes is unknown. Based on their size and abundance, I hypothesize that these are ribosomal proteins. It seems possible that these proteins are especially aggregation prone in the absence of rRNA after RNase treatment.

These data indicate that proteins can form aggregates large enough to spin out at 3000 g, though it is not certain from these data that stress-induced assemblies also represent large assemblies or unlysed cells.

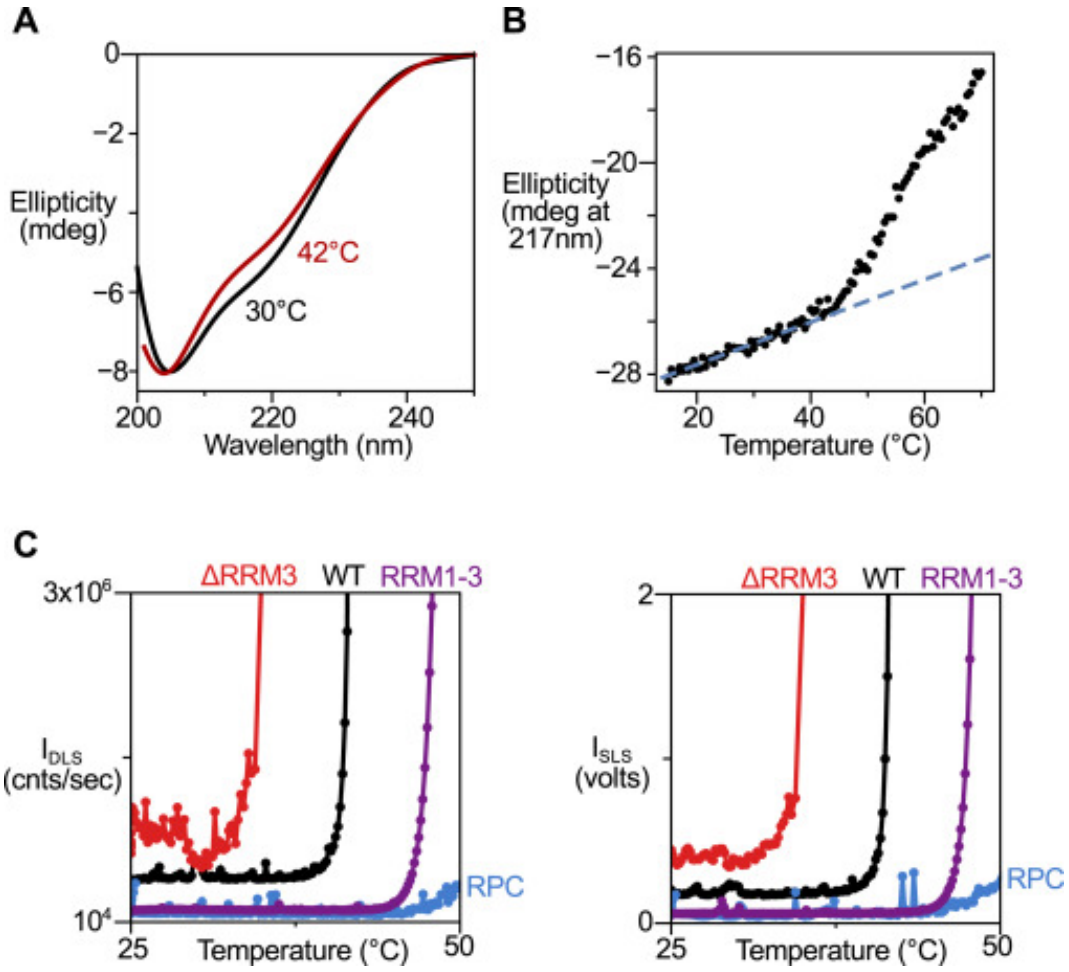

Figure 3.13: **Characterization of Folded-State Temperature Changes in RRM123, Related to 3.2 G and 3.3 F** (A) CD spectra of RRM123 at 30°C and 42°C at 0.2 μM. Unlike Pab1 in 3.2 E, no time-dependent changes were observed. (B) Temperature melt of RRM123 at 1 μM with best-fit line fit from 15°C to 30°C with extrapolation shown demonstrating that at 42°C RRM123 is still in the folded state baseline. At 47°C, RRM123 signal deviates from this native baseline, likely signifying the onset of RRM123 demixing and/or unfolding. (C) Normalized scattering intensity from DLS and SLS shown at left and right, respectively. Pab1, DRRM3, RRM1-3, and RPC are shown as indicated. In the case of DRRM3, low-temperature aggregation results in difficult-to-purify multimeric states preventing analysis of dynamic light scattering (DLS) to determine an (intensity-weighted) average hydration radius (Rh).

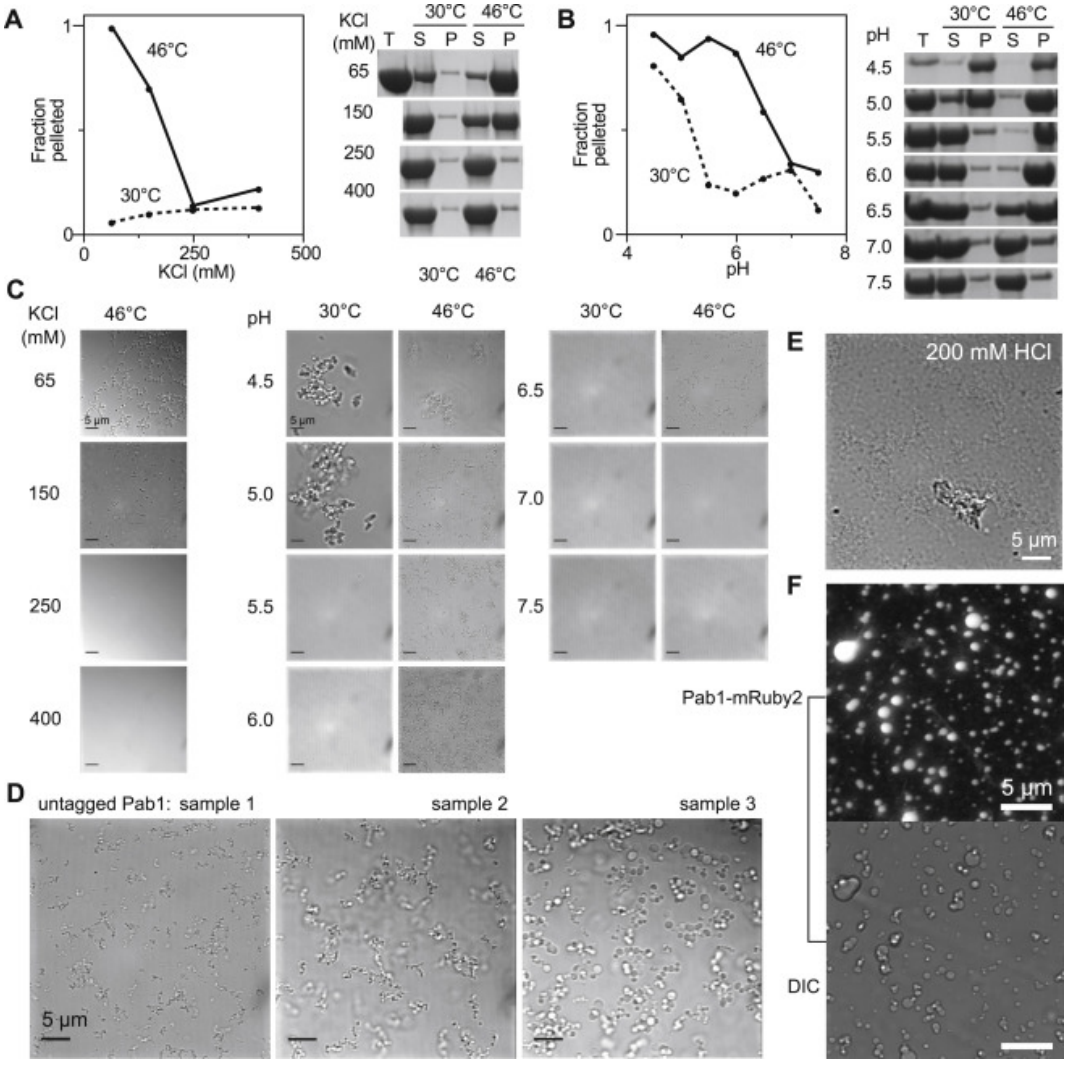

Figure 3.14: **Morphology of, and Conditions for, Pab1 Phase Separation, Related to 3.3** (A–C) Plots in (A) and (B) are reproduced from 3.3 A, with corresponding gels used to quantify fraction pelleted, where (T) is total, (P) is 20,000 g pellet fraction, and (S) is supernatant. Morphology of corresponding Pab1 assemblies are shown in (C). (D) Variation in size of heat-induced droplets (46°C, 5 min) is observed from day to day, and between sample preparations, possibly due to subtle variation in salt or pH. (E) At a pH of 0.7, Pab1 denatures and has a morphology which is distinct from phase-separated Pab1 droplets. (F) Image at the slide surface showing adherent Pab1-mRuby2 droplets wetting the surface.

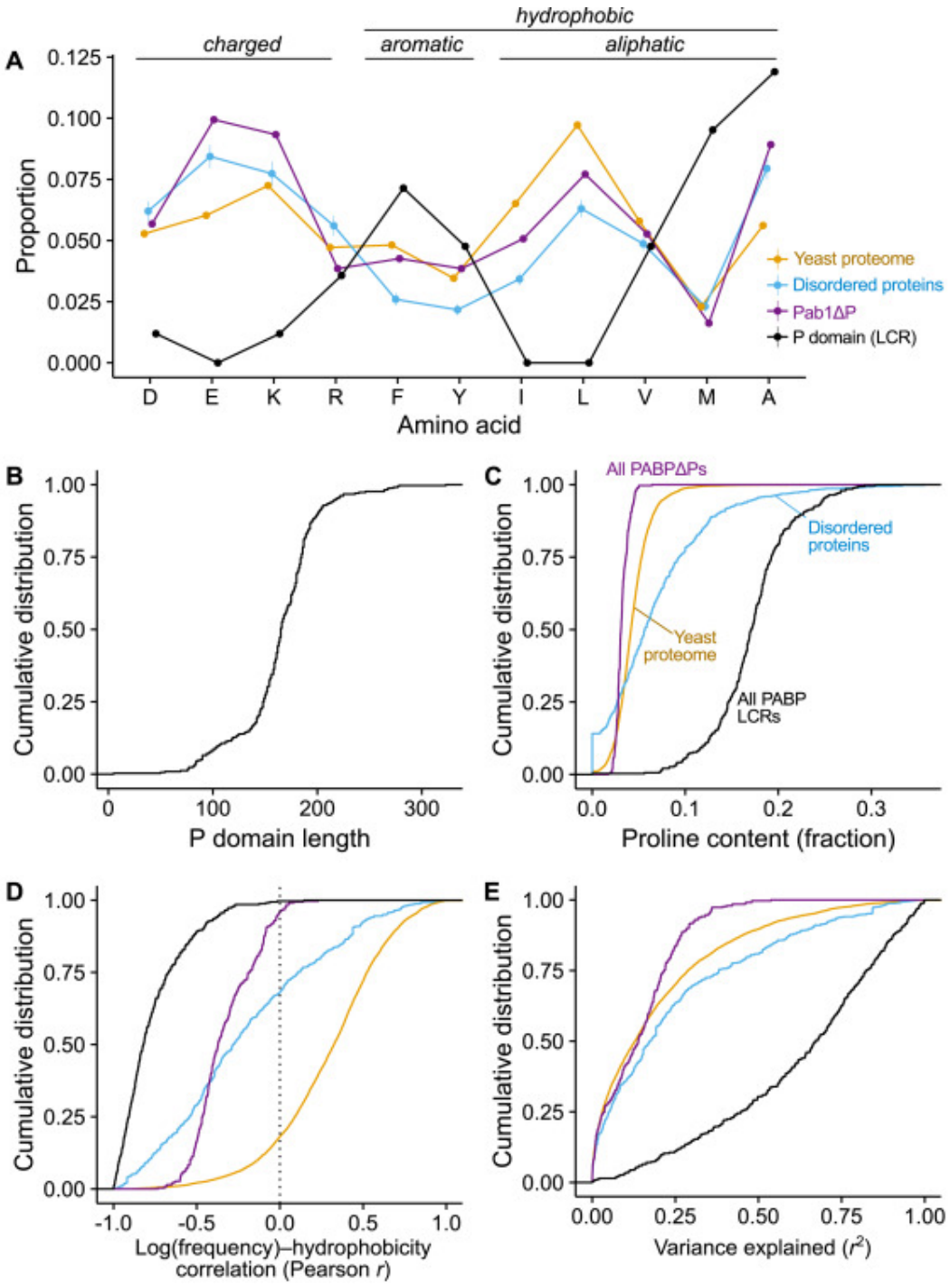

Figure 3.15: **The Pab1 Proline-Rich Domain Has Unusual Composition, and a Proline-Rich Domain Is Conserved across Species, Related to 3.4**
Continued on next page.

Figure 3.15: 3.15 continued. (A) Data in 3.4 B reordered to emphasize differences in charged and hydrophobic amino acids. Error bars show standard error on the mean. (B and C) Cumulative distributions for length (B) and proline fraction (C) for PABP sequences between RRM4 and the CTD (putative P domains). (D) Cumulative distribution of the log(frequency)-hydrophobicity correlation for ILVMA residues, for sets of sequences colored as in (C). (E) Variance explained (r2) for correlations in (D).

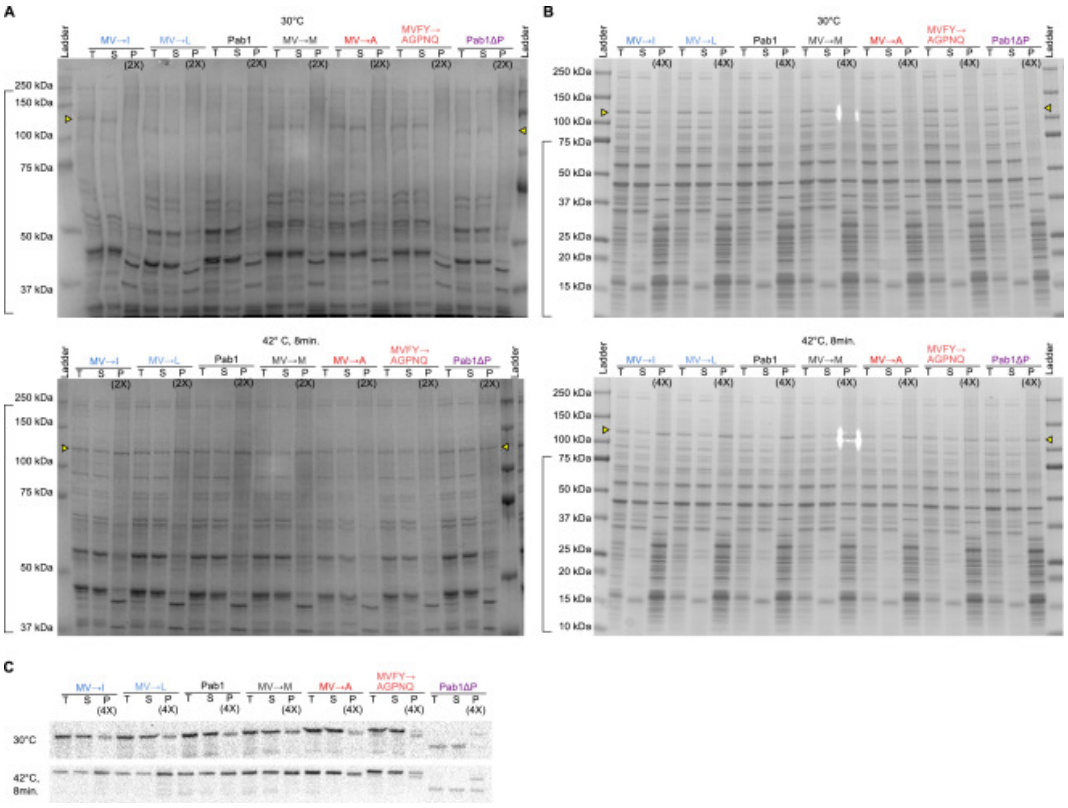

Figure 3.16: **P Domain Tunes the Demixing of Pab1 *in vivo*, Related to 3.6** (A and B) Coomassie-stained SDS-PAGE gel of samples quantified in 3.6 D for replicates 1 and 2, respectively. Top and bottom correspond to cells incubated at 30°C and 42°C, respectively. Yef3 is annotated with a yellow arrow. The bracket indicates the region that was used for quantification. (C) Pab1 western blot for replicate 2 of yeast strains with mutated P domains; replicate 1 is shown in 3.6 C.

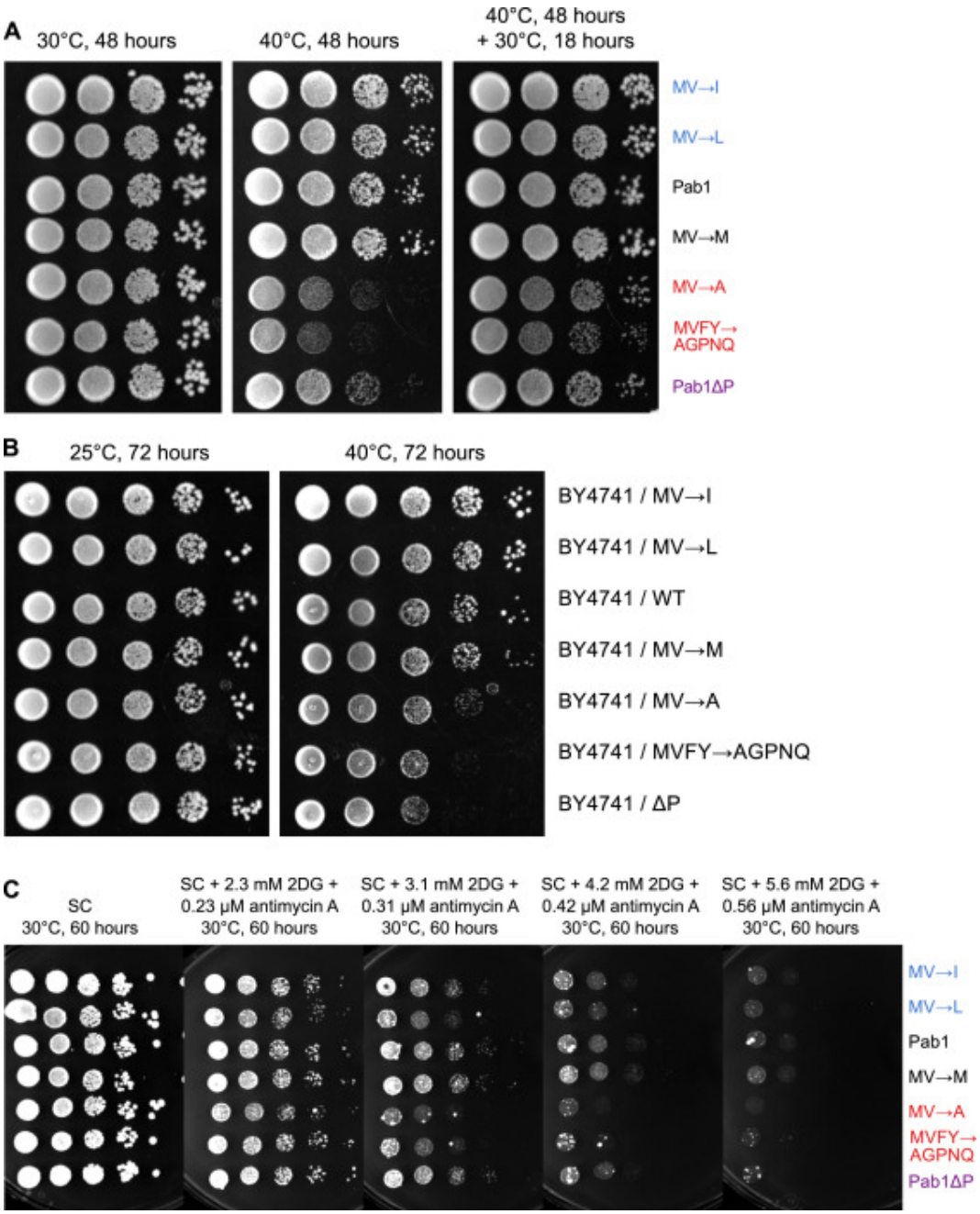

Figure 3.17: **P domain Stress-Sensitive Phenotype Is Reversible, Genetically Dominant, and Concentration-Sensitive during Energy Depletion, Related to 3.6** (A) The heat-sensitive phenotype from 3.6 E represents growth arrest, not death, since cells resume growth when shifted down to 30°C. (B) Diploid yeast expressing both WT Pab1 and P domain mutant Pab1 variants show a similar pattern of heat sensitivity compared to haploid strains. (C) Sensitivity of P domain mutant strains is more pronounced with increasing concentrations of 2-deoxyglucose and antimycin A. Large colonies in the presence of drug are suppressors.

3.6 Supplemental figures

3.7 Methods

3.7.1 Strain construction

Pab1 P domain swaps

Saccharomyces cerevisiae strains with substituted P domains were created by serial lithium acetate transformation as follows. First, BY4742 was transformed with dsDNA corresponding to a URA3 expression cassette with flanking DNA for integration. This cassette integrated such that a stop codon is inserted after RRM4, the P domain DNA was knocked out, and the C-domain DNA is preserved, but knocked out of frame. Transformants were selected on –Ura plates. This intermediate strain (yCDK059) was then transformed with dsDNA for a new P domain with flanking DNA for homologous recombination. The flanking DNA guides integration such that the URA3 cassette is knocked out and the C domain is brought back into frame after the new P domain. Transformants were selected with 5-FOA. Transformants were confirmed by PCR and sequencing. These strains are scarless, with no leftover selectable markers and native 30 UTRs (yCDK060, yCDK061, yCDK062, yCDK063, yCDK065, yCDK066).

Diploid strains

Diploid strains were constructed by standard mating procedure. BY4741 was streaked onto YPD plates, then appropriate BY4742- background Pab1 mutant strains were streaked through. Cells were incubated at room temperature for 5 hr, then replica-plated onto selective plates: SC -lys -met -cys. Resulting colonies were further purified by streaking onto selective plates (yCDK084, yCDK085, yCDK086, yCDK087, yCDK088, yCDK089). BY4743 was used as a control.

3.7.2 Plate growth

Heat sensitivity

For each strain, a dense overnight culture was diluted into fresh YPD and allowed to grow for 5 hr, when all cultures reached optical densities (OD600s) above 0.2. Cultures for each strain were diluted to matching OD600. Cultures were then serially diluted into fresh YPD. 7 mL of each dilution was spotted onto plates. For 3.6 F, one YPD plate was incubated for four days at 30°C and another for four days at 40°C. Plates were then imaged. For 3.17 A, one YPD plate was incubated at 30C for 2 days, then imaged; another YPD plate was incubated at 40°C for 2 days, imaged, then shifted to a 30°C incubator for an additional 18 hr, then imaged. For 3.17 B, diploid cells on a YPD plate were incubated at room temperature for 3 days then imaged; another YPD plate was incubated at 40C for 3 days then imaged. Energy depletion For 3.6 H, energy depletion plates were YPD with 4.2 mM 2-deoxyglucose and 0.42 mM antimycin A added, and were grown at room temperature (25C) for 5 days them imaged. For concentration dependence in 3.17 C, yeast were grown on SC plates with indicated amount of 2-deoxyglucose and antimycin A at 30C for 60 hr then imaged.

3.7.3 Total/soluble/pellet (TSP) assay in vivo

Serial fractionation and RNase sensitivity

For in vivo experiments, strains were grown in YPD from OD600 = 0.010 and harvested starting at OD600 = 0.400 (5.3 doublings) where the first 50 mL cells were harvested by 3000 g spin for one minute then decanted. Then cells were subjected to 8 min heat shock at 42C in the tube, fluid volume less than 500 mL. Yeast were immediately put on ice and washed with ice cold soluble protein buffer (SPB: 20 mM HEPES pH 6.5, 120 mM KCl, 2 mM EDTA) and resuspended in 200 mL SPB. Then 100 mL aliquots were frozen in liquid nitrogen. Total handling time was 40 min. Then another 50 mL of yeast were harvested,

OD600 had correspondingly increased. Cells were pelleted and mock treated for 8 min in 30C incubator. Samples were collected as for 42C. 100 mL aliquots were cryogenically lysed by pulverization in a Retsch MM100: 6 cycles of 90 s at 30 Hz. Samples were thawed on ice in 400 mL of SPB + PMSF and 0.2 mM DTT. Lysate is clarified at 3000 g for 30 s. 50 mL of that supernatant is taken as the total fraction. For Figure 1B, to 200 mL of that supernatant RNase1 was added to a concentration of 0.3U/mL and digested at room temp for 30 min. RNase-treated lysate was then spun at 4C for 5 min at 8,000 rcf. That supernatant was separated to a new tube and spun at a 100,000 rcf for 20 min.

Pab1 P domain mutant assembly

For Figure 6D and Figure S5, to 200 mL of that supernatant, 5 mL of RNase A (5 mg/mL) was added and digested at room temp for 20 min. RNase-treated lysate was then spun at 4C for 5 min at 20,000 rcf. Finally, 50 mL supernatant was taken as supernatant fraction, the rest is discarded. As a wash step, the pellet was suspended in SPB and re-pelleted. The pellet was then suspended in 50 mL of SPB (4X). 50 mL of loading buffer was added to all samples, then boiled and vortexed. Samples were then diluted 4-fold in 1X loading buffer. Dilutions were run 45 min on TGX 4%–20% acrylamide gel at 200 V. Region between 37 kDa and 150 kDa was cut out and transferred to nitrocellulose membrane, 100 V for 1 hr. Monoclonal anti-Pab1 antibody (EnCor MCA-1G1 lot 020407) was used for western blot. Semiquantitative lanes were included: 30C - WT total was included at 1/4 and 1/16 dilutions; 42C - I pellet was included at 1/4 and 1/16 dilution. Quantification of all gels was performed in ImageJ.

3.7.4 Protein sequences used in this study Protein construct sequences

The five WT constructs utilized in this study were 8xHis-(TevC)-Pab1, 8xHis-hyperstable Protein G-(TevC)-P domain, 8xHis-(TevC)- P domain, 6xHis-(TevC)-Pab1-clover, and 6xHis-

(TevC)-Pab1-mRuby2. Sequences for all constructs are listed in the Key Resources table. Final protein sequences lacked the His-tag, due to TEV protease cleavage; cleavage occurred between Q and S residues in TevC site (ENLYFQ/S).

3.7.5 Physiological conditions for in vitro studies Buffering and protein concentration

Physiological conditions, unless otherwise specified, were 150mM KCl at pH 6.4 to match intracellular pH conditions within 5 min of heat shock ([200]). We used Pab1 at 15 mM. Pab1 is not induced during heat shock, and has a log-phase concentration of roughly 20 mM, 120,000 molecules per cell ([201]) almost entirely in the cytosol ([64]) assuming a cytosolic volume of 10 fL.

3.7.6 Expression and purification of proteins

Expression and purification of Pab1 and Pab1 variants

Recombinant 6x or 8xHis-tagged Pab1 constructs were overexpressed in E. coli strain BL21(DE3), using a pET28a plasmid backbone (pESN07, pESN08, pJAR006, pJAR016, pJAR033, pJAR034, pJAR035, pJAR036, pJAR037, pJAR038, pJAR039). Cells were lysed via sonication on ice, in buffer containing 20 mM HEPES, pH 6.5, 150 mM KCl, 25 mM imidazole, and EDTA-free cOmplete protease inhibitor tablets (Roche 05 056 489 001). Clarified lysate was loaded onto a buffer-equilibrated 5 mL HiTrap chelating HP column (GE Healthcare Life Sciences 17-0409) on an AKTA system with automated fraction collector; bound protein was washed with loading buffer and eluted over an imidazole gradient. Fractions containing the target protein were pooled and loaded into dialysis tubing with b-mercaptoethanol and tobacco etch virus (TEV) protease, for removal of N-terminal tags and simultaneous reduction of imidazole concentration. Protein was subsequently loaded onto a second HiTrap Chelating

HP column to remove tags and uncleaved protein. Fractions were pooled, then exchanged to buffer containing 20mM HEPES, pH 6.5, 50 mM KCl, and loaded onto a 1 mL HiTrap heparin HP column for removal of nucleic acid contaminants (GE Healthcare Life Sciences 17-0406-01), with elution over a KCl gradient. If needed, protein was then loaded onto a 5 mL HiTrap Q HP column, in buffer 1 pH unit above the isoelectric point of the construct, and eluted over a KCl gradient. Finally, and if needed, protein was concentrated and loaded onto a Superdex 200 10/300 GL size exclusion column.

Expression and purification of Pab1 truncation variants

Recombinant 8xHis-tagged Pab1 truncation constructs were overexpressed from a pET28a plasmid backbone (pJAR011, pJAR012, pJAR013, pJAR014, pJAR015, pJAR029, pJAR030, pJAR031) in E. coli strain BL21 (DE3) and purified according to general Pab1 methodology listed above.

Expression and purification of protein G fusion constructs

Recombinant 8xHis-tagged protein G-Pab1 fusion constructs were overexpressed from a pET21 plasmid backbone (pJAR032, pJAR019, pJAR021, pJAR020, pJAR023, pJAR022, pJAR018, pJAR017, pJAR027, pJAR028, pJAR025, pJAR026, pJAR024), in E. coli strain BL21(DE3) according to the Pab1 protocol, then purified using a HiTrap Chelating HP column with subsequent TEV cleavage of tags when applicable. P domain-protein G fusion variants Randomized 1 and 2, and His-tagged P domain were partially insoluble upon overexpression, and thus 8M urea was added to all purification buffers prior to SEC-SAXS.

3.7.7 Dynamic and static light scattering SLS and DLS measurements

SLS and DLS measurements were performed in a DynaPro NanoStar. For DLS, each time point was the average of five 6 s acquisitions filtering out samples with a baseline higher than

1.003 and analyzed in the DYNAMICS software with a cumulant fit to the autocorrelation function. Measurements were performed either as a temperature fast jump (1C/min up to a specific temperature) or a slow ramp (0.25C/min continuously). All experiments, unless noted, were performed at 15 mM protein in 20mM HEPES, pH 6.4 with 150mM KCl and 2.5 mM MgCl2. Samples were centrifuged for 30 min at 20,000 g at 20C before DLS experiments. For samples below pH 6, concentrated stocks at pH 6.4 buffered in HEPES were diluted 10-fold into 50 mM sodium acetate, 150 mM KCL, buffered to the indicated pH and samples were spun at 4C, 20,000 g for 5 min.

3.7.8 Small-angle X-ray scattering (SEC-SAXS) Size-exclusion chromatography coupled to small-angle X-ray scattering (SEC-SAXS)

SAXS measurements were performed at the Advanced Photon Source at Argonne National Laboratory with in-line SEC columns (Superdex 75) equilibrated with 20 mM HEPES, pH 7.4, and with either 150 mM KCl (representing 0M GdnHCl) or 2M GdnHCl. We chose to include 150mM KCl in the 0M GdnHCl condition to mimic physiological ionic strength. The samples were injected onto the SEC with a starting concentration ranging from 100 mM to 1 mM. During sample concentration, prior to injection, 6M GdnHCl was added to samples to increase solubility and break up potential oligomers, as needed. Proteins were primarily eluted as monomers with some variants having large aggregates that eluted in the void volume. For the one or two mutants that expressed with a 30% cleavage product, SEC was able to separate the two forms. Typically, samples were spun at 16,000 g for 5 min before injecting.

3.7.9 Circular dichroism (CD) spectroscopy; CD measurements

Experiments were performed on a Jasco J-715 CD spectrometer in a 10 mm path length cuvette with a bandwidth of 5 nm, scan speed of 20 nm/min, a 4 s integration time with

data collected every 1 nm. Spectra were smoothed using the BezierFunction in Mathematica software with default settings. Experiments on isolated P domain (after TEV cleavage of the P domain fusion to the expression tag) were performed in 5 mM phosphate at pH 6.9 at 1 mM at 20C. Pab1 and RRM123 wavelength spectra were in 2.5 mM phosphate at pH 6.4 and 150 mM NaF at 0.2 mM. RRM123 temperature melts were in 2.5mM phosphate at pH 6.4 and 150 mM NaF at 1 mM taken at 217 nm with temperature increasing from 15C to 70C in increments of 1C/min.

3.7.10 Size-exclusion chromatography (SEC) Pab1:RNA complex characterization

15 mM Pab1 was incubated alone or with 100 mg/ml A_{19} RNA in 120 mL reaction in 20 mM HEPES (pH 6.4), 150 mM KCl, 2.5 mM MgCl2 buffer at 30C for 30 min. Pab1 and Pab1:A_{19} pre-formed complexes were then heated at 46C for 30 min when indicated. Each reaction was centrifuged 3 min at 8,000 g and 100 mL supernatant was subjected to size exclusion FPLC using Superose 6 10/300 GL (GE Healthcare) equilibrated with 20 mM HEPES (pH 6.4), 400 mM KCl buffer. Chromatography was carried out at 4C by use of an AKTA Purifier P10 system (GE Healthcare).

3.7.11 Light and fluorescence microscopy

Live cell imaging

Diploid yeast strains (yAER77, imaged alive) and purified recombinant proteins were imaged on an Olympus DSU spinning-disk confocal microscope using a 100x oil immersion objective and FITC/Cy2 and DsRed filter sets for Clover and mRuby2, respectively. Strains used for microscopy and detailed protocols for imaging strains were identical to those previously reported ([64]).

Protein assembly imaging

Purified recombinant proteins were imaged using either 63x or 100x oil immersion objectives, on a Leica SP5 II STED-CW super-resolution laser scanning confocal microscope with Gallium arsenide phosphide (GaAsP) / Photon Multiplier Tube (PMT) hybrid detectors and LASAF Leica proprietary software. For in vitro studies, purified recombinant protein was subjected to brief heat shock (when applicable) using an Eppendorf ThermoMixer F1.5 heat block, deposited on a slide and immediately imaged. For imaging experiments performed between pH 5.7 and pH 6.4, purified protein samples were buffered in 20mM HEPES, 150mM KCl. For imaging experiments performed between pH 5.0 and 5.6, purified protein samples were buffered in 20mM sodium acetate, 150mM KCl.

Mixing experiment

15 mM 1:20 Clover:unlabeled Pab1 was assembled, on-slide, via a 10x dilution with buffer containing 50 mM sodium acetate and 150 mM KCl. After 5 min, 15 mM 1:20 mRuby2: unlabeled Pab1 was added to the sample slide, then imaged using an Olympus DSU spinning-disk confocal microscope, with 100x oil immersion objective and FITC/Cy2 and DsRed filter sets for Clover and mRuby2, respectively.

Fluorescence recovery after photobleaching

Fluorescence recovery after photobleaching (FRAP) experiments were performed on a Leica SP5 II STED-CW super-resolution laser scanning confocal microscope with FRAP wizard, using a 63x oil objective. Droplet formation was triggered in a 15 mM 1:20 Clover: unlabeled Pab1 solution, either by heat treatment or a drop to pH 5 at room temperature. Pab1 droplets were imaged prior to photobleaching, bleached for 100 ms using the argon laser at 488nm, then imaged for up to 10 min at equal intervals. Total pixel intensity per unit area over time, in circular regions of interest drawn in ImageJ, was plotted in R.

3.7.12 Total/soluble/pellet (TSP) assay in vitro; Fractionation of Pab1 assemblies

Purified proteins were incubated at specified temperatures for 10 min, unless otherwise specified. For pH 4.5 and 5 treatments, samples were buffered in 50 mM sodium acetate. For pH 5.5, 6, and 6.5 treatments, samples were buffered in 50 mM MES. pH 7 and 7.5 samples were buffered in 20 mM HEPES. All sample buffers contained 150mM KCl and 2.5 mM MgCl2. For pH 4.5 and 5 treatments, samples were buffered in 50 mM sodium acetate. In all other cases, they were buffered in 20 mM HEPES. Samples were pelleted by sedimentation at 10,000 g for 10 min.

3.7.13 Poly(A)-binding protein mutant design; P domain mutations

Mutations to Pab1's low-complexity region were designed by replacing all instances of a set of residues, e.g., M and V, with another set, e.g., A. Two randomized mutants were designed by reordering all residues in the LCR according to the output of a pseudorandom number generator. Two additional mutants were constructed as follows. The MV/AGQ mutant was made by pseudorandom selection of replacements of MV (12 instances) from the set AGQ. The MVFY/AGPNQ was made starting from the MV/AGQ mutant, adding pseudorandom replacements of FY (10 instances) from the set AGPNQ. The intention behind the construction of these mutants was to replace aromatic and/or hydrophobic residues with polar residues. These were the only two such mutants constructed; no selection process was imposed.

3.7.14 QUANTIFICATION AND STATISTICAL ANALYSIS

Unless otherwise indicated, statistical tests were employed with only an informal analysis of whether the data conformed to the assumptions of the methods, reflecting the limited

assumptions of the few statistical tests employed.

3.7.15 Gel quantification

In vivo Total/Soluble/Pellet fractionation. Total protein Coomassie-stained gels were quantified using the gel quantification tool in ImageJ. Lanes loaded 1/4 X and 1/16 X were used to construct a standard curve for Figure 6; total protein intensity was used to verify consistent loading. Sensitivity of in vitro assemblies to pH and [KCl] gels were quantified in ImageJ with gel quantification tool by comparing total lane intensity. SEC pelleted material was compared to semiquantitative lanes.

3.7.16 Western blot quantification

All western blots were quantified using ImageJ's gel quantification tool. Semiquantitative lanes (loaded with less material) were used to construct a standard curve for Figure 6; fraction pelleted was computed as pelleted material divided by total and divided by a factor to account for pellet loading (2X or 4X). Proportions reported in Figure 1 is the blot intensity of the fraction divided by the sum of supernatant, 8,000 g pellet, and 100,000 g pellet.

3.7.17 DLS/SLS - Rh calculation

Calculation of T_{demix}: The apparent radius of hydration (Rh) reported is the Z-average, an intensity-weighted harmonic mean size calculated using DYNAMICS software with a cumulant fit to the autocorrelation function. T_{demix} is calculated as the temperature at which this Rh reaches double the value at 25C, calculated as the mean of the first 20 points. For the phase diagrams and Pab1dRRM3, T_{demix} was calculated as the temperature where the SLS normalized intensity doubled from its mean value of the first 40 points. To verify these definitions of T_{demix} were compatible, we compared their values on all traces having T_{demix} calculated using both methods, obtaining a standard deviation between the two

methods of 0.3C. Kinetic data were analyzed according to ([202]). DLS Z-average Rh was fit, in Mathematica, to Rh(t) = Rh(0)*(1+a*(Exp [K*t*Log[(a+1)/a]]-1)) where k is the rate of change. The data range spanned 20 min before to 80 min after reaching the target temperature. The temperature dependence, here denoted 'm', was quantified by the slope of the log(k) versus temperature. Q_{10} 36 C was calculated as Exp[m*10]. Each kinetic experiment was done twice at each temperature.

3.7.18 Temperature/pH phase boundary

We fit SLS-derived T_{demix} values (see Calculation of T_{demix} for details) at a range of pH levels for WT and mutant (MV/A, MV/I) Pab1 variants using nonlinear least-squares in R. Starting values were the same for all constructs. The functional form was: pHdemix = a + b*T_{demix}c with initial values a = 4.5, b = 1e-6, c = 4. All fits converged within 1000 iterations. Example call in R: fit < - nls(pHdemix a + b*T_{demix}.SLSĉ, start = list(a = 4.5, b = 1e-6, c = 4), data = subset(x, construct = = 'WT'), control = list(max- iter = 1000)) Each phase boundary was derived from temperature-ramp curves taken at three or more pH values with at least two replicates; all data are shown.

3.7.19 SAXS - Rg calculation; Calculation of Rg

Samples were analyzed with autorg and datgnom with the commands "autorg–sminrg 0.55–smaxrg 1.1" and "datgnom '1'.dat -r '2'– skip '3' -o '1'.out," respectively, where '1' is the file name, '2' is the Rg determined by autorg, and '3' is the number of points determined to skip at low q as specified from the output of autorg. For MVFY/AGPNQ, the parameter–sminrg is replaced with 0.7 due to an unphysical Rg from poor signal at low q for this mutant. Rg values and associated errors were determined in datgnom. For the P domain alone, the dependence on Rg with denaturant was fit, in Mathematica, with the functional form Rg0+a*x/(1+b*x) where a, b, and Rg0 (the extrapolated Rg without denaturant) are fit

parameters and x is the denaturant concentration. This ad hoc form has been used previously (Hofmann et al., 2012) for intrinsically disordered or unfolded states. Calculated Rg expected for folded and denatured proteins given for a 108 amino acid protein, the same number as in the His-tagged P domain construct, in Figure 5B right are 3*1080.3414.7$Aand2 *$ 1080.5931.7A [203]). For figures, error bars represent standard error on the mean within either linearly or logarithmically spaced bins.

3.7.20 Protein alignment and sequence analysis

Poly(A)-binding protein alignment

Orthologs of Pab1 were retrieved from SMART (http://smart.embl.de, ([204])) on the basis of possessing a specific domain architecture: four RRM domains and a PolyA (poly(A)-binding protein C-terminal) domain, resulting in 742 sequences. No constraint for the presence or absence of a proline-rich low-complexity region was imposed. We aligned these sequences using MUSCLE ([205]). We then filtered these sequences by identity to produce an alignment where all sequences share no more than 95% identity and each species contributes at most one sequence, resulting in 351 sequences in a master PABP alignment. For display in Figure 4, we further filtered sequences to eliminate those inducing large gaps (e.g., due to insertion specific to small numbers of species) to 295. All quantitative analyses were performed using the full 351-species alignment.

Proteome datasets

Intrinsically disordered proteins were retrieved from DisProt ([186]) release 6.02 after removing regions shorter than 40 residues and those with non-canonical amino acid entries ('Z' and 'B'). The yeast proteome (translated coding sequences) was retrieved from the Saccharomyces Genome Database (SGD) ([206], release 64-2-1.

Sequence analysis

To isolate the P domain, regions in the master PABP alignment aligned with the beginning and end of the S. cerevisiae P domain (beginning with YQQATAAAAAAAAGMP..., ending with ...ANDNNQFYQ) were extracted. The remaining sequences were designated PABPDP. Amino acid proportions (alternatively referred to as fractions) were computed by counting the number of amino-acid occurrences and dividing by the total amino-acid length of the respective subsequence, omitting gaps. Log-linear correlations between ILMVA frequencies and hydrophobicity were performed as follows. Given the absolute amino-acid frequencies for these amino-acid types, as in the table below (data from H. sapiens):

We compute the Pearson linear correlation between log-transformed frequencies and hydrophobicity. To avoid taking the logarithm of zero, a pseudocount of 1 is added to all frequencies. In the illustrated case, the correlation is r = 0.94. The proportion of variation in (log) residue frequencies explained by residue hydrophobicity is r2 = 0.89. Error bars in 3.4 show standard error on the mean. All statistical calculations were carried out in using the statistical package R (R Core Team, 2016).

As described in the main text, the Spearman rank correlation (nonparametric) was used to compare amino acid frequencies in the proline-rich domain. The Wilcoxon signed rank test (nonparametric) was used to determine whether frequency/hydrophobicity correlations were stronger in proline-rich domains than comparison sets. The Pearson correlation was used to test explicitly for a linear relationship between log-frequency and hydrophobicity.

3.7.21 DATA AND SOFTWARE AVAILABILITY

Example collapsed conformations

Single model P domain fusion conformations, shown in 3.5 D, were chosen from ensembles produced by RANCH ([207]), side chain atoms were added back using SABBAC ([208]),

and SAXS curves were generated with Crysol version 2.83 ([207]). For comparing Rgs in these models to the extrapolated His-tagged P domain Rg in water, 108 residues from the C terminus of the model were entered into Crysol yielding an Rg.

Custom software

Availability of custom scripts used in this manuscript is described in the Key Resources Table.

CHAPTER 4

A SPECIFIC REGULATORY FUNCTION FOR PHASE SEPARATION DURING THE STRESS RESPONSE (KATANSKI ET AL., UNPUBLISHED)

The material presented in this chapter is unpublished work representing my continued inquiry into the mechanism of Pab1-mediated gene regulation during stress. Christiane Iserman with the Alberti lab performed *in vitro* translation using yeast lysate in 4.3. Haneul Yoo assisted with measuing fluorescence anisotropy duing Pab1 phase separation in 4.2. Catherine Triandafillou assisted with data analysis of flow cytometry data for figure 4.4 and 4.6. Evgeny Pilipenko assisted with *in vitro* translation experiments using rabbit reticulocyte lysate.

I performed all flow cytometry experiments. I designed and performed all qPCR measurements. I designed and assisted with performance of *in vitro* translation using rabbit reticulocyte lysate, and fluorescence anisotropy measurement. I performed data analysis of Pab1 CLIP-seq data, and of data relating to 5' UTRs of related fungal species.

4.1 Summary

Authors:
Christopher D. Katanski, Haneul Yoo, Christiane Iserman, Evgeny Pilipenko, Catherine Triandafillou, Simon Alberti, and D. Allan Drummond

How do cells sense and respond to stressful environmental changes? In eukaryotic cells, stress triggers synthesis of specific molecular chaperones and the simultaneous condensation of many proteins and RNA, in certain cases by phase separation, into macromolecular assemblies such as stress granules. Here we show a connection between these two long-

observed phenomena: phase separation of an abundant, conserved, stress granule protein — poly(A)-binding protein (Pab1 in *S. cerevisiae*) — regulates translation of mRNAs encoding molecular chaperones during stress. We find that poly(A)-binding protein binds to A-rich regions in the 5' untranslated region (5' UTR) of mRNA that encodes heat-induced chaperones. In response to heat shock, poly(A)-binding protein phase separates and releases these RNAs. We show that poly(A)-binding protein represses translation when bound to the 5' UTR of mRNA, whereas phase-separated Pab1 neither binds nor represses translation. The induced chaperones, once translated, disperse poly(A)-binding protein back into functional monomers, which rebind the heat-induced mRNAs, repressing translation. Together, these results reveal an autoregulatory mechanism wherein stress-triggered phase separation of Pab1 facilitates high level translation of stress-induced chaperones, whose capacity to disperse phase-separated Pab1 leads to the attenuation of their translation after sufficient chaperones have been produced. This mechanism connects direct environmental sensing by phase separation to the adaptive cellular stress response.

4.2 Introduction

In response to stressful changes in the environment, eukaryotic cells respond in archetypal ways including global repression of translation, upregulation of a small set of stress response genes known as heat shock proteins (HSPs), and the formation of massive assemblies of protein and mRNA such as stress granules [209, 140, 137]. The relationship between these phenomena is largely unknown.

The predominant model for induction and regulation of the heat shock response posits a relationship between stress-induced assemblies and upregulation of stress response genes. In this model, heat and other stresses lead to protein misfolding and aggregate formation[139]. Aggregates are engaged by HSP70s - which titrates the chaperones away from a transcription factor, HSF1[141]. HSF1 unbound by HSP70 drives transcription of a small set of stress

response genes including more HSP70. These stress response genes are produced until there is enough HSP70 to both engage aggregates, and repress HSF1[28, 140]. HSP70, in concert with other chaperones, is known to disperse stress induced aggregates[19, 18]. However, the precise protein substrates that engage and titrate HSP70 are unknown [28].

Coincident with assembly formation and transcription of HSPs, translation is globally attenuated; this is referred to as polysome-collapse[19]. With the exception of stresses that trigger eIF2α phosphorylation, the mechanism causing reduced translation is unknown[56]. During stress, many initiation factors and mRNAs localize to visible foci known as stress granules. While significant literature has focused on these microscopically visible foci, less severe stresses still trigger formation of massive protein assemblies without visible stress granule formation [64, 61, 50, 19]. For this reason, we consider not just stress granules, but more generally, stress-induced assemblies of RNA and protein. Recent evidence suggests that these stress-induced assemblies form by phase separation and do not rely on membranes for their physical coherence [61, 20, 66, 68, 67, 73]. While phase separation of at least one stress-assembling protein, poly(A)-binding protein (Pab1 in *S. cerevisiae*), has been shown to be adaptive for cell growth under stressful conditions, the precise molecular function of these structures is unknown[61].

Poly(A)-binding protein, Pab1, is an abundant RNA binding protein known for its role in binding the 3' poly(A)-tail of mRNAs and regulating mRNA decay [210]. Pab1 is also thought to function as an initiation factor by interacting with eIF4G near the 5' end of the mRNA and to help circularize the RNA, leading to ribosome recycling [211]. We previously showed the Pab1 is capable of autonomously sensing temperature and pH and undergoing phase separation into gel-like structures. This phase separation is modulated by a low-complexity region enriched for hydrophobic amino acids [61]. Poly(A)-binding protein also has a lesser known function: to repress translation when bound to genetically encoded A-tracts in the 5' UTR of its own mRNA [127, 125, 126]. Poly(A)-binding protein has also

been shown to regulate the translation of other genes by this mechanism [130].

Despite reduced global translation in stressed cells, the newly transcribed HSP mRNAs are robustly translated [212]). The disparity in translation between HSP mRNAs and other mRNAs is known as preferential translation. The precise mechanism behind preferential translation is unknown; however, the 5' UTR of their mRNAs are known to be necessary [212, 37, 38, 40, 39, 41]. Translation of some of these transcripts has further been shown to be cap-independent, not requiring the full suite of cap-dependent translation initiation machinery [37, 42, 38].

To understand the relationship between stress-induced assemblies and other hallmarks of the stress response, we turn to a model system: heat stress in *Saccharomyces cerevisiae*. We show that an abundant RNA-binding protein, Pab1, binds the 5' UTR of HSP mRNAs, and releases them when the protein phase separates during stress. We show that Pab1 can repress translation of the HSP mRNAs when bound, but has no effect when the protein is phase separated. We find that inhibiting the dispersal of stress-induced structures causes continued production of SSA4, an HSP70, but without a concomitant increase in transcription. Together with historical results, these data support a mechanism of regulation for the heat shock response at the level of translation — stress-induced phase separation regulates translation of HSP mRNA.

4.3 Results

4.3.1 The 5' UTR of HSP mRNAs are bound by poly(A)-binding protein

The 5' UTR of HSP mRNAs are known to play a role in preferential translation of these genes during stress, likely by mediating a form of cap-independent translation [37, 38, 39, 212]. However, the precise mechanism remain unknown. These leader sequences are exceptionally high in A-content — a feature that seems to be conserved and specific to heat-induced

chaperones compared to constitutively expressed chaperones (4.1 A and 4.5 A)[22]. A notable example of this is the cytoplasmic HSP70s: SSA1, SSA2, SSA3, and SSA4. SSA3 and SSA4 are ohnologs resulting from a whole genome duplication; species that diverged from *S. cerevisiae* before the duplication have an ortholog of either SSA3 or SSA4 — as determined by gene synteny [213]. Similarly, SSA1 and SSA2 are ohnologs; however, SSA1 is only seen in species closely related to *S. cerevisiae*. SSA2 is constitutively expressed at high levels in *S. cerevisiae* and shows only modest transcript induction during heat. By contrast SSA1, SSA3, and SSA4 are induced more than 25 fold during stress at the transcript level(4.1 A)[169]. To determine if the A-content in a gene's 5' UTR was enriched, we compared the fraction of A nucleotides in 75 bases upstream of the start codon, with the A-content of all genes in that organism. The induced set of SSA genes and their orthologs have A-rich 5' UTRs. By contrast, SSA2 and its orthologs have near average A-content in their 5' UTRs. This suggests that an A-rich 5' UTR is a conserved feature of heat-stress-induced chaperone genes.

While A-rich 5' UTRs are important for translation during stress, they also reveal a potential translational inhibitor: poly(A)-binding protein [130, 126, 127, 125]. To determine if Pab1 binds to the 5' UTR of HSP mRNAs, we mined published CLIP-seq data against Pab1 [214]. Pab1 binding along a gene was matched to annotated 5' and 3' UTR regions, and the number of reads per nucleotide was normalized to the median of the ORF to account for transcript expression (4.1 B)[215]. As expected, many reads mapped to the 5' UTR of the PAB1 mRNA compared to its own ORF, consistent with specific binding to this region. Also, many reads map to the 3' UTR, consistent with PAB1 binding to the poly(A)-tail of the transcript. By contrast, for PGK1, an abundant glycolytic enzyme, many reads map to the 3' UTR, but not to the 5' UTR. HSP mRNAs SSA4 and HSP26 match the binding pattern of the Pab1 mRNA, indicating that Pab1 does bind the A-rich 5' UTR of these HSPs *in vivo*. To get a global sense of Pab1 5' UTR binding, we condensed CLIP-seq data to a

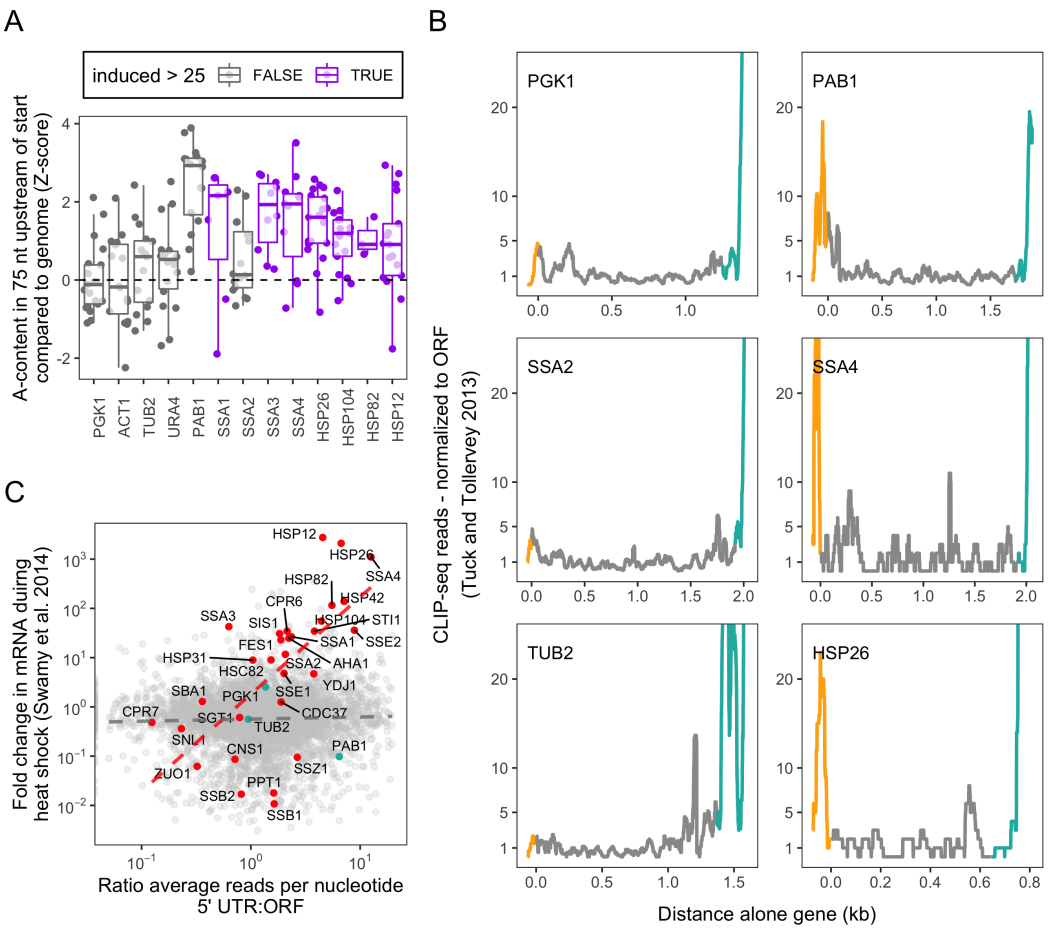

Figure 4.1: **Pab1 binds conserved A-rich 5' UTRs of heat-induced chaperones.** A) The A-content in the 75 nucleotides upstream of the start codon for each gene was compared to its associated genome average to get a Z-score. This score was compared between orthologs of several *S. cerevisiae* genes [213]. PAB1 is known to have highly conserved A-tracts in the 5' UTR region. A similar pattern is seen in select heat-induced chaperone genes (purple) compared to constitutively expressed genes (grey) such as PGK1, ACT1, TUB2, URA4, and SSA2. B) CLIP-seq data against Pab1 was mined from [214]. The number of reads mapping to each nucleotide was scaled by the median number of read per nucleotide in the ORF. The 5' UTR (orange) of the PAB1, the gene, shows enhanced binding of Pab1, the protein, to its own mRNA compared to the ORF (grey). Enhanced binding is also seen in the 3' UTR (blue) consistent with binding to a 3' poly(A)-tail. Enriched Pab1 binding in the 5' UTR is visible in heat induced genes, including SSA4 and HSP26, but not in constitutively expressed genes like PGK1, SSA2, or TUB2. C) Pab1 binding in the 5' UTR was quantified by taking the ratio of average CLIP-seq reads per nucleotide in the 5' UTR versus average reads per nucleotide in the ORF. This ratio was plotted against mRNA fold change during heat stress [169]. Among genes annotated as chaperones (red) there is a correlation between Pab1 binding to the 5' UTR and mRNA induction ($R^2 = 0.385$) compared to all genes (grey) ($R^2 = 0.001$)[140].

ratio of average reads per nucleotide in the 5' UTR vs. the ORF and plotted this against mRNA fold change during heat shock (4.1 C)[169]. Among genes annotated as cytoplasmic molecular chaperones, there is a positive correlation with Pab1 binding in the 5' UTR and transcript induction during heat shock ($R^2 = 0.385$ vs. 0.001 for all genes)[140].

4.3.2 Pab1 releases RNA during phase separation

Translational repression by poly(A)-binding protein has been found to regulate its own expression — when protein levels are low, there isn't enough protein to repress all the transcripts, so more protein is produced until the concentration is high enough to repress translation [127, 125, 126]. SILAC mass spectrometry indicates that Pab1 levels do not change appreciably during stress and recovery [64]. How then is the repressive activity of Pab1 modulated?

As noted before, Pab1 joins stress-induced assemblies, and is a defining component of stress granules. Our previous work suggests that during phase separation, Pab1 released RNA [61]. To monitor Pab1 RNA interactions during phase separation *in vitro*, we used a fluorescence anisotropy-based assay. Purified RNA, A_{19}, labeled with FAM, is mixed with purified Pab1. Fluorescence anisotropy of the labeled RNA is monitored as the temperature of the mixture increases. The anisotropy of the RNA begins to drop starting at 42°C — the temperature where Pab1 phase separation begins (4.2A)[61]. The change in anisotropy indicates a pseudo-melt temp at 48.3°C. The anisotropy of Pab1-bound RNA drops to the levels of RNA alone at temperatures that correspond to Pab1 phase separation. This indicates that Pab1 does indeed release RNA during phase separation and as a function of temperature.

To determine if Pab1 releases A-tracts in the mRNA of HSPs *in vivo*, we used qPCR to identify regions of an mRNA that are enriched in a Pab1 immunoprecipitation (IP). For each gene, 3 qPCR probes were designed to measure RNA at the 5', middle, and 3' end of the

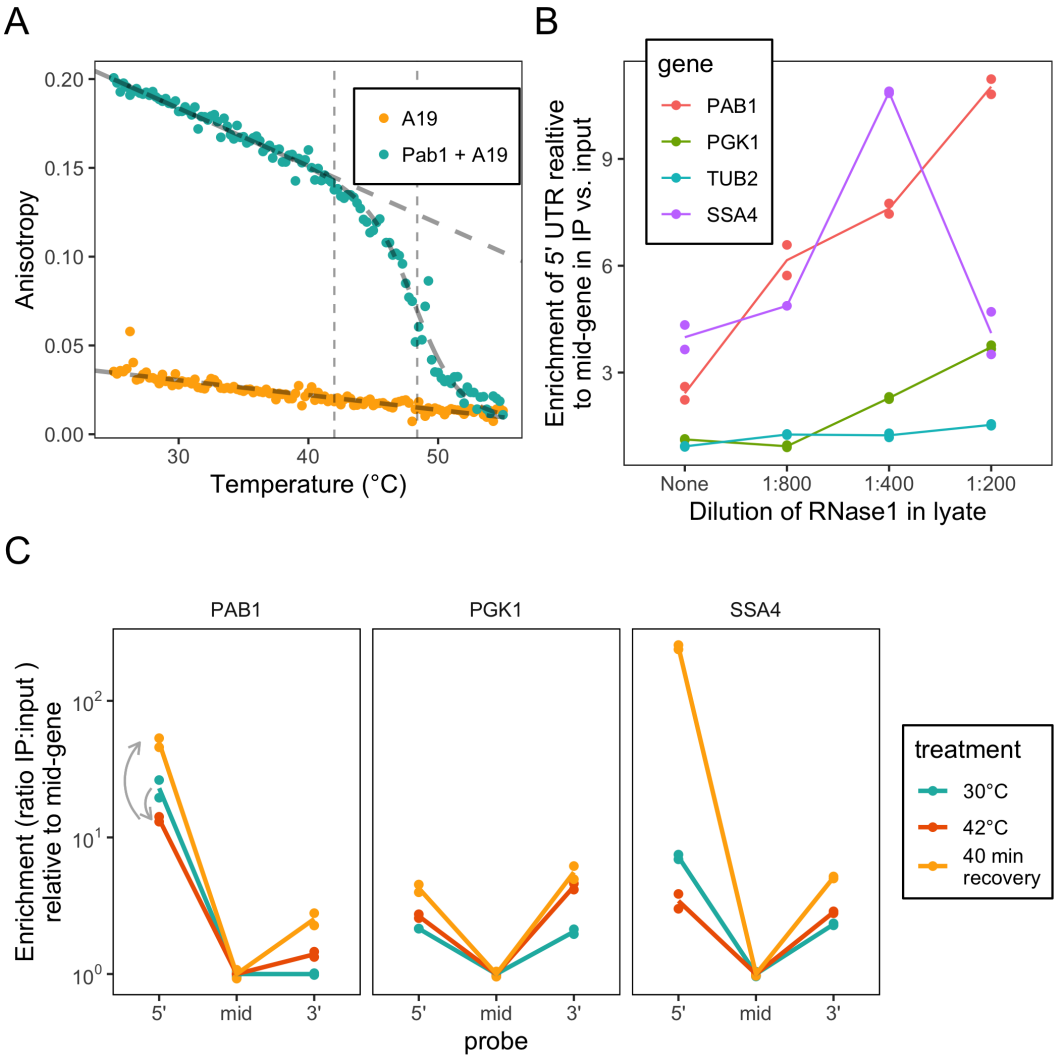

Figure 4.2: **Pab1 releases RNA *in vitro* and *in vivo* during phase separation.** A) Anisotropy of fluorescently labeled A_{19} RNA alone or when mixed with Pab1 was measured during a slow temperature ramp. Anisotropy of A_{19} alone slopes down as temperature is increased — consistent with faster tumbling at high temperature. A_{19} mixed with Pab1 shows a large drop in anisotropy as temperature increases, beginning when Pab1 phase separation starts. B) RNA was purified both from cell lysate, and from Pab1 immunoprecipitation (IP) following a mild RNase digest. Cell lysate was subjected to increasingly harsh RNase1 digest. qPCR was performed with probes against the 5', middle, or 3' end of several mRNAs to determine if one section was enriched in the IP fraction. For each gene, the ratio of 5' UTR RNA to ORF RNA in the IP is first normalized by the same ratio from the input RNA, then plotted as a function of RNase digest intensity. C) This experiment was repeated in cells stressed at 42°C for 10 min, and in cells stressed and then allowed to recover at 30°C for 40 min.

transcript; this method was modeled after similar work [216]. Yeast lysates were treated with RNase to fragment long mRNAs, then Pab1 was immunoprecipitated. RNA was isolated from both RNase-treated lysate, and Pab1 IP fractions, and then used in RT-qPCR analysis. For each probe, the ratio of RNA in the IP to input was calculated, then normalized to the ratio for the middle of the respective gene. We verified that enrichment of one RNA fragment could be disentangled from the rest of the transcript by showing enrichment is sensitive to increasing RNase digest (4.2 B). Increasing digest results in greater enrichment of the Pab1 5' UTR, a target expected to be bound by Pab1. We interpret this as showing that non-specific binding to the ORF is decreased by digest, but specific binding to the 5' UTR of PAB1 persists - thus the ratio of 5' UTR to ORF increases. Digest has little effect on the enrichment of negative control genes, PGK1 and TUB2, suggesting that the 5' UTR is as likely to be bound non-specifically as the ORF. Similar to PAB1, SSA4 shows increased enrichment with stronger digest, until the 1:200 dilution. This drop could indicate over-digest since, this mRNA is very low expression in unstressed cells. When this experiment is repeated with yeast subjected to mild heat stress, enrichment for binding the 5' UTR of SSA4 and PAB1 decreases, which is consistent with release (4.2 C). These data agree with reduced crosslinking of bulk RNA to Pab1 during stress[136]. When cells are allowed to recover from heat stress, enrichment for binding in the 5' UTR of SSA4 increases dramatically. The timescale of this rebinding is consistent with dispersal of Pab1 assemblies [64].

4.3.3 Pab1 selectively represses translation of HSP mRNAs

Poly(A)-binding protein is known to repress translation of its own mRNA and a few other genes. We sought to confirm this effect on mRNAs bearing the HSP mRNA UTRs. We used translation-competent yeast lysate to measure the effects of Pab1 on the translation of mRNAs bearing the 5' UTRs of HSPs [217]. As expected, increasing the concentration of Pab1 represses translation of mRNA with A-rich 5' UTRs, but has minimal effect on mRNAs

with control UTRs (4.3 A).

To determine if phase separation affects Pab1's ability to repress translation, we used a dual luciferase reporter assay with rabbit reticulocyte lysate. Two mRNAs were mixed, one with an A-rich HSP UTR and one with a control UTR. The two mRNAs encode firefly luciferase and renilla luciferase, respectively, which can be independently detected, and their relative productions compared. As before, when purified monomeric Pab1 is added to the translation mixture, translation of the mRNA with an HSP UTR is repressed compared to the control. However, if Pab1 is first phase separated by heat in isolation, then added to the translation mix, almost no effect is seen (4.3 B). These data support a model where phase separation not only causes Pab1 to release RNA, but it also renders it incompetent to repress translation.

4.3.4 Inhibition of chaperones leads to increased chaperone production, without concomitant mRNA production

To probe the relationship between stress-induced assemblies and molecular chaperone production, we used flow cytometry and qPCR to monitor protein and mRNA induction of SSA4, a heat-induced HSP70, fused to a fluorescent protein, Clover. Cells were subjected to a mild stress of 42°C for 20 minutes, before recovering at 30°C. The same experiment was done with cells grown in a low concentration of guanidinium chloride (GdnHCl) — a treatment known to inhibit the activity of HSP104, which is a chaperone involved in dispersal of Pab1 stress-induced assemblies [20, 19]. Cells grown in GdnHCl produced almost double the amount of SSA4 following stress — approaching levels of cells continuously grown at 42°C (4.4 A, 4.6 A). The rate of production matched untreated cells for the first 60 minutes following stress, but when untreated cells attenuated production, GdnHCl-treated cells continued to produce protein for another 60 minutes (4.4 A, 4.6 C). To verify that this effect was due to inhibition of HSP104, and not an off-target effect of GdnHCl treatment,

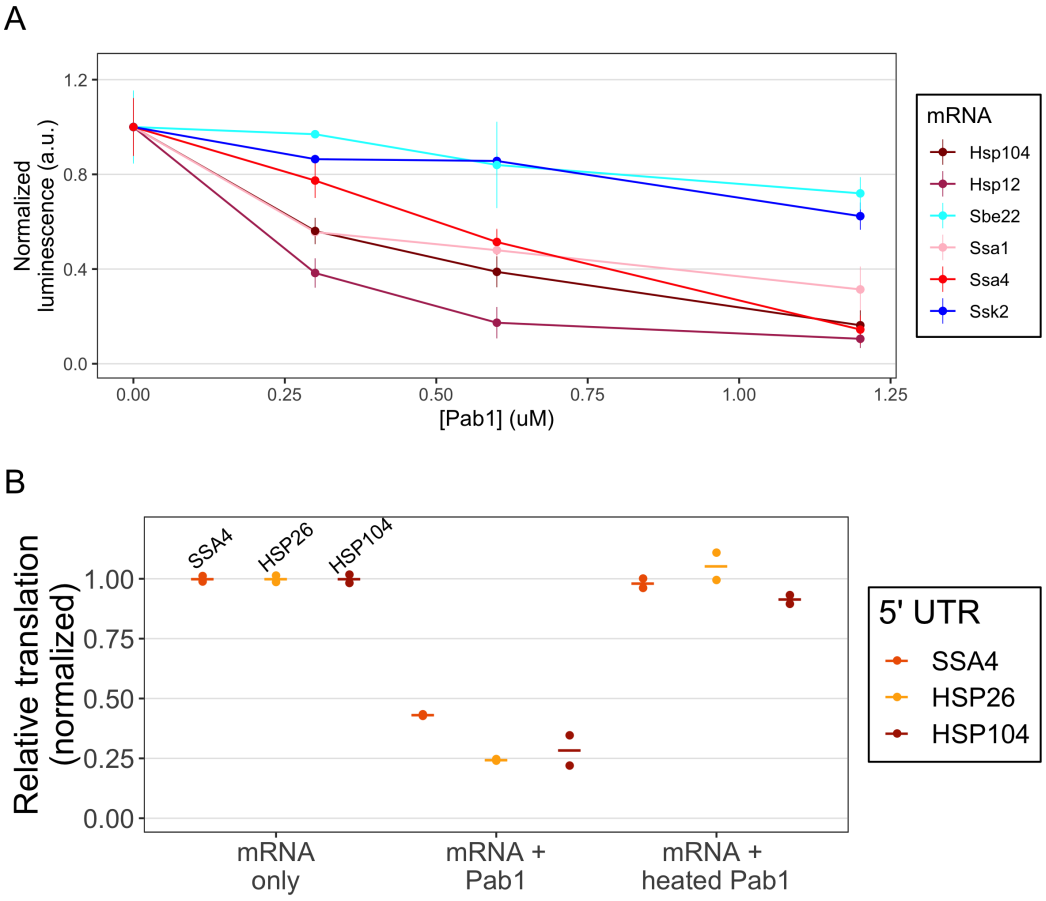

Figure 4.3: **Pab1 selectively represses the translation of mRNAs with A-rich 5' UTRs; phase separated Pab1 has no effect.** A) Translation-competent yeast lysate was mixed with luciferase mRNA preceded by different endogenous 5' UTRs. Luminescence of the produced protein was measured when the reaction was carried out with increasing concentration of purified Pab1 added. Results are normalized to no added Pab1. mRNAs with A-rich UTRs such as SSA4 and HSP12 are repressed by Pab1, while UTRs from SSK2 and SBE22 are minimally affected — indicating specific repression of A-rich sequences. B) Two mRNAs were mixed: one encoding firefly luciferase preceded by a control UTR from SSZ1; the other encoding renilla luciferase preceded by an A-rich 5' UTR from SSA4, HSP26, or HSP104. The mRNA mixture was translated using rabbit reticulocyte lysate; luminescences of firefly and renilla luciferase were independently detected. The reaction was repeated with the addition of purified Pab1 as in A, or with phase separated Pab1 — the ratio of firefly to renilla luciferase was normalized to the reaction with no added Pab1.

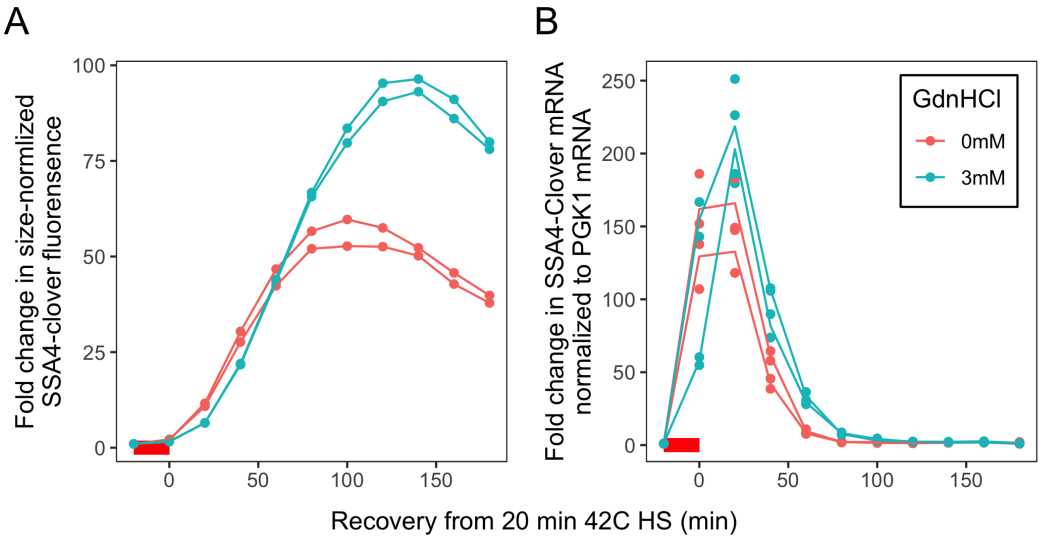

Figure 4.4: **Inhibition of chaperones leads to increased chaperone production, without concomitant mRNA production.** A) Cells expressing SSA4-Clover were preincubated in 0 mM or 3 mM Guanidinium hydrochloride for 3 hours. Then cells were shifted to 42°C for 20 minutes followed by recovery at 30°C for 3 hours. Flow cytometry was used to measure average fluorescence of cells during recovery. B) mRNA was isolated from cells treated as in A and qPCR was performed against SSA4-Clover and normalized to PGK1.

we deleted HSP104 and observed similar results (4.6 B). To determine if these differences in protein production are related to mRNA production, we used qPCR to monitor SSA4-Clover transcription relative to a glycolytic enzyme known to be minimally affected by heat shock, PGK1 (4.4 B)[169, 64]. Cells treated with GdnHCl induce more mRNA for SSA4; however, this mRNA is similarly short lived in treated and untreated cells. Transcript levels fall dramatically after 20 minutes recovery for both treated and untreated cells.

While treated cells do experience greater transcription of SSA4, it is difficult to reconcile the similar mRNA decay dynamics with the disparate rates of protein production (4.6 C, D, and E). Broadly, mRNA levels are expected to correspond with the rate of protein translation. Since we measured protein level by fluorescence, our detection is delayed by fluorophore maturation [218]. In order to roughly compare mRNA level and rate of protein production, we offset the rate data by 40 min, and plot it on top of mRNA levels with an arbitrary Y-axis (4.6 D). In untreated cells mRNA levels and the rate of protein production increase and

decrease with similar timing. By contrast, in GdnHCl treated cells, low levels of mRNA seem to support high levels of protein production. This result is difficult to rationalize if mRNA levels strictly determine translation rate, as one may expect based upon untreated cells. However, it is well known that mRNA for HSPs is preferentially translated during stress, consistent with small amounts of mRNA supporting robust protein production [44, 212, 37, 38]. Why then does translation rate decrease in untreated cells? One explanation is that translation of these transcripts is repressed at the same time they are being degraded. By contrast, in GdnHCl-treated cells, repression is impaired, resulting in continued translation. The time scales are consistent with the dispersal of Pab1 from stress-induced assemblies.

In summary, we find that there is translational regulation during heat shock and recovery of HSP genes. This regulation is related to the activity of molecular chaperones. These chaperones disperse phase separated Pab1 from an RNA-binding incompetent state back to an RNA-binding state. When bound to the 5' UTR of mRNA, including those encoding HSPs, like SSA4, Pab1 can repress translation. Pab1 does bind to the 5' UTR of SSA4 *in vivo* during recovery from stress. Together, these data suggest that phase separation of Pab1 facilitates high-level translation of HSPs during stress and helps to attenuate translation during recovery.

4.4 Discussion

How are the induction of molecular chaperones, global repression of translation, and formation of stress-induced assemblies related? The latter of these phenomena is of particular interest, because mounting evidence indicates that these structures form by phase separation, and this mechanism appears related to the formation of similar structures in neurodegenerative disease [219]. While aggregation in some diseases is the result of pathological mutation, stress-induced assemblies can be adaptive. However, the precise mechanisms of these adaptive processes have remained elusive [61]. Here we show that phase separation

of poly(A)-binding protein could act in translational regulation of the heat shock response. This supports the idea that formation of massive protein assemblies can be functional and adaptive, and not simply a result of pathologic protein misfolding.

Early work regarding regulation of the heat shock response suggests that there is an autoregulatory facet to the response [36]. Additionally, lysate from heat shocked cells lacks a dominant soluble inhibitor of translation [212]. Poly(A)-binding protein is a promising candidate for this factor for several reasons: 1) phase separation causes Pab1 to become sedimentable after heat shock (insoluble and RNA-binding incompetent) [64, 61]; 2) Pab1 can act as an inhibitor of translation for HSP mRNAs [127, 125, 126, 130]; 3) a fitness defect resulting from inhibiting phase separation of Pab1 is genetically dominant [61]. Our data support a role for Pab1 as a factor in translational regulation. However, it is unlikely to act alone. For example, assembly of cap-dependent initiation factors is also likely to affect preferential translation during stress [212, 64, 183, 56].

4.4.1 Poly(A)-binding protein maybe an important foil to cap-independent initiation

Translation of some stress-induced genes is regulated without use of traditional cap-dependent translation initiation machinery [37, 42, 38]. While it is known that the 5' UTR of these genes is important for translation initiation, the precise mechanism is unknown. These A-rich regions are thought to be minimally structured, unlike some viral IRESs, which can mediate cap-independent translation initiation [40]. However, a poly(A)-mediated mechanism, similar to pox virus, could support initiation [168, 41]. This alludes to a mechanism of preferential translation wherein initiation factors required for cap-dependent initiation are sequestered into stress-triggered assemblies, thus advancing genes capable of cap-independent initiation to a preferred status. However, this model introduces a problem: how to regulate translation of these genes after cap-dependent initiation resumes? One possible solution is repression by

Pab1 following dispersal of stress-triggered assemblies. Thus, phase separation and assembly of initiation factors in addition to Pab1 could regulate global changes to translation during stress.

4.4.2 Stress-triggered phase separation as a general mechanism for regulation

More broadly, phase separation is an attractive mechanism for regulation of the stress response because it can integrate many environmental cues — temperature, acidification from starvation, osmolytes and cytoplasmic crowding [64, 20, 91, 61]. Phase separation can be both protein-autonomous — not requiring additional signaling factors and thus reducing the time required to adapt to a rapidly changing environment — and distributive — many different proteins can phase separate independently and respond to different stimuli to tune the proper response [61, 64, 20, 86, 68, 67, 66, 220, 73].

4.4.3 A function of stress granules beyond sequestration

Most of our knowledge of stress-induced protein assemblies focuses around the study of visible foci known as stress granules. While the precise composition of stress granules varies by organism and stress, generally they contain poly(A)+ RNA and translation initiation factors [56, 19, 51]. Since stress granule formation is coincident with global attenuation of translation and they colocalize with initiation factors, it seems clear that they are somehow connected to translation [19]. Initially stress granule formation was thought to strictly require phosphorylation of translation initiation factor eIF2α [47, 48]. This phosphorylation would lead to stalled 43S preinitiation complexes. As ribosomes run off of mRNAs, mRNA would become exposed. Exposed mRNA would be bound by a variety of non-specific RNA binding proteins, which would then aggregate, thus recruiting the mRNA and associated initiation machinery to foci. Sequestered in foci, translation machinery and mRNA are protected [34, 47, 53]. This model is supported by the effect of cyclohexamide: cyclohexamide stalls ribosomes

on mRNA, and prevents stress granule formation — presumably by preventing TIA-1 from binding mRNA [53]. While this model effectively explains phenomena in mammalian cells subjected to arsenite stress, the model fails to explain a growing variety of observations from other stresses and other organisms. First, eIF2α phosphorlyation is not strictly necessary for stress granule formation; *S. cerevisiae* do not require eIF2α phosphorylation during heat stress, human cells do not require eIF2α phosphorylation during hypertonic stress [50, 221]. Second, the composition of stress granules varies, and components of a stalled 43S preinitiation complex do not always colocalize, including the 40S ribosome [50, 143, 222]). Third, crosslinking suggests that many initiation factors no longer physically associate with RNA following stress (eIF4E, eIF4G, Pab1)[136]. Fourth, cycloheximide does not block the formation of sedimentable aggregates [64]. Fifth, there has been no demonstration that mRNA localization to foci has a physiological consequence [223].

An alternative to the sequestration model, described above, is autonomous phase separation of many different stress granule components into small, but sedimentable species, followed by coalescence into visible foci [64]. This model reconciles the colocalization of Pab1 with poly(A)+ RNA despite our evidence that the protein releases RNA [61]. Additionally, crosslinking data suggests that eIF4E and eIF4G do not associate with mRNA following stress, despite colocalization in stress granules — independent phase assembly processes followed by coalescence can reconcile these observations [136]. It has further been shown that RNA can autonomously phase separate in certain conditions [224]). This model provides an elegant way for cells to sense different environmental cues quickly, and integrate the cues into a regulated gene expression pattern.

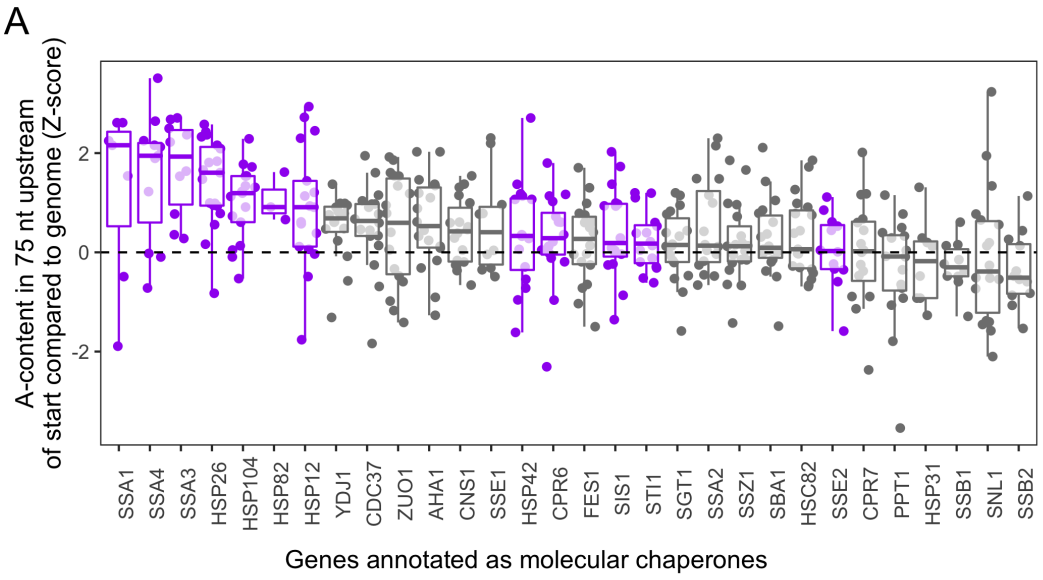

Figure 4.5: **Heat-induced chaperones have conserved A-rich UTRs.** A) As in 4.1 A, the A-content in the 75 nucleotides upstream of the start codon was plotted for cytoplasmic chaperones from *S. cerevisiae* genes and their orthologs in 20 related fungal species [213]. Genes are ordered by median A-content. Genes that are induced by more than 25-fold at the mRNA level during heat-shock are colored purple [169].

4.5 Supplemental figures

4.6 Methods

4.6.1 In vitro translation experiments using rabbit reticulocyte lysate

Related to 4.3 B: from a plasmid encoding firefly luciferase fused to the SSZ1 5' UTR, dsDNA was generated by PCR using primes to add a T7 transcription site and a poly(A)-tail of 30 nucleotides. DNA was used as the template for the NEB T7 HiScribe kit (NEB E2040S). Transcription included addition of cap-analogue (NEB S1407S) according to manufacturer's instructions. mRNA was purified by phenol-chloroform extraction and two rounds of ethanol precipitation. The same protocol was used to generate mRNA encoding renilla luciferase preceded by 5' UTRs of HSP26, HSP104, and SSA4. Pab1 was purified as previously described ([61]). mRNAs were mixed together with either buffer, Pab1, or Pab1 that had been as-

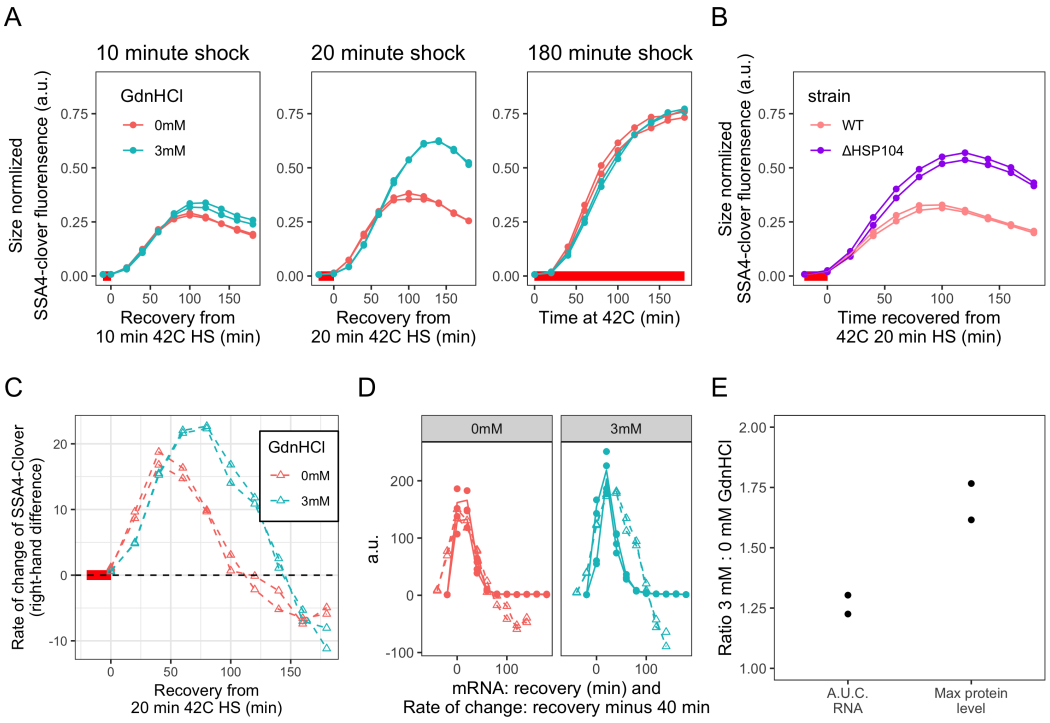

Figure 4.6: **HSP104 is involved in translational regulation during recovery from heat shock** A) Cells were grown and treated as in 4.4, but stressed at 42°C for 10 and 180 minutes -indicated by a red bar on the X-axis- for comparison to the 20 min stress in 4.4. B) Instead of pretreatment with guanidinium hydrochloride, SSA4-Clover expression was measured in wild type cells and ΔHSP104 cells C) The rate of change in protein abundance from 4.4A was computed using a right-hand difference. D) The rate of change in SSA4-Clover production (dashed, triangles) was overlaid with mRNA levels (solid, circles) from 4.4B. Protein production was left-shifted by 40 minutes to correct for Clover fluorophore maturation time. E) Area under the curve for mRNA expression for guanidinium treated cells was compared to untreated cells to quantify differences in gene expression at the mRNA level. Similarly, the ratio of of maximum protein levels achieved for treated and untreated cells was compared.

sembled by incubation at 46°C for 20 min at 40 μM (?) before mixing with RNA. RNA mixture was then added to promega rabbit reticulocyte lysate *in vitro* translation system (Promega L4960). Final concentration of each mRNA was 40 nM and the final concentration of Pab1 when present was 4.5 μM. Translation reactions were run at 30°C for 60 minutes, then quenched with 5 volumes of passive lysis buffer included with the translation system. Luciferase activity was assayed using Dual-Luciferase® Reporter Assay System (Promega E1910) according to manufacturer's instructions. Briefly, 5 uL of quenched translation reaction was mixed with 25 uL of firefly luciferase reagent; luminescence was measured with promega GloMax® 20/20 Single-Tube Luminometer. Then 30 uL of renilla luciferase reagent was mixed in and luminescence was measured again. Experiments were done in duplicate. The ratio of renilla to firefly luminescence for each mRNA pair across all additives (buffer only, Pab1, assembled Pab1) was normalized to the buffer only control ratio. Values are reported.

4.6.2 UTR sequences

SSZ1:

TACTACCACAATCACAGTTAAAATTACAAATAAG

HSP26:

CACCGATAAAGATATATCAGATCTCTATTAAAAC

AGGTATCCAAAAAAGCAAACAAACAAACTAAACA

AATTAAC

HSP104:

AGCAATAACAAAGAAAAAAGAAATCAACTACACG

TACCATAAAATATACAGAATAT

SSA4:

TCCACAACTTTCGAATAAAAACCACTAATAAAAA

GTAAATAACAAAAACAAGAAAAAAAATAAACAAA

ACAATAATC

4.6.3 Pab1 release of RNA during stress in vivo

Related to 4.2 C:

Cell growth: Cells were grown by innoculating 300 mL YPD with yCDK071 (SSA4-Clover) the, grow overnight (13.5 hours) such that they reach OD 0.430. Harvest 3 tube of 50 mL cells each by spinning in 50 mL conical tube 1.5 min 3000g. Decant cells. Resuspend cells 1 mL ICE COLD SPB; transfer to new tube; spin 30 sec 3000g, decant. Add 250 uL of SPB. Mix, freeze 2 aliquots of 150 uL in safelock tubes.

Cell stress: Cells were grown as above. Then stressed in the following way. Harvest 2 tubes of 50 mL; 1.5 min 3000g. Decant cells - leave 500 uL of media to keep cells wet. Heat shock in 42C water bath for 10 min. Put on ice. Resuspend 1 tube in 50 mL pre-warmed YPD, recover at 30C for 40 min. Resuspend the other tube in 1 mL ICE COLD SPB; pellect cells 3000g 30 sec, decant. Resuspend 200 uL SPB; freeze two 150 uL aliquots. Repeat harvest procedure for recovering cells.

Preparation of protein G beads for immunoprecipitation: Start with 50 uL proteinG surebeads per IP. Wash 3X PBST (PBS + 0.1% tween20) add 200 uL PBST. Add 5 uL Anti-Pab1 per IP; incubate / mix at RT 30 min. Wash 3 more times with PBST. Resuspend 50 uL PBST per IP

Cell lysis and RNase digest: Cells were cryogenically lysaed as described ([61]) into 600 uL of NEB buffer 3 + 1 mM DTT (fresh), 1:500 disution of Roche protease inhibitor IV, and NEB RNase1f diluted with NEB buffer 3 as follows: For unstressed cells used to investigate the effects of RNase treatment, Rnase1f was added to a final concentration in the lysate of 0, 1:200, 1:400, or 1:800. For cells stressed and recovered, RNase digest of 1:1000 was used. Mix and spin lysate 3000g 30 sec. Move 500 uL lysate to fresh tube. Take 30 uL as total

protein sample. Spin lysate 10000g 5 min. Move 450 uL supernatant to new tube. Wash pellet once. Resuspend in 450 uL PBS and save. Taken 30 uL Sup as protein sample and save. Take 100 uL sup as Sup RNA. Keep at room temperature. Add 50 uL Pab beads to remaining 300 uL lysate. Vortex. Incubate lysate mixed with beads at 25 C, in thermomixer with agitation for 20 min. Incubate "Sup RNA" sample same temp, same time. Magnetize the beads; keep the flow through for protein sampling. Add 200 uL HES buffer to "Sup RNA", mix, add 300 uL acid Phenol. Vortex and incubate 65 C. Wash beads 3X in 1 mL SPB400. Resuspend in 300 uL PBS. Take 30 uL protein sample and save it. Magnetize, remove PBS. Resuspend 300 uL HES buffer. Add 300 uL Acid phenol.

Extract RNA: Add 300 uL acid phenol. Incubate 65 C 10 min. [Likely already did this just before]. Spin mixture for 10 minutes at 20000g at room temperature. Move Aqueous top phase to a fresh tube. Add 300 uL acid pheonl and extract again. Extract twice with with chloroform. Precipitate with 1/10th volume 3M amonium acetate and 2 uL glyco-blue.

DNase treatment: Resuspend precipitated RNA in 45 uL H2O. Nano drop (Sup fractions will likely need dilution to 44 uL at 200 ng/uL). Add 5 uL of 10X Turbo DNase buffer to each sample. Add 1 uL turbo DNase. Incubate 37C for 30 min. Clean RNA through RNA clean column according to manufacturer's instructions. Elute in 14 uL. (IP RNA will be low 10-20 ng/uL). Nanodrop to get ng and check for phenol contamination.

Reverse transcription: Reverse transcription was done using iScript^{TM} Select cDNA Synthesis Kit, (BioRad 1708897). Reverse transcription was done with a cocktail of gene specific primers, each at 5 uM final concentration. Efficiency of the reverse transcription cocktail was checking with qPCR. 1 ug DNase treated RNA was used for each 20 uL RT reaction when the source was total RNA. For immunoprecipitation fractions, 100 ng of RNA was used. After reactions were complete, 60 uL of water was used to dilute the reaction. 2 uL of diluted reaction was used as template for each qPCR reaction described below.

qPCR Primers and probes for qPCR were designed using IDT primerQuest tool. Primers

are listed below. Each qPCR reaction was 10 uL, composed of 5 uL 2X IDT PrimeTime qPCR master mix, 2 uL of Reverse transcription reaction template, and 3 uL of a mixture of primers and probe (1.5 uM for primers; 600 nM probe). The final concentration of primes and probe in the mix is 500 nM and 300 nM respectively. Reactions were done in a biorad CFX96 Touch^{TM} Real-Time PCR Detection System with annealing at 55 C for 45 cycles.

4.6.4 Anisotropy temperature ramp

Related to 4.2 A: FAM-labeled A_{19} RNA was purchased from IDT. The oligo was diluted to a final concentration of 5 uM, combine with 0.2 mg/mL yeast tRNA (Roche 10109517001), and buffered with 20 mM HEPES pH 6.4, 150 mM KCl, 2 mM MgCl2. Anisotropy of the mixture was measured using HORIBA FluoroLog-3 Spectrofluorometer at the University of Chicago Biophysics core. Temperature was increased at a rate of 0.25 C per minute. Anisotropy was measured every minute. The experiment was repeated with the addition of 5 uM Pab1 purified as previously described ([61]).

4.6.5 Yeast strain construction (SSA4-Clover

Related to 4.4: yCDK071, SSA4 was tagged with the fluorophore clover at the 3' end using a scarless procedure previously described ([61]). Briefly, strain BY4742 was transformed with a URA3 selection cassette with flanking regions to direct homologous recombination between the endogenous stop codon of SSA4 and the endogenous 3' UTR; transformants were selected based on uracil auxotroph using standard lithium acetate procedure and verified by PCR and Sanger sequencing. Next, DNA encoding Clover preceded by a short GlySerSer repeat linker was transformed. Flanking regions were chosen to recombine out the endogenous SSA4 stop codon and the URA3 cassette, but leave the endogenous 3' UTR after the Clover stop codon. Transformants were selected using 5 FOA and verified using PCR and Sanger sequencing. yCDK113 (HSP104) is derived from yCDK071; HSP104 was knocked out with

a URA3 cassette as before, and selected using uracil auxotrophy.

4.6.6 Flow cytometry and qPCR following and guanidinium treatment

Related to 4.4: Yeast strain yCDK071 was inoculated from glycerol stocks and grown overnight to OD 0.02. Cultures were split; half of the culture continued to grow a 30 C, the other half was supplemented with 3mM guanidinium hydrochloride and grown for another 3 hours as in ([20]). Cells were analyzed on flow cytometer LSR Fortessa 4-15 and the University of Chicago flow cytometry core. Cells were measured for forward scatter (488), side scatter (488), BV421(405:450/50) fluorescence , and FITC (488:525/50) as reported here ([225]). 1 mL of cells from both treated and non treated cultures were heat shocked at 42 C for 20 minutes (unless otherwise indicated) in a heat block. After stress, cells were moved back to 30 C heat block and grown with agitation for 3 hours. Aliquots of cells were taken and analyzed on the flow cytometer every 20 minutes for 3 hours as cells recover from heat shock. Data was analyzed using custom scripts. Briefly, the ratio of FITC fluorescence to forward scatter was taken as size-normalized fluorescence; the medianfluroseence was found across 20000 cells analyzed per sample and reported. To analyze mRNA production, cells were grown, treated, and stress as above, however 50 mL cultures were used instead of 1 mL cultures. Every 20 minutes, 1 mL of cells was collected. Cells were pelleted, decanted, and flash frozen in liquid nitrogen. Once all samples were collected, Cell pellets were resuspended in 300 uL HES buffer (20 mM HEPES pH 6.5, 50 mM EDTA, 2% SDS), mixed with 300 uL acid buffered phenol, and RNA was extracted as described in this manuscript. Samples were extracted, DNase treated, reverse transcribed, and used for qPCR as described.

4.6.7 Analysis of fungal 5' UTR sequences

Related to 4.1 A and 4.5 A: Homologs of S. cerevisiae genes from ([213]) were gathered, then the 75 nucleotides upstream of each start codon for each gene was parsed from the

genomes. The fraction of A nucleotides was calculated. This process was repeated for every annotated genome so that a Z-score could be assigned to each gene relative to the A-content of 5' regions within its endogenous genome.

4.6.8 Analysis of CLIP-seq data

Related to 4.1 B and C: CLIP-seq data against Pab1 published ([214]) and available at Gene Expression Omnibus GSM1137787. Starting from data where reads were collapsed down to read count at each genomic coordinate, the coordinates for each gene extended by 5' and 3' UTRs as annotated from ([215]). To plot traces for each gene, the median number of mapped reads per nucleotide in the ORF was used to scale reads to account for differences in gene expression. Next, to condense the data into a enrichment score, the average number of reads mapped per nucleotide in the 5' UTR was compared to the average reads per nucleotide in the ORF. This data was plotted against data from ([169]) to show fold-change change in gene expression during heat shock.

CHAPTER 5

CONCLUSIONS AND FUTURE DIRECTIONS

The previous chapters describe work characterizing the composition of stress-induced assemblies, their mechanism of formation, and coincident production of molecular chaperones. This chapter will highlight how these findings have challenged previous models about assembly formation and function. This chapter will also acknowledge questions that remain open, and suggest possible experimental approaches to answer them.

5.1 Protein assembly is adaptive

Chapter 2 adopts a functional definition of stress-induced assemblies as sedimentable species - a definition which overlaps but is distinct from a definition related to formation of visible cellular foci. This definition makes no assumption regarding mechanism or adaptive/maladaptive function. We found that specific protein species joined sedimentable species from different cellular compartments under different stress severities 2.1. Specificity among the set of translation initiation factors that assemble suggests one function of this assembly process: to direct translation to a set of mRNAs requiring only a minimal set of initiation factors [64, 168]. Sedimentable species are not degraded, but dispersed back to a soluble form; this was taken as evidence that sedimentable species are not irreparably damaged or misfolded 2.5. Moreover, heat-triggered sedimentation of some proteins can be reconstituted, and the assembled proteins are still enzymatically functional 2.5. These data again suggest that sedimentable species are not misfolded. Formation of sedimentable species is not affected by the drug cycloheximide, unlike formation of visible foci. This result requires reinterpretation of a model for stress granule formation that required ribosome runoff [56].

Chapter 3 reports that another stress granule protein can be reconstituted to form stress-triggered assemblies *in vitro*: poly(A)-binding protein (Pab1). This protein displayed unique

assembly properties compared to other known assembling proteins: 1) Pab1 releases RNA during assembly 2) assembly of Pab1 does not require its low-complexity domain 3) Pab1 assemblies are gel-like, not liquid-like in character [61]. Pab1 does not appear to undergo global unfolding during assembly, again suggesting that the protein is not misfolding and undergoing nonspecific aggregation 3.2. The assembly of Pab1 appears to proceed via a phase separation mechanism that is tuned by the hydrophobicity of its low-complexity region. Pab1 autonomous phase separation also integrates environmental cues of temperature and pH. This suggest a mechanism for how cells can response to multiple simultaneous stresses. Importantly, I show that reducing the hydrophobicity in this domain reduces phase separation of the protein *in vivo* and results in reduced organismal fitness during growth at high temperature. We found signatures of evolutionary selection on the hydrophobicity of this domain, and additionally found environments that favor either high hydrophobicity or low hydrophobicity, consistent with selection on regulated assembly of Pab1 in response to the environment 3.4 3.9.

Chapter 4 focuses on one unique feature of Pab1 phase separation compared to other assembling RNA-binding proteins is how it releases bound RNA. I showed that Pab1 binds the A-tracts in the 5' untranslated region (UTR) of mRNA that encodes stress-induced chaperones. I further showed that Pab1 releases these RNA regions during stress *in vivo*. When bound to these regions soluble Pab1 can repress translation of mRNAs *in vitro*, while phase separated Pab1 has little effect. Together these data suggest that Pab1 releases HSP mRNAs during stress and facilitates their efficient translation. Moreover, HSPs are known to disperse Pab1 back to an RNA binding state, which is expected to repress further HSP translation. This mechanism is consistent with observation of self-regulating aspects of the cellular heat shock response [36, 32]. Finally, I showed that inhibiting the activity of chaperones, which results in persistence of Pab1 assemblies, results in greater HSP production - regulated at the post-transcriptional level.

Together these data support a reframing of how we understand the effect of heat shock on the proteome. Instead of heat leading to catastrophic protein misfolding and non-specific aggregation, we see specific assembly via phase separation, and not misfolding, that leads to increased organismal fitness. Thus, formation of these massive structures is unlikely due to unfolding and generating toxic species. Instead, assembly is cytoprotective, regulated, specific, and ultimately adaptive.

5.2 Future directions

There are many remaining open questions regarding the function of protein and RNA assembly during stress and how organisms sense and adapt to changing environments. Below I explore how to approach some questions and explain why they are important for our understanding of cell adaptation.

5.2.1 The adaptive function of Pab1

Chapter 4 explores how phase separation of Pab1 can affect translation of HSPs during acute stress. While this work is highly suggestive, it remains to be shown that altered phase separation of Pab1 leads to different protein expression *in vivo*. Similarly, it is not clear whether the long-term growth phenotype associated with the Pab1 P domain is related to regulating translation of the HSPs during acute stress, because the timescales are different. Clues as to source of a long term growth defect related to the P domain come from additional phenotypes, including differential sensitivity to caffeine and tuned sensitivity to buffered citrate. These phenotypes suggest a role for TOR signaling, which is known to be related to dispersal of assemblies [226, 97]. These data further suggest that assembly processes, which are sensitive to TOR signaling and phosphorlyation are also adaptive. One model is that assembly-impaired P domain mutants are especially sensitive to caffeine, because TOR would normally compensate for reduced Pab1 assembly by stimulating assembly of other factors

as part of an adaptive stress response. This model suggests that blocking TOR signaling during acute stress will also lead to reduced assembly of specific protein factors. While it has been shown that TOR is indeed necessary for certain proteins to join heat-induced foci, the full suite of affected proteins is unknown. To understand the adaptive consequences of impaired Pab1 phase separation, aside from TOR sensitivity, proteomic analysis of cells after long-term growth may reveal a defect. One possibility is that cells impaired for growth have produced too many HSPs. Since the cells are arrested, not dead, catastrophic damage is not expected. Instead, impaired mutants are likely to transcribe excess amounts of HSP mRNA to compensate for constitutive Pab1 repression of HSP translation, ultimately leading to overexpression of HSPs. It is known that cells that grow slowly, due either to mutation or nutrient limitation, are more resistant to stress due to higher chaperone expression [227, 228]. It is not clear if high chaperone expression leads to reduced growth rate. If so, this would explain reduced growth of yeast expressing assembly-impaired Pab1.

5.2.2 Role of RNA in recruiting proteins to assemblies

During acute stress, as studied in [64, 61], what is the mechanism of initiation factor assembly? Are these proteins autonomously phase separating, or do they join sedimentable species by virtue of binding mRNA? It has been reported that "purified stress granules" are resistant to RNase digest, which supports RNA-independent assembly [229]. However, RNA could simply be tightly protected. Alternatively, one protein factor may assemble and simply recruit the others. In addition to Pab1, recent evidence indicates the eIF4E and eIF4G, involved in 5' cap binding, have reduced crosslinking to RNA during stress [136]. This evidence is contrary to a well-cited model of stress granule formation where RNA is recruited to assemblies, and the rest of the 43S preinitation complex simply follows along [56]. Understanding recruitment to assembly for initiation factors is part of a broader question about how proteins are recruited to assemblies, and the role of RNA in recruitment.

Experiments *ex vivo* with RNase are likely a fruitful direction to identify RNA dependent and independent assembly processes.

5.2.3 Mechanism of HSP mRNA initiation

Further, what is the function of initiation factor assembly on continuing translation? Does their sequestration actually focus translation of HSPs? It is highly suggestive that the remaining soluble initiation factors are those required for poly(A)-mediated cap-independent initiation. However, it is not yet demonstrated that the HSPs are initiated via a pox virus-like poly(A)-mediated initiation mechanism [168]. Experiments exploiting translation-competent yeast lysate generated from various knockout yeast strains will help establish specific initiation factor requirements for HSP mRNAs. *In vivo* mRNAs with strong 5' hairpins will also help establish whether conventional 5' cap-dependent ribosome scanning is necessary for translation of HSPs. Further, it is unclear whether the set of mRNAs that can be translated is affected by stress-specific changes to which proteins are recruited to assemblies [51]. This would require multiple independent assembly processes, and would present an elegant mechanism for how cells can sense and adapt to different environments while harnessing the same basic mechanisms. Understanding how the HSPs are translated is an important step in understanding how cells distinguish stress and alter gene production.

5.2.4 Long-term adaptation

Aside from acute stress, many questions remain about how cells adapt to long-term changes in the environment. For example, yeast stressed at 42°C upregulate HSPs, slow growth, from protein assemblies, etc. However, after many hours at elevated temperature, growth will resume. It has been shown that cells re-enter the cell cycles upon clearance of stress granules when recovering in non-stressful environments [54]. Have assemblies been cleared in yeast that grow at high temperature? If so, how is this possible? For example, Pab1 phase

separates at 42°C, so how could the cell prevent phase separation of Pab1 while remaining at elevated temperature? One likely answer is that HSPs actively suppress protein assembly, such as HSP70. Alternatively, small heat shock proteins like HSP26 may alter the solvent properties of the cytoplasm inhibiting phase separation. Regulation of small molecules may also play a role. Proteins may be phosphorylated to alter the biophysical properties of assembly. Understanding how cells control and suppress protein assembly will provide us insight into the mechanism of assembly formation. Is suppression of assembly ATPase-driven or does it result from altered assembly requirements? Is assembly even suppressed at all, and if not, how is the cell able to grow with so many sequestered factors? I believe these questions are extremely fertile ground for discovery of mechanisms relating protein assembly and gene regulation.

References

[1] F Ritossa. Discovery of the heat shock response. *Cell Stress Chaperones*, 1(2):97–98, June 1996.

[2] Virginia M Weis. Cellular mechanisms of cnidarian bleaching: stress causes the collapse of symbiosis. *J. Exp. Biol.*, 211(Pt 19):3059–3066, October 2008.

[3] Lagering: A complete overview. `https://www.mainbrew.com/lagering-ExtraPages.html`. Accessed: 2019-1-8.

[4] Devastating drought, heat wave hammer farmers across northern europe. `https://www.nbcnews.com/news/world/drought-brings-big-worries-farmers-across-northern-europe-n896096`. Accessed: 2019-1-8.

[5] Heat wave taking toll on california crops. `https://www.farmprogress.com/crops/heat-wave-taking-toll-california-crops`, July 2018. Accessed: 2019-1-8.

[6] Carl I Schulman, Nicholas Namias, James Doherty, Ronald J Manning, Pamela Li, Ahmed Elhaddad, David Lasko, Jose Amortegui, Christopher J Dy, Lucie Dlugasch, Gio Baracco, and Stephen M Cohn. The effect of antipyretic therapy upon outcomes in critically ill patients: a randomized, prospective study. *Surg. Infect.*, 6(4):369–375, 2005.

[7] James F Morley and Richard I Morimoto. Regulation of longevity in caenorhabditis elegans by heat shock factor and molecular chaperones. *Mol. Biol. Cell*, 15(2):657–664, February 2004.

[8] Kyeongjin Kang, Vincent C Panzano, Elaine C Chang, Lina Ni, Alexandra M Dainis, Adam M Jenkins, Kimberly Regna, Marc A T Muskavitch, and Paul A Garrity. Modulation of TRPA1 thermal sensitivity enables sensory discrimination in drosophila. *Nature*, 481(7379):76–80, December 2011.

[9] Klaus Richter, Martin Haslbeck, and Johannes Buchner. The heat shock response: life on the verge of death. *Mol. Cell*, 40(2):253–266, October 2010.

[10] F Ritossa. A new puffing pattern induced by temperature shock and DNP in drosophila. *Experientia*, 18(12):571–573, December 1962.

[11] Michael Ashburner and J Jose Bonner. The induction of gene activity in drosophila by heat shock. *Cell*, 17(2):241–254, June 1979.

[12] A Spradling, M L Pardue, and S Penman. Messenger RNA in heat-shocked drosophila cells. *J. Mol. Biol.*, 109(4):559–587, February 1977.

[13] A Tissières, H K Mitchell, and U M Tracy. Protein synthesis in salivary glands of drosophila melanogaster: relation to chromosome puffs. *J. Mol. Biol.*, 84(3):389–398, April 1974.

[14] S L McKenzie, S Henikoff, and M Meselson. Localization of RNA from heat-induced polysomes at puff sites in drosophila melanogaster. *Proc. Natl. Acad. Sci. U. S. A.*, 72(3):1117–1121, March 1975.

[15] M J Lewis and H R Pelham. Involvement of ATP in the nuclear and nucleolar functions of the 70 kd heat shock protein. *EMBO J.*, 4(12):3137–3143, December 1985.

[16] J Ellis. Proteins as molecular chaperones. *Nature*, 328(6129):378–379, 1987.

[17] J P Hendrick and F U Hartl. Molecular chaperone functions of heat-shock proteins. *Annu. Rev. Biochem.*, 62:349–384, 1993.

[18] J R Glover and S Lindquist. Hsp104, hsp70, and hsp40: a novel chaperone system that rescues previously aggregated proteins. *Cell*, 94(1):73–82, July 1998.

[19] Valeria Cherkasov, Sarah Hofmann, Silke Druffel-Augustin, Axel Mogk, Jens Tyedmers, Georg Stoecklin, and Bernd Bukau. Coordination of translational control and protein homeostasis during severe heat stress. *Curr. Biol.*, 23(24):2452–2462, December 2013.

[20] Sonja Kroschwald, Matthias C Munder, Shovamayee Maharana, Titus M Franzmann, Doris Richter, Martine Ruer, Anthony A Hyman, and Simon Alberti. Different material states of pub1 condensates define distinct modes of stress adaptation and recovery. *Cell Rep.*, 23(11):3327–3339, June 2018.

[21] R J Ellis and S M van der Vies. Molecular chaperones. *Annu. Rev. Biochem.*, 60:321–347, 1991.

[22] R Holmgren, V Corces, R Morimoto, R Blackman, and M Meselson. Sequence homologies in the 5' regions of four drosophila heat-shock genes. *Proc. Natl. Acad. Sci. U. S. A.*, 78(6):3775–3778, June 1981.

[23] D A Parsell, A S Kowal, M A Singer, and S Lindquist. Protein disaggregation mediated by heat-shock protein hsp104. *Nature*, 372(6505):475–478, December 1994.

[24] Y Sanchez and S L Lindquist. HSP104 required for induced thermotolerance. *Science*, 248(4959):1112–1115, June 1990.

[25] S Lindquist and G Kim. Heat-shock protein 104 expression is sufficient for thermotolerance in yeast. *Proc. Natl. Acad. Sci. U. S. A.*, 93(11):5301–5306, May 1996.

[26] A D Grossman, D B Straus, W A Walter, and C A Gross. Sigma 32 synthesis can regulate the synthesis of heat shock proteins in escherichia coli. *Genes Dev.*, 1(2):179–184, April 1987.

[27] Xu Zheng, Joanna Krakowiak, Nikit Patel, Ali Beyzavi, Jideofor Ezike, Ahmad S Khalil, and David Pincus. Dynamic control of hsf1 during heat shock by a chaperone switch and phosphorylation. *Elife*, 5, November 2016.

[28] Joanna Krakowiak, Xu Zheng, Nikit Patel, Zoë A Feder, Jayamani Anandhakumar, Kendra Valerius, David S Gross, Ahmad S Khalil, and David Pincus. Hsf1 and hsp70 constitute a two-component feedback loop that regulates the yeast heat shock response. *Elife*, 7, February 2018.

[29] E A Craig and C A Gross. Is hsp70 the cellular thermometer? *Trends Biochem. Sci.*, 16(4):135–140, April 1991.

[30] Audrey P. Gasch,*¶ Paul T. Spellman,†¶ Camilla M. Kao,*¶ Orna Carmel-Harel,‡ Michael B. Eisen,§ Gisela Storz,‡ David Botstein,† and Patrick O. Brown*i. Genomic expression programs in the response of yeast cells to environmental changes. *Molecular Biology of the Cell*, 11:4241–4257, December 2000.

[31] Noritaka Yamamoto, Yuka Maeda, Aya Ikeda, and Hiroshi Sakurai. Regulation of thermotolerance by stress-induced transcription factors in saccharomyces cerevisiae. *Eukaryot. Cell*, 7(5):783–790, May 2008.

[32] S Lindquist and R Petersen. Selective translation and degradation of heat-shock messenger RNAs in drosophila. *Enzyme*, 44(1-4):147–166, 1990.

[33] Yosuke Yamamoto and Shingo Izawa. Adaptive response in stress granule formation and bulk translational repression upon a combined stress of mild heat shock and mild ethanol stress in yeast. *Genes Cells*, 18(11):974–984, November 2013.

[34] Nancy Kedersha, Samantha Chen, Natalie Gilks, Wei Li, Ira J Miller, Joachim Stahl, and Paul Anderson. Evidence that ternary complex (eIF2-GTP-tRNA(i)(Met))-deficient preinitiation complexes are core constituents of mammalian stress granules. *Mol. Biol. Cell*, 13(1):195–210, January 2002.

[35] Natalie G Farny, Nancy L Kedersha, and Pamela A Silver. Metazoan stress granule assembly is mediated by P-eIF2alpha-dependent and -independent mechanisms. *RNA*, 15(10):1814–1821, October 2009.

[36] Beth J Didomenico, Gabrielle E Bugaisky, and Susan Lindquist. The heat shock response is self-regulated at both the transcriptional and posttranscriptional levels. *Cell*, 31(3, Part 2):593–603, December 1982.

[37] B Gerstel, M F Tuite, and J E McCarthy. The effects of 5'-capping, 3'-polyadenylation and leader composition upon the translation and stability of mRNA in a cell-free extract derived from the yeast saccharomyces cerevisiae. *Mol. Microbiol.*, 6(16):2339–2348, August 1992.

[38] C A Barnes, M M MacKenzie, G C Johnston, and R A Singer. Efficient translation of an SSA1-derived heat-shock mRNA in yeast cells limited for cap-binding protein and eIF-4F. *Mol. Gen. Genet.*, 246(5):619–627, March 1995.

[39] Ruhi Ahmed and Roger F Duncan. Translational regulation of hsp90 mRNA: AUG-PROXIMAL 5-UNTRANSLATED REGION ELEMENTS ESSENTIAL FOR PREFERENTIAL HEAT SHOCK TRANSLATION. *J. Biol. Chem.*, 279(48):49919–49930, November 2004.

[40] M A Hess and R F Duncan. Sequence and structure determinants of drosophila hsp70 mRNA translation: 5'UTR secondary structure specifically inhibits heat shock protein mRNA translation. *Nucleic Acids Res.*, 24(12):2441–2449, June 1996.

[41] R E Rhoads and B J Lamphear. Cap-Independent translation of heat shock messenger RNAs. In Peter Sarnow, editor, *Cap-Independent Translation*, pages 131–153. Springer Berlin Heidelberg, Berlin, Heidelberg, 1995.

[42] I Novoa and L Carrasco. Cleavage of eukaryotic translation initiation factor 4G by exogenously added hybrid proteins containing poliovirus 2apro in HeLa cells: effects on gene expression. *Mol. Cell. Biol.*, 19(4):2445–2454, April 1999.

[43] W R Boorstein and E A Craig. Structure and regulation of the SSA4 HSP70 gene of saccharomyces cerevisiae. *J. Biol. Chem.*, 265(31):18912–18921, November 1990.

[44] Susan LINDQUISTt. Translational efficiency of heat-induced messages in drosophila melanogaster cells. *Biol.*, 137:151–158, 1980.

[45] L Nover, K D Scharf, and D Neumann. Formation of cytoplasmic heat shock granules in tomato cell cultures and leaves. *Mol. Cell. Biol.*, 3(9):1648–1655, September 1983.

[46] L Nover, K D Scharf, and D Neumann. Cytoplasmic heat shock granules are formed from precursor particles and are associated with a specific set of mRNAs. *Mol. Cell. Biol.*, 9(3):1298–1308, March 1989.

[47] N L Kedersha, M Gupta, W Li, I Miller, and P Anderson. RNA-binding proteins TIA-1 and TIAR link the phosphorylation of eIF-2 alpha to the assembly of mammalian stress granules. *J. Cell Biol.*, 147(7):1431–1442, December 1999.

[48] N Kedersha and P Anderson. Stress granules: sites of mRNA triage that regulate mRNA stability and translatability. *Biochem. Soc. Trans.*, 30(Pt 6):963–969, November 2002.

[49] Natalie Gilks, Nancy Kedersha, Maranatha Ayodele, Lily Shen, Georg Stoecklin, Laura M Dember, and Paul Anderson. Stress granule assembly is mediated by prion-like aggregation of TIA-1. *Mol. Biol. Cell*, 15(12):5383–5398, December 2004.

[50] Tomás Grousl, Pavel Ivanov, Ivana Frýdlová, Pavla Vasicová, Filip Janda, Jana Vojtová, Katerina Malínská, Ivana Malcová, Lenka Nováková, Dana Janosková, Leos Valásek, and Jirí Hasek. Robust heat shock induces eIF2alpha-phosphorylation-independent assembly of stress granules containing eIF3 and 40S ribosomal subunits in budding yeast, saccharomyces cerevisiae. *J. Cell Sci.*, 122(Pt 12):2078–2088, June 2009.

[51] J Ross Buchan and Roy Parker. Eukaryotic stress granules: the ins and outs of translation. *Mol. Cell*, 36(6):932–941, December 2009.

[52] J Ross Buchan, Tracy Nissan, and Roy Parker. Chapter 25 - analyzing P-Bodies and stress granules in saccharomyces cerevisiae. In *Methods in Enzymology*, volume 470, pages 619–640. Academic Press, January 2010.

[53] N Kedersha, M R Cho, W Li, P W Yacono, S Chen, N Gilks, D E Golan, and P Anderson. Dynamic shuttling of TIA-1 accompanies the recruitment of mRNA to mammalian stress granules. *J. Cell Biol.*, 151(6):1257–1268, December 2000.

[54] Sonja Kroschwald, Shovamayee Maharana, Daniel Mateju, Liliana Malinovska, Elisabeth Nüske, Ina Poser, Doris Richter, and Simon Alberti. Promiscuous interactions and protein disaggregases determine the material state of stress-inducible RNP granules. *Elife*, 4:e06807, August 2015.

[55] J Ross Buchan, Denise Muhlrad, and Roy Parker. P bodies promote stress granule assembly in saccharomyces cerevisiae. *J. Cell Biol.*, 183(3):441–455, November 2008.

[56] Pavel Ivanov, Nancy Kedersha, and Paul Anderson. Stress granules and processing bodies in translational control. *Cold Spring Harb. Perspect. Biol.*, page a032813, 2018.

[57] Maurice L Huggins. Some properties of solutions of long-chain compounds. *J. Phys. Chem.*, 46(1):151–158, January 1942.

[58] Paul J Flory. Thermodynamics of high polymer solutions. *J. Chem. Phys.*, 10(1):51–61, January 1942.

[59] Lin Guo and James Shorter. It's raining liquids: RNA tunes viscoelasticity and dynamics of membraneless organelles. *Mol. Cell*, 60(2):189–192, October 2015.

[60] Yongdae Shin and Clifford P Brangwynne. Liquid phase condensation in cell physiology and disease. *Science*, 357(6357), September 2017.

[61] Joshua A Riback, Christopher D Katanski, Jamie L Kear-Scott, Evgeny V Pilipenko, Alexandra E Rojek, Tobin R Sosnick, and D Allan Drummond. Stress-Triggered phase separation is an adaptive, evolutionarily tuned response. *Cell*, 168(6):1028–1040.e19, March 2017.

[62] Peter Chien and Lila M Gierasch. Challenges and dreams: physics of weak interactions essential to life. *Mol. Biol. Cell*, 25(22):3474–3477, November 2014.

[63] S J Edelstein. Patterns in the quinary structures of proteins. plasticity and inequivalence of individual molecules in helical arrays of sickle cell hemoglobin and tubulin. *Biophys. J.*, 32(1):347–360, October 1980.

[64] Edward W J Wallace, Jamie L Kear-Scott, Evgeny V Pilipenko, Michael H Schwartz, Pawel R Laskowski, Alexandra E Rojek, Christopher D Katanski, Joshua A Riback, Michael F Dion, Alexander M Franks, Edoardo M Airoldi, Tao Pan, Bogdan A Budnik, and D Allan Drummond. Reversible, specific, active aggregates of endogenous proteins assemble upon heat stress. *Cell*, 162(6):1286–1298, September 2015.

[65] Yuan Lin, David S W Protter, Michael K Rosen, and Roy Parker. Formation and maturation of Phase-Separated liquid droplets by RNA-Binding proteins. *Mol. Cell*, 60(2):208–219, October 2015.

[66] Masato Kato, Tina W Han, Shanhai Xie, Kevin Shi, Xinlin Du, Leeju C Wu, Hamid Mirzaei, Elizabeth J Goldsmith, Jamie Longgood, Jimin Pei, Nick V Grishin, Douglas E Frantz, Jay W Schneider, She Chen, Lin Li, Michael R Sawaya, David Eisenberg, Robert Tycko, and Steven L McKnight. Cell-free formation of RNA granules: low complexity sequence domains form dynamic fibers within hydrogels. *Cell*, 149(4):753–767, May 2012.

[67] Amandine Molliex, Jamshid Temirov, Jihun Lee, Maura Coughlin, Anderson P Kanagaraj, Hong Joo Kim, Tanja Mittag, and J Paul Taylor. Phase separation by low complexity domains promotes stress granule assembly and drives pathological fibrillization. *Cell*, 163(1):123–133, September 2015.

[68] Avinash Patel, Hyun O Lee, Louise Jawerth, Shovamayee Maharana, Marcus Jahnel, Marco Y Hein, Stoyno Stoynov, Julia Mahamid, Shambaditya Saha, Titus M Franzmann, Andrej Pozniakovski, Ina Poser, Nicola Maghelli, Loic A Royer, Martin Weigert, Eugene W Myers, Stephan Grill, David Drechsel, Anthony A Hyman, and Simon Alberti. A Liquid-to-Solid phase transition of the ALS protein FUS accelerated by disease mutation. *Cell*, 162(5):1066–1077, August 2015.

[69] Elvan Boke, Martine Ruer, Martin Wühr, Margaret Coughlin, Regis Lemaitre, Steven P Gygi, Simon Alberti, David Drechsel, Anthony A Hyman, and Timothy J Mitchison. Amyloid-like Self-Assembly of a cellular compartment. *Cell*, 166(3):637–650, July 2016.

[70] Simon Alberti, Randal Halfmann, and Susan Lindquist. Chapter 30 - biochemical, cell biological, and genetic assays to analyze amyloid and prion aggregation in yeast. In *Methods in Enzymology*, volume Volume 470, pages 709–734. Academic Press, 2010.

[71] Melinda Balbirnie, Robert Grothe, and David S Eisenberg. An amyloid-forming peptide from the yeast prion sup35 reveals a dehydrated β-sheet structure for amyloid. *Proc. Natl. Acad. Sci. U. S. A.*, 98(5):2375, February 2001.

[72] S B Joseph and M Kirkpatrick. Effects of the [PSI+] prion on rates of adaptation in yeast. *J. Evol. Biol.*, 21(3):773–780, May 2008.

[73] Titus M Franzmann, Marcus Jahnel, Andrei Pozniakovsky, Julia Mahamid, Alex S Holehouse, Elisabeth Nüske, Doris Richter, Wolfgang Baumeister, Stephan W Grill, Rohit V Pappu, Anthony A Hyman, and Simon Alberti. Phase separation of a yeast prion protein promotes cellular fitness. *Science*, 359(6371), January 2018.

[74] Tetsuro Murakami, Seema Qamar, Julie Qiaojin Lin, Gabriele S Kaminski Schierle, Eric Rees, Akinori Miyashita, Ana R Costa, Roger B Dodd, Fiona T S Chan, Claire H Michel, Deborah Kronenberg-Versteeg, Yi Li, Seung-Pil Yang, Yosuke Wakutani, William Meadows, Rodylyn Rose Ferry, Liang Dong, Gian Gaetano Tartaglia, Giorgio Favrin, Wen-Lang Lin, Dennis W Dickson, Mei Zhen, David Ron, Gerold Schmitt-Ulms, Paul E Fraser, Neil A Shneider, Christine Holt, Michele Vendruscolo, Clemens F Kaminski, and Peter St George-Hyslop. ALS/FTD Mutation-Induced phase transition of FUS liquid droplets and reversible hydrogels into irreversible hydrogels impairs RNP granule function. *Neuron*, 88(4):678–690, November 2015.

[75] Ankur Jain and Ronald D Vale. RNA phase transitions in repeat expansion disorders. *Nature*, 546(7657):243–247, June 2017.

[76] Clifford P Brangwynne, Christian R Eckmann, David S Courson, Agata Rybarska, Carsten Hoege, Jöbin Gharakhani, Frank Jülicher, and Anthony A Hyman. Germline P granules are liquid droplets that localize by controlled dissolution/condensation. *Science*, 324(5935):1729–1732, June 2009.

[77] Shana Elbaum-Garfinkle, Younghoon Kim, Krzysztof Szczepaniak, Carlos Chih-Hsiung Chen, Christian R Eckmann, Sua Myong, and Clifford P Brangwynne. The disordered P granule protein LAF-1 drives phase separation into droplets with tunable viscosity and dynamics. *Proc. Natl. Acad. Sci. U. S. A.*, 112(23):7189–7194, June 2015.

[78] Timothy J Nott, Evangelia Petsalaki, Patrick Farber, Dylan Jervis, Eden Fussner, Anne Plochowietz, Timothy D Craggs, David P Bazett-Jones, Tony Pawson, Julie D Forman-Kay, and Andrew J Baldwin. Phase transition of a disordered nuage protein generates environmentally responsive membraneless organelles. *Mol. Cell*, 57(5):936–947, March 2015.

[79] Clifford P Brangwynne, Timothy J Mitchison, and Anthony A Hyman. Active liquid-like behavior of nucleoli determines their size and shape in xenopus laevis oocytes. *Proc. Natl. Acad. Sci. U. S. A.*, 108(11):4334–4339, March 2011.

[80] Marina Feric, Nilesh Vaidya, Tyler S Harmon, Diana M Mitrea, Lian Zhu, Tiffany M Richardson, Richard W Kriwacki, Rohit V Pappu, and Clifford P Brangwynne. Coexisting liquid phases underlie nucleolar subcompartments. *Cell*, 165(7):1686–1697, June 2016.

[81] R A Laskey, B M Honda, A D Mills, and J T Finch. Nucleosomes are assembled by an acidic protein which binds histones and transfers them to DNA. *Nature*, 275(5679):416–420, October 1978.

[82] Lindsay J Frehlick, José María Eirín-López, and Juan Ausió. New insights into the nucleophosmin/nucleoplasmin family of nuclear chaperones. *Bioessays*, 29(1):49–59, January 2007.

[83] Jeffrey B Woodruff, Beatriz Ferreira Gomes, Per O Widlund, Julia Mahamid, Alf Honigmann, and Anthony A Hyman. The centrosome is a selective condensate that nucleates microtubules by concentrating tubulin. *Cell*, 169(6):1066–1077.e10, June 2017.

[84] Jeffrey B Woodruff, Oliver Wueseke, Valeria Viscardi, Julia Mahamid, Stacy D Ochoa, Jakob Bunkenborg, Per O Widlund, Andrei Pozniakovsky, Esther Zanin, Shirin Bahmanyar, Andrea Zinke, Sun Hae Hong, Marcus Decker, Wolfgang Baumeister, Jens S Andersen, Karen Oegema, and Anthony A Hyman. Centrosomes. regulated assembly of a supramolecular centrosome scaffold in vitro. *Science*, 348(6236):808–812, May 2015.

[85] Changhwan Lee, Huaiying Zhang, Amy E Baker, Patricia Occhipinti, Mark E Borsuk, and Amy S Gladfelter. Protein aggregation behavior regulates cyclin transcript localization and cell-cycle control. *Dev. Cell*, 25(6):572–584, June 2013.

[86] Huaiying Zhang, Shana Elbaum-Garfinkle, Erin M Langdon, Nicole Taylor, Patricia Occhipinti, Andrew A Bridges, Clifford P Brangwynne, and Amy S Gladfelter. RNA controls PolyQ protein phase transitions. *Mol. Cell*, 60(2):220–230, October 2015.

[87] Erin M Langdon, Yupeng Qiu, Amirhossein Ghanbari Niaki, Grace A McLaughlin, Chase A Weidmann, Therese M Gerbich, Jean A Smith, John M Crutchley, Christina M Termini, Kevin M Weeks, Sua Myong, and Amy S Gladfelter. mRNA structure determines specificity of a polyq-driven phase separation. *Science*, 360(6391):922–927, May 2018.

[88] Changhwan Lee, Patricia Occhipinti, and Amy S Gladfelter. PolyQ-dependent RNA-protein assemblies control symmetry breaking. *J. Cell Biol.*, 208(5):533–544, March 2015.

[89] Elizabeth S Freeman Rosenzweig, Bin Xu, Luis Kuhn Cuellar, Antonio Martinez-Sanchez, Miroslava Schaffer, Mike Strauss, Heather N Cartwright, Pierre Ronceray, Jürgen M Plitzko, Friedrich Förster, Ned S Wingreen, Benjamin D Engel, Luke C M Mackinder, and Martin C Jonikas. The eukaryotic CO2-Concentrating organelle is liquid-like and exhibits dynamic reorganization. *Cell*, 171(1):148–162.e19, September 2017.

[90] Tobias Wunder, Steven Le Hung Cheng, Soak-Kuan Lai, Hoi-Yeung Li, and Oliver Mueller-Cajar. The phase separation underlying the pyrenoid-based microalgal rubisco supercharger. *Nat. Commun.*, 9(1):5076, November 2018.

[91] Elisabeth Nueske, Guendalina Marini, Doris Richter, Weihua Leng, Aliona Bogdanova, Titus M Franzmann, Gaia Pigino, and Simon Alberti. Filament formation by the translation factor eIF2B regulates protein synthesis in starved cells. November 2018.

[92] Qing-Ji Shen, Hakimi Kassim, Yong Huang, Hui Li, Jing Zhang, Guang Li, Peng-Ye Wang, Jun Yan, Fangfu Ye, and Ji-Long Liu. Filamentation of metabolic enzymes in saccharomyces cerevisiae. *J. Genet. Genomics*, 43(6):393–404, June 2016.

[93] J N Telford, P M Lad, and G G Hammes. Electron microscope study of native and crosslinked rabbit muscle phosphofructokinase. *Proc. Natl. Acad. Sci. U. S. A.*, 72(8):3054–3056, August 1975.

[94] Bradley A Webb, Anne M Dosey, Torsten Wittmann, Justin M Kollman, and Diane L Barber. The glycolytic enzyme phosphofructokinase-1 assembles into filaments. *J. Cell Biol.*, 216(8):2305–2313, August 2017.

[95] Ivana Petrovska, Elisabeth Nüske, Matthias C Munder, Gayathrie Kulasegaran, Liliana Malinovska, Sonja Kroschwald, Doris Richter, Karim Fahmy, Kimberley Gibson, Jean-Marc Verbavatz, and Simon Alberti. Filament formation by metabolic enzymes is a specific adaptation to an advanced state of cellular starvation. *Elife*, April 2014.

[96] Stephan Wullschleger, Robbie Loewith, and Michael N Hall. TOR signaling in growth and metabolism. *Cell*, 124(3):471–484, February 2006.

[97] Terunao Takahara and Tatsuya Maeda. Transient sequestration of TORC1 into stress granules during heat stress. *Mol. Cell*, 47(2):242–252, July 2012.

[98] Eva Kummer, Yuki Oguchi, Fabian Seyffer, Bernd Bukau, and Axel Mogk. Mechanism of Hsp104/ClpB inhibition by prion curing guanidinium hydrochloride. *FEBS Lett.*, 587(6):810–817, March 2013.

[99] Diana F Colgan and James L Manley. Mechanism and regulation of mRNA polyadenylation. *Genes Dev.*, 11(21):2755–2766, November 1997.

[100] Uwe Kühn and Elmar Wahle. Structure and function of poly(a) binding proteins. *Biochim. Biophys. Acta*, 1678(2-3):67–84, May 2004.

[101] S A Adam, T Nakagawa, M S Swanson, T K Woodruff, and G Dreyfuss. mRNA polyadenylate-binding protein: gene isolation and sequencing and identification of a ribonucleoprotein consensus sequence. *Mol. Cell. Biol.*, 6(8):2932–2943, August 1986.

[102] G Blobel. A protein of molecular weight 78,000 bound to the polyadenylate region of eukaryotic messenger RNAs. *Proc. Natl. Acad. Sci. U. S. A.*, 70(3):924–928, March 1973.

[103] A B Sachs, M W Bond, and R D Kornberg. A single gene from yeast for both nuclear and cytoplasmic polyadenylate-binding proteins: domain structure and expression. *Cell*, 45(6):827–835, June 1986.

[104] David A Mangus, Matthew C Evans, and Allan Jacobson. Poly(A)-binding proteins: multifunctional scaffolds for the post-transcriptional control of gene expression. *Genome Biol.*, 4(7):223, July 2003.

[105] A B Sachs, R W Davis, and R D Kornberg. A single domain of yeast poly(a)-binding protein is necessary and sufficient for RNA binding and cell viability. *Mol. Cell. Biol.*, 7(9):3268–3276, September 1987.

[106] J A Deardorff and A B Sachs. Differential effects of aromatic and charged residue substitutions in the RNA binding domains of the yeast poly(a)-binding protein. *J. Mol. Biol.*, 269(1):67–81, May 1997.

[107] Morgan Tucker, Robin R Staples, Marco A Valencia-Sanchez, Denise Muhlrad, and Roy Parker. Ccr4p is the catalytic subunit of a Ccr4p/Pop2p/Notp mRNA deadenylase complex in saccharomyces cerevisiae. *EMBO J.*, 21(6):1427–1436, March 2002.

[108] M Tucker and R Parker. Mechanisms and control of mRNA decapping in saccharomyces cerevisiae. *Annu. Rev. Biochem.*, 69:571–595, 2000.

[109] C J Wilusz, M Gao, C L Jones, J Wilusz, and S W Peltz. Poly(A)-binding proteins regulate both mRNA deadenylation and decapping in yeast cytoplasmic extracts. *RNA*, 7(10):1416–1424, October 2001.

[110] Ewan F Dunn, Christopher M Hammell, Christine A Hodge, and Charles N Cole. Yeast poly(a)-binding protein, pab1, and PAN, a poly(a) nuclease complex recruited by pab1, connect mRNA biogenesis to export. *Genes Dev.*, 19(1):90–103, January 2005.

[111] Sandra E Wells, Paul E Hillner, Ronald D Vale, and Alan B Sachs. Circularization of mRNA by eukaryotic translation initiation factors. *Mol. Cell*, 2(1):135–140, July 1998.

[112] A B Sachs and R W Davis. The poly(a) binding protein is required for poly(a) shortening and 60S ribosomal subunit-dependent translation initiation. *Cell*, 58(5):857–867, September 1989.

[113] S Z Tarun, Jr and A B Sachs. Association of the yeast poly(a) tail binding protein with translation initiation factor eIF-4G. *EMBO J.*, 15(24):7168–7177, December 1996.

[114] Dmitry A Belostotsky. Unexpected complexity of poly(a)-binding protein gene families in flowering plants: three conserved lineages that are at least 200 million years old and possible auto- and cross-regulation. *Genetics*, 163(1):311–319, January 2003.

[115] B W Baer and R D Kornberg. Repeating structure of cytoplasmic poly(a)-ribonucleoprotein. *Proc. Natl. Acad. Sci. U. S. A.*, 77(4):1890–1892, April 1980.

[116] A B Sachs and R D Kornberg. Nuclear polyadenylate-binding protein. *Mol. Cell. Biol.*, 5(8):1993–1996, August 1985.

[117] C G Burd, E L Matunis, and G Dreyfuss. The multiple RNA-binding domains of the mRNA poly(a)-binding protein have different RNA-binding activities. *Mol. Cell. Biol.*, 11(7):3419–3424, July 1991.

[118] Guennadi Kozlov, Gregory De Crescenzo, Nadia S Lim, Nadeem Siddiqui, Daniel Fantus, Avak Kahvejian, Jean-François Trempe, Demetra Elias, Irena Ekiel, Nahum Sonenberg, Maureen O'Connor-McCourt, and Kalle Gehring. Structural basis of ligand recognition by PABC, a highly specific peptide-binding domain found in poly(a)-binding protein and a HECT ubiquitin ligase. *EMBO J.*, 23(2):272–281, January 2004.

[119] Gang Yao, Yueh-Chin Chiang, Chongxu Zhang, Darren J Lee, Thomas M Laue, and Clyde L Denis. PAB1 self-association precludes its binding to poly(a), thereby accelerating CCR4 deadenylation in vivo. *Mol. Cell. Biol.*, 27(17):6243–6253, September 2007.

[120] Richard W P Smith and Nicola K Gray. Poly(A)-binding protein (PABP): a common viral target. *Biochem. J*, 426(1):1–12, January 2010.

[121] N Muge Kuyumcu-Martinez, Marc E Van Eden, Patrick Younan, and Richard E Lloyd. Cleavage of poly(a)-binding protein by poliovirus 3C protease inhibits host cell translation: a novel mechanism for host translation shutoff. *Mol. Cell. Biol.*, 24(4):1779–1790, February 2004.

[122] W Nietfeld, H Mentzel, and T Pieler. The xenopus laevis poly(a) binding protein is composed of multiple functionally independent RNA binding domains. *EMBO J.*, 9(11):3699–3705, November 1990.

[123] T Grange, C M de Sa, J Oddos, and R Pictet. Human mRNA polyadenylate binding protein: evolutionary conservation of a nucleic acid binding motif. *Nucleic Acids Res.*, 15(12):4771–4787, June 1987.

[124] D A Belostotsky and R B Meagher. Differential organ-specific expression of three poly(a)-binding-protein genes from arabidopsis thaliana. *Proc. Natl. Acad. Sci. U. S. A.*, 90(14):6686–6690, July 1993.

[125] J Bag and J Wu. Translational control of poly(a)-binding protein expression. *Eur. J. Biochem.*, 237(1):143–152, April 1996.

[126] O P de Melo Neto, N Standart, and C Martins de Sa. Autoregulation of poly(a)-binding protein synthesis in vitro. *Nucleic Acids Res.*, 23(12):2198–2205, June 1995.

[127] Jun Wu and Jnanankur Bag. Negative control of the Poly(A)-binding protein mRNA translation is mediated by the adenine-rich region of its 5-untranslated region. *J. Biol. Chem.*, 273(51):34535–34542, December 1998.

[128] Eduardo O Melo, Osvaldo P de Melo Neto, and Cezar Martins de Sá. Adenosine-rich elements present in the 5'-untranslated region of PABP mRNA can selectively reduce the abundance and translation of CAT mRNAs in vivo. *FEBS Lett.*, 546(2-3):329–334, July 2003.

[129] Eduardo O Melo, Rafael Dhalia, Cezar Martins de Sa, Nancy Standart, and Osvaldo P de Melo Neto. Identification of a c-terminal Poly(A)-binding protein (PABP)-PABP interaction domain: ROLE IN COOPERATIVE BINDING TO POLY(A) AND EFFICIENT CAP DISTAL TRANSLATIONAL REPRESSION. *J. Biol. Chem.*, 278(47):46357–46368, November 2003.

[130] Hemant K Kini, Ian M Silverman, Xinjun Ji, Brian D Gregory, and Stephen A Liebhaber. Cytoplasmic poly(a) binding protein-1 binds to genomically encoded sequences within mammalian mRNAs. *RNA*, 22(1):61–74, January 2016.

[131] Wendy V Gilbert, Kaihong Zhou, Tamira K Butler, and Jennifer A Doudna. Cap-Independent translation is required for Starvation-Induced differentiation in yeast. *Science*, 317(5842):1224–1227, August 2007.

[132] Nathaniel P Hoyle, Lydia M Castelli, Susan G Campbell, Leah E A Holmes, and Mark P Ashe. Stress-dependent relocalization of translationally primed mRNPs to cytoplasmic granules that are kinetically and spatially distinct from p-bodies. *J. Cell Biol.*, 179(1):65–74, October 2007.

[133] Muriel Brengues and Roy Parker. Accumulation of polyadenylated mRNA, pab1p, eIF4E, and eIF4G with p-bodies in saccharomyces cerevisiae. *Mol. Biol. Cell*, 18(7):2592–2602, July 2007.

[134] Aya Iwaki, Shinsuke Ohnuki, Yohei Suga, Shingo Izawa, and Yoshikazu Ohya. Vanillin inhibits translation and induces messenger ribonucleoprotein (mRNP) granule formation in saccharomyces cerevisiae: application and validation of high-content, image-based profiling. *PLoS One*, 8(4):e61748, April 2013.

[135] Paul Anderson and Nancy Kedersha. Stressful initiations. *J. Cell Sci.*, 115(Pt 16):3227–3234, August 2002.

[136] Vadim Shchepachev, Stefan Bresson, Christos Spanos, Elisabeth Petfalski, Lutz Fischer, Juri Rappsilber, and David Tollervey. Defining the RNA interactome by total RNA-Associated protein purification. October 2018.

[137] S Lindquist. The heat-shock response. *Annu. Rev. Biochem.*, 55:1151–1191, 1986.

[138] A Mogk, T Tomoyasu, P Goloubinoff, S Rüdiger, D Röder, H Langen, and B Bukau. Identification of thermolabile escherichia coli proteins: prevention and reversion of aggregation by DnaK and ClpB. *EMBO J.*, 18(24):6934–6949, December 1999.

[139] R Martin Vabulas, Swasti Raychaudhuri, Manajit Hayer-Hartl, and F Ulrich Hartl. Protein folding in the cytoplasm and the heat shock response. *Cold Spring Harb. Perspect. Biol.*, 2(12):a004390, December 2010.

[140] Jacob Verghese, Jennifer Abrams, Yanyu Wang, and Kevin A Morano. Biology of the heat shock response and protein chaperones: budding yeast (saccharomyces cerevisiae) as a model system. *Microbiol. Mol. Biol. Rev.*, 76(2):115–158, June 2012.

[141] R Baler, W J Welch, and R Voellmy. Heat shock gene regulation by nascent polypeptides and denatured proteins: hsp70 as a potential autoregulatory factor. *J. Cell Biol.*, 117(6):1151–1159, June 1992.

[142] Balasubrahmanyam Medicherla and Alfred L Goldberg. Heat shock and oxygen radicals stimulate ubiquitin-dependent degradation mainly of newly synthesized proteins. *J. Cell Biol.*, 182(4):663–673, August 2008.

[143] Tomas Grousl, Pavel Ivanov, Ivana Malcova, Petr Pompach, Ivana Frydlova, Renata Slaba, Lenka Senohrabkova, Lenka Novakova, and Jiri Hasek. Heat shock-induced accumulation of translation elongation and termination factors precedes assembly of stress granules in s. cerevisiae. *PLoS One*, 8(2):e57083, February 2013.

[144] J Ross Buchan, Je-Hyun Yoon, and Roy Parker. Stress-specific composition, assembly and kinetics of stress granules in saccharomyces cerevisiae. *J. Cell Sci.*, 124(2):228–239, January 2011.

[145] Jarrod W Heck, Samantha K Cheung, and Randolph Y Hampton. Cytoplasmic protein quality control degradation mediated by parallel actions of the E3 ubiquitin ligases ubr1 and san1. *Proc. Natl. Acad. Sci. U. S. A.*, 107(3):1106–1111, January 2010.

[146] Eric K Fredrickson, Pamela S Gallagher, Sarah V Clowes Candadai, and Richard G Gardner. Substrate recognition in nuclear protein quality control degradation is governed by exposed hydrophobicity that correlates with aggregation and insolubility. *J. Biol. Chem.*, 288(9):6130–6139, March 2013.

[147] J Ross Buchan, Regina-Maria Kolaitis, J Paul Taylor, and Roy Parker. Eukaryotic stress granules are cleared by autophagy and Cdc48/VCP function. *Cell*, 153(7):1461–1474, June 2013.

[148] J Michael Cherry, Eurie L Hong, Craig Amundsen, Rama Balakrishnan, Gail Binkley, Esther T Chan, Karen R Christie, Maria C Costanzo, Selina S Dwight, Stacia R Engel, Dianna G Fisk, Jodi E Hirschman, Benjamin C Hitz, Kalpana Karra, Cynthia J Krieger, Stuart R Miyasato, Rob S Nash, Julie Park, Marek S Skrzypek, Matt Simison, Shuai Weng, and Edith D Wong. Saccharomyces genome database: the genomics resource of budding yeast. *Nucleic Acids Res.*, 40(Database issue):D700–5, January 2012.

[149] Amy J Lam, François St-Pierre, Yiyang Gong, Jesse D Marshall, Paula J Cranfill, Michelle A Baird, Michael R McKeown, Jörg Wiedenmann, Michael W Davidson, Mark J Schnitzer, Roger Y Tsien, and Michael Z Lin. Improving FRET dynamic range with bright green and red fluorescent proteins. *Nat. Methods*, 9(10):1005–1012, October 2012.

[150] Bahram Samanfar, Le Hoa Tan, Kristina Shostak, Firoozeh Chalabian, Zongbin Wu, Md Alamgir, Noor Sunba, Daniel Burnside, Katayoun Omidi, Mohsen Hooshyar, Imelda Galván Márquez, Matthew Jessulat, Myron L Smith, Mohan Babu, Ali Azizi, and Ashkan Golshani. A global investigation of gene deletion strains that affect premature stop codon bypass in yeast, saccharomyces cerevisiae. *Mol. Biosyst.*, 10(4):916–924, April 2014.

[151] Stephanie B M Miller, Axel Mogk, and Bernd Bukau. Spatially organized aggregation of misfolded proteins as cellular stress defense strategy. *J. Mol. Biol.*, 427(7):1564–1574, April 2015.

[152] Hugo Aguilaniu, Lena Gustafsson, Michel Rigoulet, and Thomas Nyström. Asymmetric inheritance of oxidatively damaged proteins during cytokinesis. *Science*, 299(5613):1751–1753, March 2003.

[153] Beidong Liu, Lisa Larsson, Antonio Caballero, Xinxin Hao, David Oling, Julie Grantham, and Thomas Nyström. The polarisome is required for segregation and retrograde transport of protein aggregates. *Cell*, 140(2):257–267, January 2010.

[154] Chuankai Zhou, Brian D Slaughter, Jay R Unruh, Fengli Guo, Zulin Yu, Kristen Mickey, Akshay Narkar, Rhonda Trimble Ross, Melainia McClain, and Rong Li. Organelle-based aggregation and retention of damaged proteins in asymmetrically dividing cells. *Cell*, 159(3):530–542, October 2014.

[155] Therese Jacobson, Clara Navarrete, Sandeep K Sharma, Theodora C Sideri, Sebastian Ibstedt, Smriti Priya, Chris M Grant, Philipp Christen, Pierre Goloubinoff, and Markus J Tamás. Arsenite interferes with protein folding and triggers formation of protein aggregates in yeast. *J. Cell Sci.*, 125(Pt 21):5073–5083, November 2012.

[156] Helena Firczuk, Shichina Kannambath, Jürgen Pahle, Amy Claydon, Robert Beynon, John Duncan, Hans Westerhoff, Pedro Mendes, and John Eg McCarthy. An in vivo control map for the eukaryotic mRNA translation machinery. *Mol. Syst. Biol.*, 9:635, 2013.

[157] Steffen Preissler and Elke Deuerling. Ribosome-associated chaperones as key players in proteostasis. *Trends Biochem. Sci.*, 37(7):274–283, July 2012.

[158] Shuye Pu, Jessica Wong, Brian Turner, Emerson Cho, and Shoshana J Wodak. Up-to-date catalogues of yeast protein complexes. *Nucleic Acids Res.*, 37(3):825–831, February 2009.

[159] Mathieu Frechin, Ludovic Enkler, Emmanuel Tetaud, Daphné Laporte, Bruno Senger, Corinne Blancard, Philippe Hammann, Gaétan Bader, Sandra Clauder-Münster, Lars M Steinmetz, Robert Pierre Martin, Jean-Paul di Rago, and Hubert Dominique Becker. Expression of nuclear and mitochondrial genes encoding ATP synthase is synchronized by disassembly of a multisynthetase complex. *Mol. Cell*, 56(6):763–776, December 2014.

[160] Mónica Martínez-Alonso, Nuria González-Montalbán, Elena García-Fruitós, and Antonio Villaverde. Learning about protein solubility from bacterial inclusion bodies. *Microb. Cell Fact.*, 8:4, January 2009.

[161] Maxim V Gerashchenko and Vadim N Gladyshev. Translation inhibitors cause abnormalities in ribosome profiling experiments. *Nucleic Acids Res.*, 42(17):e134, July 2014.

[162] Stephanie B M Miller, Chi-Ting Ho, Juliane Winkler, Maria Khokhrina, Annett Neuner, Mohamed Y H Mohamed, D Lys Guilbride, Karsten Richter, Michael Lisby, Elmar Schiebel, Axel Mogk, and Bernd Bukau. Compartment-specific aggregases direct distinct nuclear and cytoplasmic aggregate deposition. *EMBO J.*, 34(6):778–797, March 2015.

[163] Richard G Gardner, Zara W Nelson, and Daniel E Gottschling. Degradation-mediated protein quality control in the nucleus. *Cell*, 120(6):803–815, March 2005.

[164] E H McConkey. Molecular evolution, intracellular organization, and the quinary structure of proteins. *Proc. Natl. Acad. Sci. U. S. A.*, 79(10):3236–3240, May 1982.

[165] Pilong Li, Sudeep Banjade, Hui-Chun Cheng, Soyeon Kim, Baoyu Chen, Liang Guo, Marc Llaguno, Javoris V Hollingsworth, David S King, Salman F Banani, Paul S Russo, Qiu-Xing Jiang, B Tracy Nixon, and Michael K Rosen. Phase transitions in the assembly of multivalent signalling proteins. *Nature*, 483(7389):336–340, March 2012.

[166] Stephanie C Weber and Clifford P Brangwynne. Getting RNA and protein in phase. *Cell*, 149(6):1188–1191, June 2012.

[167] Piali Sengupta and Paul Garrity. Sensing temperature. *Curr. Biol.*, 23(8):R304–7, April 2013.

[168] Nikolay E Shirokikh and Alexander S Spirin. Poly(A) leader of eukaryotic mRNA bypasses the dependence of translation on initiation factors. *Proc. Natl. Acad. Sci. U. S. A.*, 105(31):10738–10743, August 2008.

[169] Krishna B S Swamy, Chih-Hsu Lin, Ming-Ren Yen, Chuen-Yi Wang, and Daryi Wang. Examining the condition-specific antisense transcription in s. cerevisiae and s. paradoxus. *BMC Genomics*, 15:521, June 2014.

[170] Adrian Alexa, Jörg Rahnenführer, and Thomas Lengauer. Improved scoring of functional groups from gene expression data by decorrelating GO graph structure. *Bioinformatics*, 22(13):1600–1607, July 2006.

[171] Jeremy D O'Connell, Mark Tsechansky, Ariel Royal, Daniel R Boutz, Andrew D Ellington, and Edward M Marcotte. A proteomic survey of widespread protein aggregation in yeast. *Mol. Biosyst.*, 10(4):851–861, April 2014.

[172] D Wessel and U I Flügge. A method for the quantitative recovery of protein in dilute solution in the presence of detergents and lipids. *Anal. Biochem.*, 138(1):141–143, April 1984.

[173] Jacek R Wiśniewski, Alexandre Zougman, Nagarjuna Nagaraj, and Matthias Mann. Universal sample preparation method for proteome analysis. *Nat. Methods*, 6(5):359–362, May 2009.

[174] Paul J Boersema, Reinout Raijmakers, Simone Lemeer, Shabaz Mohammed, and Albert J R Heck. Multiplex peptide stable isotope dimethyl labeling for quantitative proteomics. *Nat. Protoc.*, 4(4):484–494, 2009.

[175] Jürgen Cox, Nadin Neuhauser, Annette Michalski, Richard A Scheltema, Jesper V Olsen, and Matthias Mann. Andromeda: a peptide search engine integrated into the MaxQuant environment. *J. Proteome Res.*, 10(4):1794–1805, April 2011.

[176] Ajit P Joglekar, E D Salmon, and Kerry S Bloom. Counting kinetochore protein numbers in budding yeast using genetically encoded fluorescent proteins. *Methods Cell Biol.*, 85:127–151, 2008.

[177] Johannes Schindelin, Ignacio Arganda-Carreras, Erwin Frise, Verena Kaynig, Mark Longair, Tobias Pietzsch, Stephan Preibisch, Curtis Rueden, Stephan Saalfeld, Benjamin Schmid, Jean-Yves Tinevez, Daniel James White, Volker Hartenstein, Kevin Eliceiri, Pavel Tomancak, and Albert Cardona. Fiji: an open-source platform for biological-image analysis. *Nat. Methods*, 9(7):676–682, June 2012.

[178] C Vonesch and M Unser. A fast thresholded landweber algorithm for wavelet-regularized multidimensional deconvolution. *IEEE Trans. Image Process.*, 17(4):539–549, April 2008.

[179] H Kirshner, F Aguet, D Sage, and M Unser. 3-D PSF fitting for fluorescence microscopy: implementation and localization application. *J. Microsc.*, 249(1):13–25, January 2013.

[180] Heather Hundley, Helene Eisenman, William Walter, Tara Evans, Yuka Hotokezaka, Martin Wiedmann, and Elizabeth Craig. The in vivo function of the ribosome-associated hsp70, ssz1, does not require its putative peptide-binding domain. *Proc. Natl. Acad. Sci. U. S. A.*, 99(7):4203–4208, April 2002.

[181] Nir Netzer, Jeffrey M Goodenbour, Alexandre David, Kimberly A Dittmar, Richard B Jones, Jeffrey R Schneider, David Boone, Eva M Eves, Marsha R Rosner, James S Gibbs, Alan Embry, Brian Dolan, Suman Das, Heather D Hickman, Peter Berglund, Jack R Bennink, Jonathan W Yewdell, and Tao Pan. Innate immune and chemically triggered oxidative stress modifies translational fidelity. *Nature*, 462(7272):522–526, November 2009.

[182] Elizabeth Wiltrout, Jeffrey M Goodenbour, Mathieu Fréchin, and Tao Pan. Misacylation of tRNA with methionine in saccharomyces cerevisiae. *Nucleic Acids Res.*, 40(20):10494–10506, November 2012.

[183] Paul Anderson and Nancy Kedersha. RNA granules. *J. Cell Biol.*, 172(6):803–808, March 2006.

[184] Saumya Jain, Joshua R Wheeler, Robert W Walters, Anurag Agrawal, Anthony Barsic, and Roy Parker. ATPase-Modulated stress granules contain a diverse proteome and substructure. *Cell*, 164(3):487–498, January 2016.

[185] Christopher Frederick Mugler, Maria Hondele, Stephanie Heinrich, Ruchika Sachdev, Pascal Vallotton, Adriana Y Koek, Leon Y Chan, and Karsten Weis. ATPase activity of the DEAD-box protein dhh1 controls processing body formation. *Elife*, 5, October 2016.

[186] Megan Sickmeier, Justin A Hamilton, Tanguy LeGall, Vladimir Vacic, Marc S Cortese, Agnes Tantos, Beata Szabo, Peter Tompa, Jake Chen, Vladimir N Uversky, Zoran Obradovic, and A Keith Dunker. DisProt: the database of disordered proteins. *Nucleic Acids Res.*, 35(Database issue):D786–93, January 2007.

[187] John J Skinner, Wookyung Yu, Elizabeth K Gichana, Michael C Baxa, James R Hinshaw, Karl F Freed, and Tobin R Sosnick. Benchmarking all-atom simulations using hydrogen exchange. *Proc. Natl. Acad. Sci. U. S. A.*, 111(45):15975–15980, November 2014.

[188] Reinhard Dechant, Matteo Binda, Sung Sik Lee, Serge Pelet, Joris Winderickx, and Matthias Peter. Cytosolic ph is a second messenger for glucose and regulates the PKA pathway through V-ATPase. *EMBO J.*, 29(15):2515–2526, August 2010.

[189] Matthias Christoph Munder, Daniel Midtvedt, Titus Franzmann, Elisabeth Nüske, Oliver Otto, Maik Herbig, Elke Ulbricht, Paul Müller, Anna Taubenberger, Shovamayee Maharana, Liliana Malinovska, Doris Richter, Jochen Guck, Vasily Zaburdaev, and Simon Alberti. A ph-driven transition of the cytoplasm from a fluid- to a solid-like state promotes entry into dormancy. *Elife*, 5, March 2016.

[190] Xiaoxue Yang, Yi Shen, Elena Garre, Xinxin Hao, Daniel Krumlinde, Marija Cvijović, Christina Arens, Thomas Nyström, Beidong Liu, and Per Sunnerhagen. Stress granule-defective mutants deregulate stress responsive transcripts. *PLoS Genet.*, 10(11):e1004763, November 2014.

[191] Anthony A Hyman, Christoph A Weber, and Frank Jülicher. Liquid-liquid phase separation in biology. *Annu. Rev. Cell Dev. Biol.*, 30:39–58, 2014.

[192] Xiaolei Su, Jonathon A Ditlev, Enfu Hui, Wenmin Xing, Sudeep Banjade, Julia Okrut, David S King, Jack Taunton, Michael K Rosen, and Ronald D Vale. Phase separation of signaling molecules promotes T cell receptor signal transduction. *Science*, 352(6285):595–599, April 2016.

[193] Claudia Weigert, Fabian Steffler, Tomas Kurz, Thomas H Shellhammer, and Frank-Jürgen Methner. Application of a short intracellular ph method to flow cytometry for determining saccharomyces cerevisiae vitality. *Appl. Environ. Microbiol.*, 75(17):5615–5620, September 2009.

[194] Kevin A Morano, Chris M Grant, and W Scott Moye-Rowley. The response to heat shock and oxidative stress in saccharomyces cerevisiae. *Genetics*, 190(4):1157–1195, April 2012.

[195] Chongxu Zhang, Darren J Lee, Yueh-Chin Chiang, Roy Richardson, Shiwha Park, Xin Wang, Thomas M Laue, and Clyde L Denis. The RRM1 domain of the poly(a)-binding protein from saccharomyces cerevisiae is critical to control of mRNA deadenylation. *Mol. Genet. Genomics*, 288(9):401–412, September 2013.

[196] Clifford P Brangwynne, Peter Tompa, and Rohit V Pappu. Polymer physics of intracellular phase transitions. *Nat. Phys.*, 11:899, November 2015.

[197] René Wuttke, Hagen Hofmann, Daniel Nettels, Madeleine B Borgia, Jeetain Mittal, Robert B Best, and Benjamin Schuler. Temperature-dependent solvation modulates the dimensions of disordered proteins. *Proc. Natl. Acad. Sci. U. S. A.*, 111(14):5213–5218, April 2014.

[198] Chi W Pak, Martyna Kosno, Alex S Holehouse, Shae B Padrick, Anuradha Mittal, Rustam Ali, Ali A Yunus, David R Liu, Rohit V Pappu, and Michael K Rosen. Sequence determinants of intracellular phase separation by complex coacervation of a disordered protein. *Mol. Cell*, 63(1):72–85, July 2016.

[199] Kosuke Shiraishi, Takahiro Hioki, Akari Habata, Hiroya Yurimoto, and Yasuyoshi Sakai. Yeast hog1 proteins are sequestered in stress granules during high-temperature stress. *J. Cell Sci.*, 131(1), January 2018.

[200] G Weitzel, U Pilatus, and L Rensing. The cytoplasmic ph, ATP content and total protein synthesis rate during heat-shock protein inducing treatments in yeast. *Exp. Cell Res.*, 170(1):64–79, May 1987.

[201] Gábor Csárdi, Alexander Franks, David S Choi, Edoardo M Airoldi, and D Allan Drummond. Accounting for experimental noise reveals that mRNA levels, amplified by post-transcriptional processes, largely determine steady-state protein levels in yeast. *PLoS Genet.*, 11(5):e1005206, May 2015.

[202] Vera A Borzova, Kira A Markossian, Dmitriy A Kara, and Boris Kurganov. Kinetic regime of dithiothreitol-induced aggregation of bovine serum albumin. *Int. J. Biol. Macromol.*, 80:130–138, September 2015.

[203] Hagen Hofmann, Andrea Soranno, Alessandro Borgia, Klaus Gast, Daniel Nettels, and Benjamin Schuler. Polymer scaling laws of unfolded and intrinsically disordered proteins quantified with single-molecule spectroscopy. *Proc. Natl. Acad. Sci. U. S. A.*, 109(40):16155–16160, October 2012.

[204] Ivica Letunic, Tobias Doerks, and Peer Bork. SMART: recent updates, new developments and status in 2015. *Nucleic Acids Res.*, 43(Database issue):D257–60, January 2015.

[205] Robert C Edgar. MUSCLE: multiple sequence alignment with high accuracy and high throughput. *Nucleic Acids Res.*, 32(5):1792–1797, March 2004.

[206] Stacia R Engel, Fred S Dietrich, Dianna G Fisk, Gail Binkley, Rama Balakrishnan, Maria C Costanzo, Selina S Dwight, Benjamin C Hitz, Kalpana Karra, Robert S Nash, Shuai Weng, Edith D Wong, Paul Lloyd, Marek S Skrzypek, Stuart R Miyasato, Matt Simison, and J Michael Cherry. The reference genome sequence of saccharomyces cerevisiae: then and now. *G3*, 4(3):389–398, March 2014.

[207] Maxim V Petoukhov, Daniel Franke, Alexander V Shkumatov, Giancarlo Tria, Alexey G Kikhney, Michal Gajda, Christian Gorba, Haydyn D T Mertens, Petr V Konarev, and Dmitri I Svergun. New developments in the ATSAS program package for small-angle scattering data analysis. *J. Appl. Crystallogr.*, 45(Pt 2):342–350, April 2012.

[208] Julien Maupetit, R Gautier, and Pierre Tufféry. SABBAC: online structural alphabet-based protein BackBone reconstruction from Alpha-Carbon trace. *Nucleic Acids Res.*, 34(Web Server issue):W147–51, July 2006.

[209] J M Sierra and J M Zapata. Translational regulation of the heat shock response. *Mol. Biol. Rep.*, 19(3):211–220, May 1994.

[210] Roy Parker and Haiwei Song. The enzymes and control of eukaryotic mRNA turnover. *Nat. Struct. Mol. Biol.*, 11(2):121–127, February 2004.

[211] A Kahvejian, G Roy, and N Sonenberg. The mRNA closed-loop model: the function of PABP and PABP-interacting proteins in mRNA translation. *Cold Spring Harb. Symp. Quant. Biol.*, 66:293–300, 2001.

[212] Robert Peterson Susan Lindquist. Selective translation and degradation of heat shock MRNAS in drosophila. Enzyme 1990; 44:147-166, 1990.

[213] Kevin P Byrne and Kenneth H Wolfe. The yeast gene order browser: combining curated homology and syntenic context reveals gene fate in polyploid species. *Genome Res.*, 15(10):1456–1461, October 2005.

[214] Alex Charles Tuck and David Tollervey. A transcriptome-wide atlas of RNP composition reveals diverse classes of mRNAs and lncRNAs. *Cell*, 154(5):996–1009, August 2013.

[215] Ugrappa Nagalakshmi, Zhong Wang, Karl Waern, Chong Shou, Debasish Raha, Mark Gerstein, and Michael Snyder. The transcriptional landscape of the yeast genome defined by RNA sequencing. *Science*, 320(5881):1344–1349, June 2008.

[216] Stuart K Archer, Nikolay E Shirokikh, Claus V Hallwirth, Traude H Beilharz, and Thomas Preiss. Probing the closed-loop model of mRNA translation in living cells. *RNA Biol.*, 12(3):248–254, 2015.

[217] N Iizuka, L Najita, A Franzusoff, and P Sarnow. Cap-dependent and cap-independent translation by internal initiation of mRNAs in cell extracts prepared from saccharomyces cerevisiae. *Mol. Cell. Biol.*, 14(11):7322–7330, November 1994.

[218] Enrique Balleza, J Mark Kim, and Philippe Cluzel. Systematic characterization of maturation time of fluorescent proteins in living cells. *Nat. Methods*, 15(1):47–51, January 2018.

[219] Shana Elbaum-Garfinkle and Clifford P Brangwynne. Liquids, fibers, and gels: The many phases of neurodegeneration. *Dev. Cell*, 35(5):531–532, December 2015.

[220] Mariya M Kucherenko and Halyna R Shcherbata. Stress-dependent mir-980 regulation of Rbfox1/A2bp1 promotes ribonucleoprotein granule formation and cell survival. *Nat. Commun.*, 9(1):312, January 2018.

[221] Ouissame Bounedjah, Loïc Hamon, Philippe Savarin, Bénédicte Desforges, Patrick A Curmi, and David Pastré. Macromolecular crowding regulates assembly of mRNA stress granules after osmotic stress: new role for compatible osmolytes. *J. Biol. Chem.*, 287(4):2446–2458, January 2012.

[222] Valeria Cherkasov, Tomas Grousl, Patrick Theer, Yevhen Vainshtein, Christine Glässer, Cyril Mongis, Günter Kramer, Georg Stoecklin, Michael Knop, Axel Mogk, and Bernd Bukau. Systemic control of protein synthesis through sequestration of translation and ribosome biogenesis factors during severe heat stress. *FEBS Lett.*, 589(23):3654–3664, November 2015.

[223] Anthony Khong, Tyler Matheny, Saumya Jain, Sarah F Mitchell, Joshua R Wheeler, and Roy Parker. The stress granule transcriptome reveals principles of mRNA accumulation in stress granules. *Mol. Cell*, 68(4):808–820.e5, November 2017.

[224] Ankur Jain and Ronald D Vale. RNA gelation in repeat expansion disorders. January 2017.

[225] Catherine G Triandafillou, Christopher D Katanski, Aaron R Dinner, and D Allan Drummond. Transient intracellular acidification regulates the core transcriptional heat shock response. September 2018.

[226] Irena Jevtov, Margarita Zacharogianni, Marinke M van Oorschot, Guus van Zadelhoff, Angelica Aguilera-Gomez, Igor Vuillez, Ineke Braakman, Ernst Hafen, Hugo Stocker, and Catherine Rabouille. TORC2 mediates the heat stress response in drosophila by promoting the formation of stress granules. *J. Cell Sci.*, 128(14):2497–2508, July 2015.

[227] Charles Lu, Matthew J Brauer, and David Botstein. Slow growth induces heat-shock resistance in normal and respiratory-deficient yeast. *Mol. Biol. Cell*, 20(3):891–903, February 2009.

[228] Anna Zakrzewska, Gerco van Eikenhorst, Johanna E C Burggraaff, Daniel J Vis, Huub Hoefsloot, Daniela Delneri, Stephen G Oliver, Stanley Brul, and Gertien J Smits. Genome-wide analysis of yeast stress survival and tolerance acquisition to analyze the central trade-off between growth rate and cellular robustness. *Mol. Biol. Cell*, 22(22):4435–4446, November 2011.

[229] Joshua R Wheeler, Tyler Matheny, Saumya Jain, Robert Abrisch, and Roy Parker. Distinct stages in stress granule assembly and disassembly. *eLife Sciences*, 5:e18413, September 2016.